

Physics Opportunities of a 100 TeV Proton-Proton Collider

Nima Arkani-Hamed^a, Tao Han^b, Michelangelo Mangano^c, Lian-Tao Wang^d

^a*Institute for Advanced Study, Princeton, NJ, 08540, USA*

^b*Department of Physics and Astronomy, Univ. of Pittsburgh, Pittsburgh, PA 15260, USA
and Department of Physics, Tsinghua University, Beijing 100086, China*

^c*Physics Department, TH Group, CERN, CH-1211 Genve 23, Switzerland*

^d*Enrico Fermi Institute, Department of Physics,
and Kavli Institute for Cosmological Physics, University of Chicago,
Chicago, IL 60637-1434, USA*

Abstract

The discovery of the Higgs boson at the LHC exposes some of the most profound mysteries fundamental physics has encountered in decades, opening the door to the next phase of experimental exploration. More than ever, this will necessitate new machines to push us deeper into the energy frontier. In this article, we discuss the physics motivation and present the physics potential of a proton-proton collider running at an energy significantly beyond that of the LHC and a luminosity comparable to that of the LHC. 100 TeV is used as a benchmark of the center of mass energy, with integrated luminosities of 3 ab^{-1} – 30 ab^{-1} .

Keywords: Higgs boson; electroweak symmetry breaking; electroweak phase transition; particle dark matter; future circular collider, high energy proton-proton collider

*Preprint numbers: PITT-PACC 1515; CERN-PH-TH-2015-259

Contents

1	Introduction	4
1.1	LHC, The Higgs Boson and Beyond	4
1.2	New Colliders for a New Frontier	6
1.3	Luminosity of the 100 TeV pp Collider	11
2	The Electroweak Phase Transition	17
2.1	General Remarks	17
2.2	Tests at the 100 TeV pp Collider	20
3	Naturalness of the Electroweak Scale	28
3.1	On the Mass of the Higgs Boson	28
3.2	Natural Theories and the Tests at the 100 TeV pp Collider . .	32
4	Dark Matter	42
4.1	WIMP Dark Matter	42
4.2	WIMP Dark Matter at the 100 TeV pp Collider	47
4.2.1	Pure Wino	49
4.2.2	Pure Higgsino	50
4.2.3	Mixed dark matter	51
4.2.4	Electroweak cascades	52
4.2.5	Co-annihilation with Bino dark matter	53
5	Other New Physics Searches	55
5.1	New Color Resonances	55
5.2	New Gauge Bosons and Vector Resonances	57
5.3	Heavy Higgs Bosons in Doublet and Triplet Models	57
5.4	Pair Production of Exotic Color States	61
5.5	Pair Production of Heavy Leptons	62
6	Benchmark Standard Model processes	63
6.1	Jets	64
6.2	W/Z Production	68
6.2.1	Multiple gauge boson production	69
6.2.2	FSR effects of the gauge bosons and initial state partons	70
6.3	Heavy Quarks	77
6.3.1	Inclusive bottom production	77
6.3.2	Inclusive top production	78

6.3.3	Bottom and top production at large Q^2	79
6.3.4	Heavy quark partons	80
6.4	Higgs Production Rates	81
6.5	Sources of Missing Transverse Energy	84
7	Directions for Further Exploration	85

1. Introduction

1.1. LHC, The Higgs Boson and Beyond

With the discovery of the Higgs boson at the Large Hadron Collider (LHC) [1, 2], fundamental physics finds itself at one of the most exciting crossroads in its history. The central questions today are the deepest ones that have been posed in decades, related to the ultimate origin of the elementary particles and even of space-time itself. Major new input from experiments is needed for progress.

The LHC restarted in 2015 at higher energies, and will eventually collect much more data. This will certainly significantly advance our understanding. As we will discuss in this report, however, attacking some of the most profound theoretical questions of the 21st century, particularly ones associated with the largely mysterious Higgs particle, will necessitate another leap to higher energies. The future of fundamental physics on the 20 – 50 year timescale hinges on starting a huge new accelerator complex that can take us at least one order of magnitude beyond the ultimate reach of the LHC.

There have been efforts in the community in planning the next step beyond the LHC, which have intensified after the discovery of the Higgs. Among the various options, a proton proton collider operating at energies far beyond that of the LHC has emerged as an appealing option, including the FCC-hh project promoted by CERN and the SppC project promoted by IHEP in China. 100 TeV is typically used as a benchmark energy for such a collider.

Many studies of the physics potential of an 100 TeV pp collider have been carried out in the recent past, and are continuously appearing in the literature. The results are still incomplete and preliminary, many years of intensive work are still needed to arrive at a complete description. At the same time, we already have a broad-brush picture of the physics capabilities of such a machine. The studies have also highlighted a number of open questions and future directions to explore. In this report we give a high-level summary of the central scientific issues at stake, and draw on the studies that have been carried out, to show that the leap in energy offered by a 100 TeV pp collider will allow us to robustly address some of the most important open questions in fundamental physics.

Many of the most profound mysteries are intimately connected with the Higgs particle, which is totally new, unlike anything we have seen before. In many ways the Higgs is the simplest particle imaginable, with no charge and no spin. This apparent simplicity is also what makes it so beguiling. All

other scalar particles we have seen have been obviously composite, with a size close to their Compton radius. The Higgs is not like this, appearing to be more point-like than naturally expected on theoretical grounds.

The Higgs must also have a dynamical property we have never seen for any of the other fundamental particles: it should be able to interact not only with other particles, but also with itself! Indeed, self-interaction is the most basic of all processes allowed by quantum field theory, but spin and charge forbid point-like self-couplings for all particles but the Higgs. The LHC will only scratch the surface of this physics, but with the data from the 100 TeV collider we will be able to unambiguously see and precisely measure the Higgs self-interaction process, whose structure is deeply related to the origin and mass of the Higgs itself. At an even more fundamental level, much of the

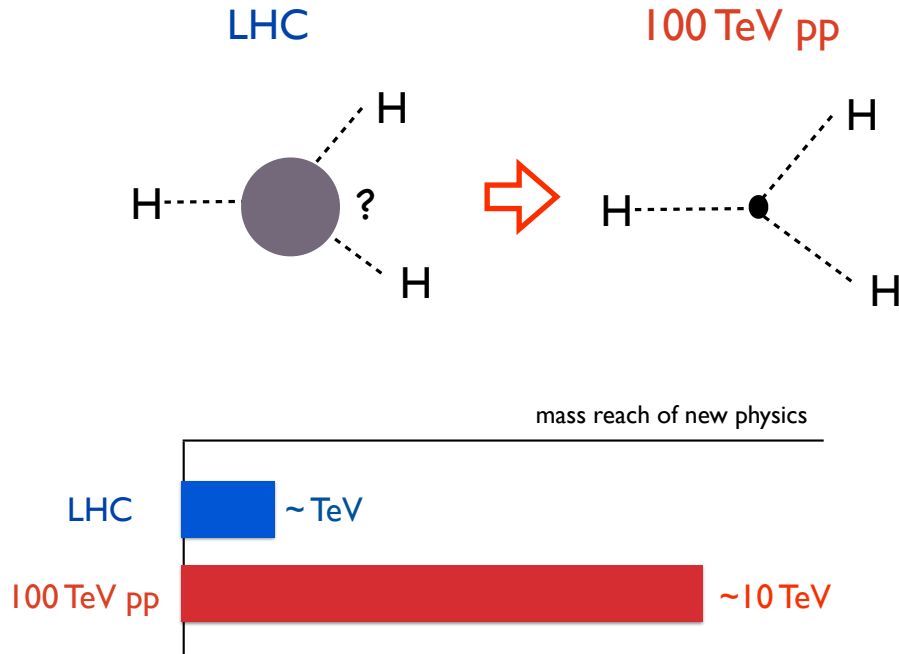


Figure 1: A sketch of two of the major advances obtained by going to a 100 TeV pp collider. The 100 TeV pp collider will see, for the first time, a fundamentally new dynamical process – the self-interaction of an elementary particle – uniquely associated with the Higgs. It will also improve the reach of the direct search of new physics particles by at least a factor of 5.

excitement surrounding the proposal of a 100 TeV pp collider stems from the bold leap into the completely uncharted new territory that it offers, probing

energy scales where we have long had reasons to expect fundamental new physical principles at play. The 100 TeV pp collider will allow us to hunt for new fundamental particles roughly an order of magnitude heavier than we can possibly produce with the LHC, and new particles the LHC may produce in small numbers will be produced with up to a thousand times higher rate, giving us a new window into the quantum-mechanical vacuum of our universe with a hundred-fold greater resolution than ever before.

These two points are sketched in Fig. 1, and represent the major advances we will make by going to a 100 TeV pp collider.

1.2. New Colliders for a New Frontier

Fundamental physics began with the twin revolutions of Relativity and Quantum Mechanics. Much of the second half of the 20th century was occupied with understanding the reconciliation of these principles within the framework of quantum field theory, and identifying a specific quantum field theory – the Standard Model (SM) of particle physics – describing all particles and interactions we know of to date.

Theoretical consistency with relativity and quantum mechanics places extremely strong constraints on theories of interacting massless particles, almost completely dictating the possible menu of spins and interactions. At energies low enough compared to some fundamental ultraviolet scale, physics is guaranteed to be described by Yang-Mills theories and gravity coupled to particles of spin 0, $1/2$, and also possibly spin $3/2$ with supersymmetry. The rigidity of this structure is striking. Of course, most elementary particles are not massless, but since the effects of mass are naively negligible at high energies, these rules fix what physics at very high energies can look like, at least until we hit the Planck scale where the usual notion of space-time itself breaks down.

For particles with nontrivial spins, there is a jump in the number of spin degrees of freedom between massless and massive particles. For instance, the massive W and Z bosons have spin one and three spin degrees of freedom, but only two helicity degrees of freedom. This discontinuous difference between “massless” and “massive” obstructs a smooth transition from the apparent complexity of low energy physics to the simplicity of the high energy world whose structure is almost entirely dictated by general principles.

Famously, in the SM, the addition of a single particle – the Higgs boson – solves this problem, allowing us to reassemble the degrees of freedom of

massive particles at low energies into the consistent high energy framework for massless particles.

The Higgs is certainly the simplest solution to the problem it solves – it is hard to imagine a simpler elementary particle, with no spin or charge. But this simplicity is actually extremely surprising and, in a literal sense, unprecedented, since we have never before seen a point-like elementary particle of spin zero. Indeed, violent ultraviolet quantum fluctuations have the potential to generate huge masses for elementary particles, but this does not happen for particles with spin, where a change from “massless” to “massive” would change the number of spin degrees of freedom discontinuously. However, the number of spin degrees of freedom for massless and massive particles of spin zero is the same, and so nothing shields the generation of huge scalar masses, near the highest ultraviolet (UV) scales of the theory.

This logic is strongly supported from analogous phenomena in condensed matter physics. Various materials can be engineered to be described by non-trivial long-distance effective theories at very low temperatures. Many of the key features of the SM, like gauge fields and chiral fermions, can arise in a beautiful way as emergent collective excitations of the system. But interacting spin zero particles like the Higgs are not seen: the only light scalars that are ubiquitously present are Goldstone bosons – like phonons – which are non-interacting at low energy. This makes sense because the emergence of fermions and gauge fields can be robust and stable against small variations in the detailed properties of the material. Since this is not true for scalars, the only way to get light scalars to emerge from a condensed matter system is to finely adjust the microphysics of the material: for instance by putting it under high pressure, looking for the thin slivers in parameter space where a Higgs-like scalar becomes accidentally light. This expectation has been borne out by recent experiments which do indeed fine-tune to produce a particle resembling the Higgs boson of an (ungauged) $SO(3) \rightarrow SO(2)$ symmetry breaking pattern [3].

These good reasons for never having seen light scalars either in particle physics or condensed matter systems make it all the more remarkable to have finally found one with the Higgs! There is an irony here: the development of the Higgs mechanism was greatly inspired by the Landau-Ginzburg model of superconductivity. However, the Landau-Ginzburg model was never a real theory, only a phenomenological model, and was replaced by BCS theory a few short years later. Many theorists expected the same fate for the Higgs model of electroweak symmetry breaking, with technicolor being the particle

physics analog of BCS theory. But it was the Higgs model that ended up being the right answer in particle physics!

So while an oft-heard desire of particle physicists for many years has been to find “new physics” beyond the Higgs, this is missing the essential point: the Higgs itself represents “new physics” in a much more profound way than any more complex discoveries would have done. Its discovery closes the 20th century chapter of fundamental physics while simultaneously kicking the door open to entirely new questions that properly belong to the 21st century. These questions on the table now are not about details, but are deeper and more structural ones, leading back to the very foundations of quantum field theory. It is striking that very similar questions are forced on us in trying to reckon with the smallness of the cosmological constant and the discovery of the accelerating expansion of the universe.

Obviously, the experimental future of the field will importantly depend on results from the next run of the LHC. However, given what we have already seen – a light Higgs, but no evidence yet for physics beyond the SM – no matter what new physics the LHC does or does not discover, building a complete picture of the relevant physics will require new machines beyond the LHC: not just for cleaning up details, but in order to answer the big-picture questions that will set the direction of fundamental physics for decades to come.

Let us begin by giving a lightning tour of the raw physics capabilities of the 100 TeV pp collider. Thanks to the asymptotic freedom and factorization theorem of QCD, hadronic collisions at high energies can be calculable in perturbation theory, and we write the production cross section of a final state X as

$$\sigma(pp \rightarrow X + \text{anything}) = \int_{\tau_0}^1 d\tau \sum_{ij} \frac{d\mathcal{L}_{ij}}{d\tau} \hat{\sigma}(ij \rightarrow X), \quad (1)$$

$$\frac{d\mathcal{L}_{ij}}{d\tau} = \frac{1}{1 + \delta_{ij}} \int_{\tau}^1 \frac{d\xi}{\xi} \left[f_{i/p}(\xi, Q_f^2) f_{j/p}\left(\frac{\tau}{\xi}, Q_f^2\right) + (i \leftrightarrow j) \right], \quad (2)$$

where the parton luminosities $d\mathcal{L}_{ij}$ are given in terms of the parton distribution functions (PDFs) $f_{i,j/p}$, whose arguments are the fractions of momenta $(\xi, \tau/\xi)$ carried by the initial partons (i, j) and the parton factorization scale Q_f , and $\tau = \hat{s}/s$, where \sqrt{s} ($\sqrt{\hat{s}}$) is the proton-proton beam (parton-parton) center of mass (CM) energy. $\hat{\sigma}$ is the partonic cross section for $ij \rightarrow X$.

Due to the rapid fall-off of parton luminosities at large τ , the rate for

processes that at a given \sqrt{s} have a large value of τ will increase dramatically when going to higher CM energies. We illustrate this point in the left panel of Fig. 2, where we show the partonic luminosity densities versus the average energy fraction $\sqrt{\tau}$ (lower scale) and the partonic CM energy $\sqrt{\hat{s}}$ (top scale), and in the right panel the luminosity ratios between 100 TeV and 14 TeV. We see the significant increase of the partonic luminosities, by a factor ranging from 20 – 100 at $\sqrt{\hat{s}} \approx 1$ TeV to 300 – 5000 at $\sqrt{\hat{s}} \approx 4$ TeV.

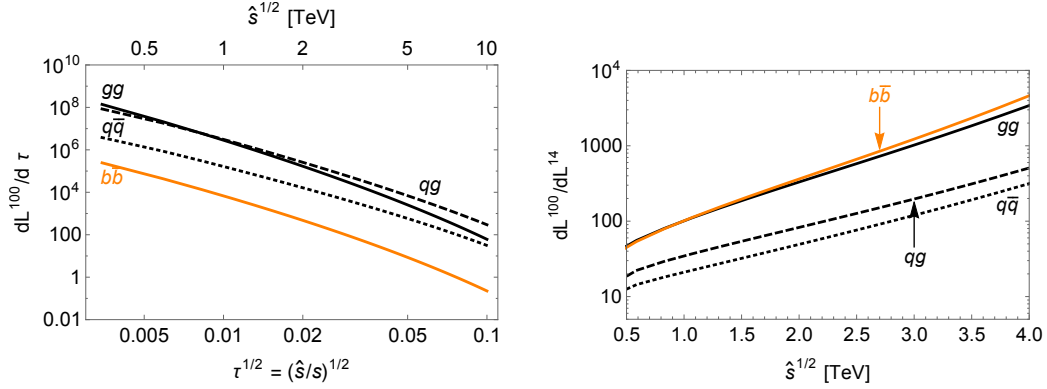


Figure 2: Left panel: Parton luminosity densities at a 100 TeV pp collider versus the average energy fraction $\sqrt{\tau}$ (lower scale) and the partonic CM energy $\sqrt{\hat{s}}$ (top scale); Right panel: luminosity ratios between 100 TeV and 14 TeV.

Most importantly, the leap in energy at the 100 TeV pp collider gives a huge increase in the reach for new physics. A seven-fold increase in CM energy relative to the LHC, with a luminosity comparable to that of the LHC, increases the mass reach for new particles significantly. For instance, the mass reach will be extended by a factor of about five relative to the LHC for resonant production of weakly or strongly interacting resonances, or by a factor of four for color-singlet pair production. We illustrate this in detail in Sec. 5.

The huge increase in parton luminosity also leads to a substantial enhancement of the production rates for the SM processes in going from 14 to 100 TeV, as illustrated in Fig. 3 [4]. This will allow several extremely rare SM processes to be potentially observable for the first time.

Measuring the triple Higgs coupling provides a direct probe of the nature of the electroweak symmetry breaking, and this is best done at the 100 TeV pp collider, by looking for double-Higgs production, which yields a sizable

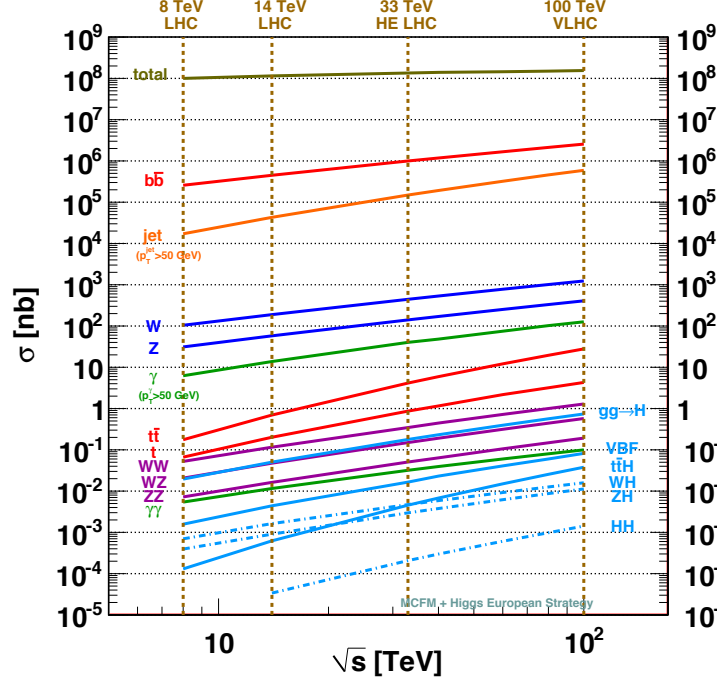


Figure 3: Production rates of SM processes versus the pp CM energy [4].

production cross section of $\mathcal{O}(1 \text{ pb})$. At the LHC, this process suffers from a low production rate and large SM backgrounds. Moreover, one needs to disentangle different contributions from different contributing diagrams. At 100 TeV, this process will however probe a SM Higgs self-coupling at about ten percent level [5, 6, 7, 8]. The 100 TeV pp collider could also directly probe the top Yukawa coupling, via $t\bar{t}H$ production, at the 1% level [9].

Experiments at 100 TeV probe the SM in a regime where the electroweak symmetry is effectively restored. A couple of new features are worth noting (more details will be given in Section 6.2.2). First of all, in processes at the very high energies $\sqrt{\hat{s}} \gg M_W$, EW gauge bosons are copiously produced by radiation. For p_T 's approaching $\sim 10 \text{ TeV}$, the electroweak Sudakov factor $4\alpha_2 \log^2(p_T^2/m_W^2) \sim 0.1$, and we have “electroweak radiation” in complete analogy with electromagnetic and gluon radiation. For instance, a W or Z gauge boson would be radiated off a light quark with 10 TeV of energy with a probability of 10% and off a gauge boson with a probability of 20%. These

production rates are one-to-two orders of magnitude higher than what we typically encounter when considering the production of gauge boson in inclusive processes at $\sqrt{\hat{s}} \sim M_W$: for example, as shown in Fig. 3, the production rate of an additional W boson in inclusive W production is only at the per-mille level, $\sigma(WW)/\sigma(W) \sim 10^{-3}$. This phenomenon makes it possible to “see” traditionally invisible particles such as neutrinos (or even weakly-interacting dark matter particles), through electroweak radiation. This can be nicely illustrated by considering the invisible decay of a $Z' \rightarrow \nu\nu$. For heavy enough Z' ’s, there is a significant rate for radiating W, Z ’s off the neutrinos. The ratio $\Gamma(Z' \rightarrow \nu\bar{\nu})/\Gamma(Z' \rightarrow \nu\bar{\nu}Z)$ only depends on the mass of the Z' , and so if this visible mode is abundant enough we can directly determine the invisible rate (and thereby also directly determine the Z' coupling to left-handed leptons) [10].

Similarly to what happens for bottom quarks at the Tevatron, at 100 TeV one can expect processes where the energy involved is so large that even a top quark can be considered as practically massless. In this case, large logarithms of \hat{s}/m_t^2 can and must be resummed, using a formalism similar to that adopted to describe the bottom quark PDF at Tevatron or LHC energies. This will be discussed in Section 6.3.4 and examples of relevant applications will be shown in Section 5. On a similar footing, as will be discussed in detail in Section 6.2.2, the electroweak gauge bosons, W, Z , may be copiously radiated off the initial-state quarks, and can be treated as partons inside the proton.

At 100 TeV, the electroweak gauge bosons and the top quark can be produced in highly boosted configurations. Their decay products will be highly collimated and thus form massive jets, W, Z - or top-jets. This new phenomena will also naturally arise when new heavy particles are produced and subsequently decay to the gauge bosons and top quarks.

1.3. Luminosity of the 100 TeV pp Collider

In this discussion of physics opportunities, some brief comments about the energy and luminosity requirements of the 100 TeV pp collider are in order. The CM energy and luminosity of a proton proton collider are crucial in determining its physics potential. Perhaps the most obvious question is how energy and luminosity impact mass reach for the production of new particles. This review uses 100 TeV as a benchmark, with integrated luminosities ranging from 3 ab^{-1} to 30 ab^{-1} . The reach will roughly scale with the CM energy, if other options are considered.

The question of required or target luminosity has been discussed in detail recently [11]. Larger integrated luminosity leads to sensitivity to new physics with smaller signal cross sections, which in turn enhances the new physics mass reach. To be concrete, let us compare the reach of the LHC and a 100 TeV pp collider for the production of massive particles with different two-parton initial states, using estimates of reach based on scaling of the parton luminosity.¹

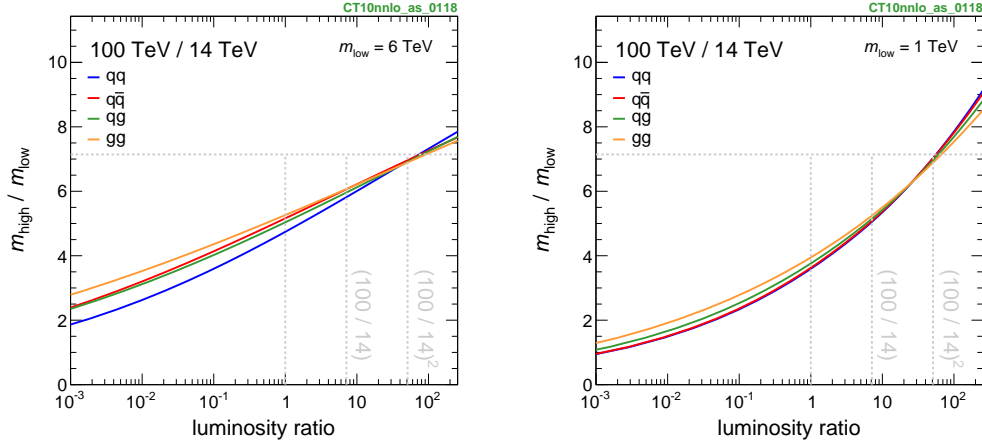


Figure 4: Ratio of the reach of new physics scale from the LHC and 100 TeV pp collider, shown as a function of the ratio of luminosity. New physics produced from different partonic initial states are considered. The limit of LHC is assumed to be 6 TeV (left) and 1 TeV (right).

First, we focus on the highest possible reach in mass. For the LHC, we assume the reach for the scale of certain type of new physics is 6 TeV, shown in the left panel of Fig. 4. This could be the case for a 6 TeV Z' , or of a ~ 3 TeV gluino, pair produced. While this is a crude estimate, it has been demonstrated to be a reasonable approximation in a wide variety of examples and suffices for our discussion here. To be more concrete, the increases of the mass reach with 10 times more luminosity for two benchmark examples, sequential W' and heavy quark, are shown in Fig. 5. We see that the much larger increase in luminosity only gives us a very modest gain in mass reach: this well-known fact is a direct consequence of the steeply falling parton

¹For a useful tool to perform such estimates, see the link by Salam and Weiler at <http://collider-reach.web.cern.ch/collider-reach/>.

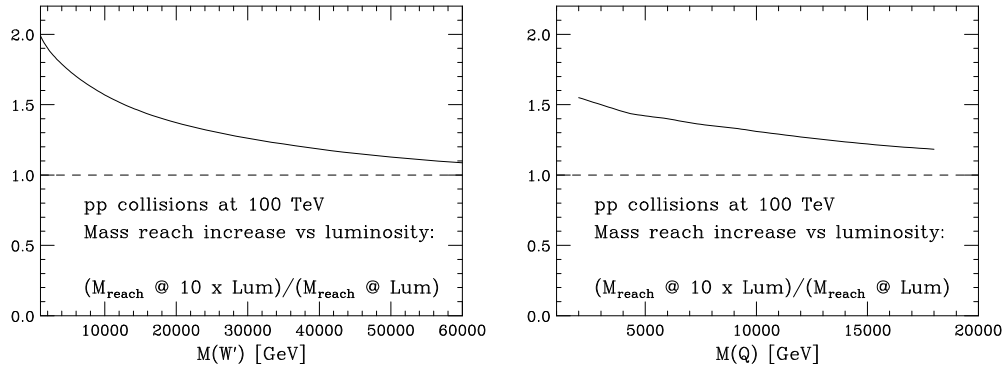


Figure 5: Two examples of the increase of the reaches of new physics with 10 times more luminosity. Left: Drell-Yan production of sequential W' . Right: Pair production of heavy quark.

luminosity as a function of parton CM energy. This is especially true when we consider the highest reach in mass, which involves a regime where the parton density falls off very fast and the ultimate reach is typically limited by the production rate. In fact, in the luminosity range of $0.1 - 10^3 \text{ ab}^{-1}$, the increase in mass reach is well approximated by a logarithmic behavior,

$$M(L) - M(L_0) \sim 7 \text{ TeV} \log_{10}(L/L_0), \quad (3)$$

with about 7 TeV increase in mass for a tenfold luminosity increase. The relative gain in mass reach therefore diminishes as the total luminosity is increased. Even with just 3 ab^{-1} , the same as the target luminosity of the HL-LHC, the 100 TeV pp collider can enhance the new physics reach by a factor of 5. This is a huge step and a large portion of the ratio of the CM energy ~ 7 . Of course, given that partonic cross sections drop with the energy as

$$\hat{\sigma} \sim \hat{s}^{-1}, \quad (4)$$

an increase of a factor of ~ 50 would be needed to extend the reach by the full factor of ~ 7 . Scaling violations in the PDFs actually call for a slightly larger luminosity increase, as discussed in detail in [12].

For the searches of lower mass particles, the parton density falls off more slowly in the relevant regime and simple scaling suggests a larger luminosity is necessary to achieve the same enhancement in the mass reach, as demonstrated in the right panel of Fig. 4. However, we note that making a sharp statement in this case is much harder, since this is usually the case with

weak signals and large backgrounds. We need to identify particular highly motivated cases to set the luminosity target. The most important example is probably the measurement of the triple Higgs coupling discussed earlier. The target here is to reach the 10% level accuracy, which is crucial in distinguishing qualitatively different characters of the Higgs potential. Preliminary studies of this process have been performed [5, 6, 7, 8]. While adopting slightly different assumptions about systematic uncertainties and backgrounds, they nevertheless converge to a precision in the range of 5 – 10% for 30 ab^{-1} . Given the fundamental importance of this question for setting an objective target for the luminosity, future studies should be undertaken to settle it decisively.

Since typically a collider will start with a lower-than-nominal luminosity, it is interesting to have a set of “minimal” luminosity goals. If we consider dijet

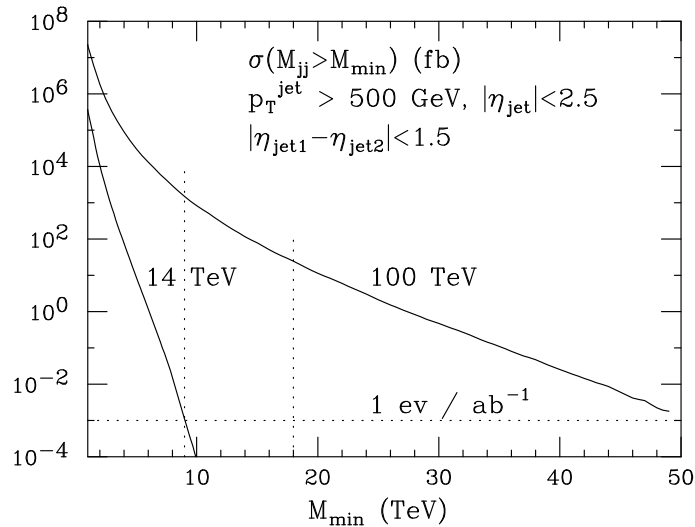


Figure 6: Cross sections for the production of dijet pairs with invariant mass $M_{jj} > M_{\min}$, at c.m. energies $\sqrt{s} = 14$ and 100 TeV. The jets are subject to the p_T and η cuts shown in the legend.

production as a probe of the shortest distances, we can extract a reference luminosity target from Fig. 6, which shows the leading-order cross section to produce central dijet pairs as a function of their invariant mass. The LHC has a sensitivity at the level of 1 event per ab^{-1} for dijet masses above ~ 9.5 TeV. At this mass, the 100 TeV cross section is 6 orders of magnitude larger, which means that the HL-LHC sensitivity can be recovered within

1 pb⁻¹, i.e., in less than a day of running at a luminosity of 10³² cm⁻²s⁻¹. The sensitivity to a mass range twice as large, 19 TeV, would require 50 pb⁻¹, namely of the order of one month at 10³² cm⁻²s⁻¹, and one year of running at this luminosity would give us events with dijet mass well above 25 TeV.

If we consider particles just outside the possible discovery reach of the HL-LHC, which therefore the LHC could not have discovered, we find the rate increases in the range of 10⁴ – 10⁵ that we discussed earlier, for $q\bar{q}$ and gg production channels, respectively. This means that integrated luminosities in the range of 0.1 – 1 fb⁻¹ are sufficient to push the discovery reach beyond what the HL-LHC has already explored. This can be obtained in one year of operations with initial luminosities as small as 2×10^{32} cm⁻²s⁻¹.

Finally, we project in Fig. 7 the temporal evolution of the extension of the discovery reach for various luminosity scenarios, relative to the reach of 3 ab⁻¹ at 14 TeV. The left (right) plot shows results for a resonance whose couplings allow discovery at HL-LHC up to 6 TeV (1 TeV). Once again, we notice that the benefit of luminosity is more prominent at low mass than at high mass. We also notice that, considering the multi-year span of the programme, and assuming a progressive increase of the luminosity integrated in a year, an early start at low luminosity does not impact significantly the ultimate reach after several years of running.

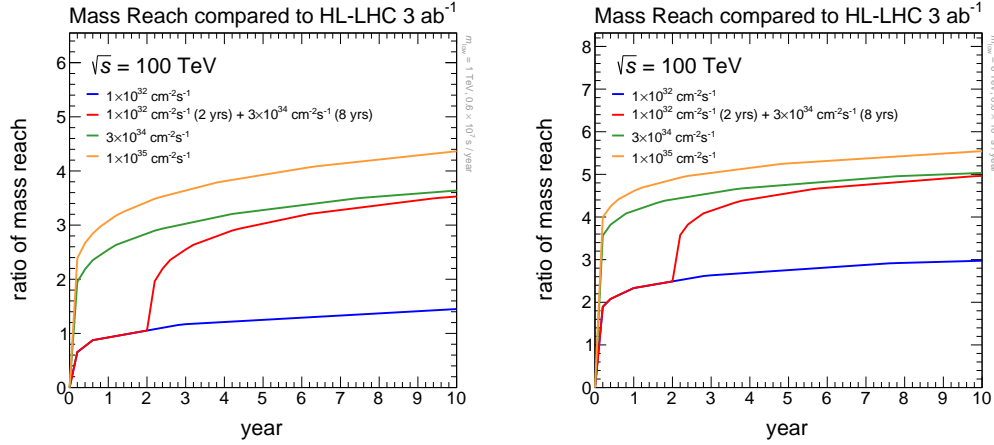


Figure 7: Evolution with time of the mass reach at $\sqrt{s} = 100$ TeV, relative to HL-LHC, under different luminosity scenarios (1 year counts for 6×10^6 sec). The left (right) plot shows the mass increase for a ($q\bar{q}$) resonance with couplings enabling HL-LHC discovery at 6 TeV (1 TeV).

The goal of an integrated luminosity in the range of $10\text{--}20\text{ ab}^{-1}$ per experiment, corresponding to an ultimate instantaneous luminosity approaching $2 \times 10^{35}\text{ cm}^{-2}\text{s}^{-1}$ [13], seems therefore well-matched to our current perspective on extending the discovery reach for new phenomena at high mass scales, high-statistics studies of possible new physics to be discovered at (HL)-LHC, and incisive studies of the Higgs boson's properties. Specific measurements may set more aggressive luminosity goals, but we have not found generic arguments to justify them. The needs of precision physics arising from new physics scenarios to be discovered at the HL-LHC, to be suggested by anomalies observed in e^+e^- collisions at a future linear or circular collider, or to be discovered at 100 TeV, may well drive the need for even higher statistics. Such requirements will need to be established on a case-by-case basis, and no general scaling law gives a robust extrapolation from 14 TeV. Further work on *ad hoc* scenarios, particularly for low-mass phenomena and elusive signatures, is therefore desirable.

For a large class of new-physics scenarios that may arise from the LHC, less aggressive luminosity goals are acceptable as a compromise between physics return and technical or experimental challenges. In particular, even luminosities in the range of $10^{32}\text{ cm}^{-2}\text{s}^{-1}$ are enough to greatly extend the discovery reach of the 100 TeV collider over that of the HL-LHC, or to enhance the precision in the measurement of discoveries made at the HL-LHC.

We have given an overview of the impressive raw capabilities of the 100 TeV pp collider. Of course, given that we can extrapolate the SM alone to ultra-high energies, there is no guarantee that this collider will see new particles. However, the production of new particles has never been an aim in itself: the driving ambition of our field has always been to uncover *new principles* of physics, as they are needed. And as we have stressed, with the discovery of the Higgs we are fortunate to find ourselves in an era where such fundamentally new principles are called for, the character of which will be illuminated by direct studies of the Higgs itself. Nonetheless, in thinking about physics that may exist beyond the Higgs, it is important to ask whether the reaches of the 100 TeV are the right ones. Our goal in the rest of this review is to address this issue, identifying fundamental physics questions which are squarely within the cross-hairs of the 100 TeV pp collider.

2. The Electroweak Phase Transition

2.1. General Remarks

For decades, particle physics has been driven by the question of what breaks the electroweak symmetry. With the discovery of the Higgs, we have discovered the broad outlines of the answer to this question: the symmetry breaking is associated with at least one weakly coupled scalar field. However, this gives us only a rough picture of the physics, leaving a number of zeroth order questions wide open that must be addressed experimentally, but cannot be definitively settled at the LHC. These questions include what is the shape of the symmetry breaking potential, and how is electroweak symmetry restored at high scales.

The SM picture for electroweak symmetry breaking follows the Landau-Ginzburg parametrization of second-order phase transitions,

$$V(h) = m_h^2 h^\dagger h + \frac{1}{2} \lambda (h^\dagger h)^2, \quad (5)$$

with $m_h^2 < 0$ and $\lambda > 0$. This is the simplest picture theoretically, and the one we would expect on the grounds of effective field theory, in which we include the leading relevant and marginal operators to describe low energy physics. On the other hand, as we will review in more detail in our discussion of naturalness, this picture is far from innocuous or “obviously correct” — for instance it is precisely this starting point that leads to the all vexing mysteries of the hierarchy problem!

The central scientific program directly continuing from the discovery of the Higgs must thus explore whether this simplest parametrization of electroweak symmetry breaking is actually the one realized in Nature. And while we have discovered the Higgs, we are very far from having confirmed this picture experimentally. As illustrated in Fig. 8, the LHC will only probe the small, quadratic oscillations around the symmetry breaking vacuum, without giving us any idea of the global structure of the potential. For example, the potential could trigger symmetry breaking by balancing a negative quartic against a positive sextic [14, 15, 16], i.e.

$$V(h) \rightarrow m_h^2 (h^\dagger h) + \frac{1}{2} \lambda (h^\dagger h)^2 + \frac{1}{3! \Lambda^2} (h^\dagger h)^3, \quad (6)$$

with $\lambda < 0$. The potential might not even be well-approximated by a polynomial function, and may instead be fundamentally non-analytic, as in the

early Coleman-Weinberg proposal for symmetry breaking [17]:

$$V(h) \rightarrow \frac{1}{2} \lambda (h^\dagger h)^2 \log \left[\frac{(h^\dagger h)}{m^2} \right]. \quad (7)$$

These possibilities are associated with totally different underlying dynamics for electroweak symmetry breaking than the SM, requiring new physics beyond the Higgs around the weak scale. They also have radically different theoretical implications for naturalness, the hierarchy problem and the structure of quantum field theory.

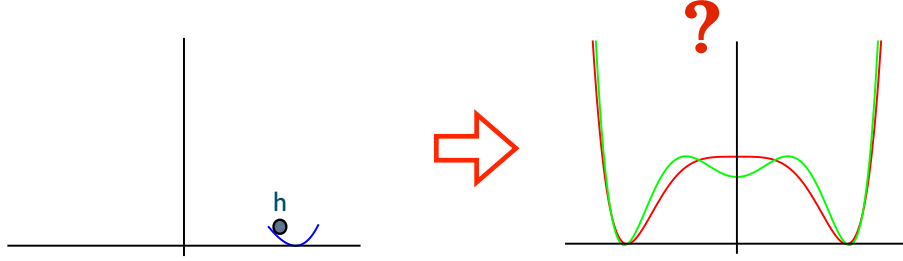


Figure 8: Question of the nature of the electroweak phase transition.

The leading difference between these possibilities shows up in the cubic Higgs self-coupling. In the SM, minimizing the potential gives $v^2 = 2|m_h|^2/\lambda$. Expanding around this minimum $h = (v + H)/\sqrt{2}$ gives

$$V(H) = \frac{1}{2} m_H^2 H^2 + \frac{1}{6} \lambda_{hhh} H^3 + \dots, \quad \text{with } m_H^2 = \lambda v^2 \quad \text{and} \quad \lambda_{hhh}^{SM} = 3(m_H^2/v). \quad (8)$$

Consider the example with the quartic balancing against a sextic and, for the sake of simplicity to illustrate the point, let us take the limit where the m_h^2 term in the potential can be neglected. The potential is now minimized for $v^2 = 2|\lambda|\Lambda^2$, and we find

$$m_H^2 = \lambda v^2, \quad \lambda_{hhh} = 7m_H^2/v = (7/3)\lambda_{hhh}^{SM}, \quad (9)$$

giving an $O(1)$ deviation in the cubic Higgs coupling relative to the SM. In the case with the non-analytic $(h^\dagger h)^2 \log(h^\dagger h)$ potential, the cubic self-coupling is $\lambda_{hhh} = (5/3)\lambda_{hhh}^{SM}$.

Even larger departures from the standard picture are possible — we don't even know whether the dynamics of symmetry breaking is well-approximated by a single light, weakly coupled scalar, as there may be a number of light scalars, and not all of them need be weakly coupled!

Understanding this physics is also directly relevant to one of the most fundamental questions we can ask about *any* symmetry breaking phenomenon, which is what is the order of the associated phase transition. Is the electroweak transition a cross-over, or might it have been strongly first-order instead? And how do we attack this question experimentally? This question is another obvious next step following the Higgs discovery: having understood what breaks electroweak symmetry, we must now undertake an experimental program to probe how electroweak symmetry is restored at high energies.

A first-order phase transition is strongly motivated by the possibility of electroweak baryogenesis [18]. While the origin of the baryon asymmetry is one of the most fascinating questions in physics, it is frustratingly straightforward to build models for baryogenesis at ultra-high energy scales, with no direct experimental consequences. However, we are not forced to defer this physics to the deep ultraviolet: as is well known, the dynamics of electroweak symmetry breaking itself provides all the ingredients needed for baryogenesis. At temperatures far above the weak scale, where electroweak symmetry is restored, electroweak sphalerons are unsuppressed, and violate baryon number. As the temperature cools to near the electroweak transition, bubbles of the symmetry breaking vacuum begin to appear. CP violating interactions between particles in the thermal bath and the expanding bubble walls can generate a net baryon number. If the phase transition is too gradual (second order), then the Higgs vacuum expectation value (VEV) inside the bubbles turns on too slowly, so the sphalerons are still active inside the bubble, killing the baryon asymmetry generated in this way. However, if the transition is more sudden (first order), the Higgs VEV inside the bubble right at the transition is large, so the sphalerons inside the bubble are Boltzmann suppressed and the baryon asymmetry can survive. This requires that

$$\exp(-\Delta E_{sph}/T_c) < \exp(-10), \quad (10)$$

and can be translated to a rough criterion on the size of the Higgs expectation value at the transition:

$$\frac{\langle h \rangle(T_c)}{T_c} > 0.6 - 1.6. \quad (11)$$

In the SM with $m_H \approx 125$ GeV, the electroweak phase transition is not strong enough to satisfy this condition. The CP violation in the Cabibbo-Kobayashi-Maskawa (CKM) quark mixing matrix is not large enough to generate the asymmetry. Hence, in order to make this beautiful idea work, we have to go beyond the SM. Getting the needed amount of CP violation is easy with the addition of new particles and interactions near the weak scale, without being in conflict with the stringent limits from electric dipole moments for the electron and neutron. However, while we can probe for new CP phases indirectly, by the continued search for electric dipole moments, it is both difficult and highly-model dependent to probe CP violation at colliders. On the other hand, the physics needed for a sufficiently first-order phase transition is a perfect target for future colliders. We will use the requirement in Eq. (11) as our benchmark for probing an “interestingly” strong first order transition.

2.2. Tests at the 100 TeV pp Collider

Colliders cannot replicate the high-temperature conditions of the early universe at the electroweak scale. However, a 100 TeV collider can provide an extremely powerful probe of physics that could alter electroweak symmetry breaking dynamics enough to make the phase transition first-order. A large change in the structure of the Higgs potential leads to an $O(1)$ deviation in the triple Higgs self-coupling relative to the SM, which will be probed to about 10% level at a 100 TeV pp collider. Furthermore, there must be additional particles beyond the Higgs, with mass not too much heavier than the weak scale, and relatively strongly coupled to the Higgs, in order to be able to qualitatively change the order of the transition relative to the minimal SM. While such particles can escape detection at the LHC, they are a perfect target for 100 TeV colliders. Even in the most difficult scenario in which the new particles only affect the phase transition at loop-level, the combination of deviations in the Higgs triple coupling and direct production of the new states at a 100 TeV collider covers most of the allowed parameter space in the examples studied to date.

Of course, we are not claiming a “no-lose” theorem, and it may be possible to engineer models that change the order of the phase transition while suppressing the 100 TeV collider signals. However, such scenarios would appear to need some contrivance. Our aim in this section is to show that a 100 TeV collider can robustly cover the space of possibilities for simple models generating a first-order phase transition.

The simplest toy model for a first-order transition simply augments the SM with a higher-dimension operator as in Eq. (6) [14, 15, 16, 19, 20]. At leading order (which suffices for our purposes here) finite temperature effects merely add the usual quadratic shift to the quadratic part of the potential $m^2(T) \rightarrow m_h^2 + cT^2$ for a positive constant c determined by the top Yukawa and gauge couplings. A first-order phase transition can be achieved if the quartic term is negative ($\lambda < 0$). As we saw earlier, in this example we have an $O(1)$ deviation in the Higgs self-coupling, and this is a general expectation for any theory where the first-order phase transition is driven by a large change in the (zero-temperature) Higgs potential.

Purely by effective field theory rules, it is consistent to have a theory where $(h^\dagger h)^3$ is the only dimension-6 operator at leading order. It is amusing that this choice is even radiatively stable at leading order: $(h^\dagger h)^3$ does not induce any of the other dimension 6 operators involving the Higgs under 1-loop RG evolution.

In any reasonable UV completions we can expect other higher-dimension operators in addition to $(h^\dagger h)^3$. While the UV physics may preserve custodial $SU(2)$ and give suppressed contributions to the precision electroweak operators, there is no symmetry distinction between the $(h^\dagger h)^3$ operator and the operator $[\partial_\mu(h^\dagger h)]^2$, so they are expected to be generated as well, and to affect the ZZH couplings, which can be probed at the per-mille level by e^+e^- Higgs factories [21, 22, 23, 24]. However it is the $(h^\dagger h)^3$ operator that is directly related to the physics of the electroweak transition, which is most powerfully probed at the 100 TeV collider.

We begin by considering the simplest example of a theory where these couplings are generated at tree-level by integrating out a massive singlet S coupled to the Higgs. As we will see, this example represents the “easiest” case, where it is straightforward to get a first-order phase transition, with large associated signals for 100 TeV colliders. Since this is an “easy” case, we will use it largely to illustrate the important physics points parametrically. We will then move to the “hard” case, where the order of the transition is only affected at 1-loop.

The important interactions for this toy model are given by

$$m_h^2 h^\dagger h + \frac{\tilde{\lambda}}{2} (h^\dagger h)^2 + \frac{1}{2} m_S^2 S^2 + a m_S S h^\dagger h + \frac{b}{3!} m_S S^3 + \frac{\kappa}{2} S^2 h^\dagger h + \frac{1}{4!} \lambda_S S^4. \quad (12)$$

The dimensionless couplings a, b can be set to zero by a Z_2 symmetry under which $S \rightarrow -S$, but in the absence of such a symmetry they should be

present. We will concentrate on the limit where the $bm_S S^3$ interaction is negligible. Integrating S out at tree-level gives rise to both the modified Higgs potential as well the oblique Higgs operator as

$$m_h^2 h^\dagger h + \frac{\lambda}{2} (h^\dagger h)^2 + \frac{\kappa a^2}{2m_S^2} (h^\dagger h)^3 + \frac{a^2}{2m_S^2} (\partial_\mu (h^\dagger h))^2. \quad (13)$$

Here $\lambda = \tilde{\lambda} - a^2$. Neglecting the m_h^2 term as above, the first-order transition is driven with $\lambda < 0$, $k > 0$, and we can determine the electroweak scale and Higgs masses as

$$v^2 = \frac{4}{3} \frac{m_S^2 |\lambda|}{\kappa a^2}, \quad m_H^2 = |\lambda| v^2. \quad (14)$$

We can also find the shift in the ZZH coupling as

$$\delta Z_H = \frac{4}{3} \frac{a^2 v^2}{m_S^2} = \frac{4}{3} \frac{|\lambda|}{\kappa}. \quad (15)$$

In order to avoid an unwanted $O(1)$ shift to the ZZH coupling, we must have $\kappa \gg \lambda$. This is perfectly consistent since λ is highly perturbative. It is interesting that despite the presence of a relatively strong coupling of the Higgs to a new massive state, there are no difficulties whatsoever with large precision electroweak corrections; this is closely related to the fact that the $O(1)$ deviation in the Higgs cubic couplings associated with the $(h^\dagger h)^3$ term does not radiatively induce precision electroweak operators at one-loop. For the couplings to be self-consistently perturbative, we must have

$$\kappa^2/16\pi^2 \lesssim |\lambda| \quad \text{and} \quad a^4/16\pi^2 \lesssim |\lambda|. \quad (16)$$

Since κ cannot become too large, the correction $\delta Z_H = (4/3)(|\lambda|/\kappa)$ cannot be too small and the singlet mass $m_S = \sqrt{\frac{3\kappa a^2}{4|\lambda|}} v$ cannot be too heavy, we thus find

$$\delta Z_H \gtrsim \frac{4}{3} \frac{\sqrt{|\lambda|}}{4\pi} = 0.05, \quad m_S \lesssim \frac{\sqrt{3}}{2} 4\pi v = 2.7 \text{ TeV}. \quad (17)$$

A similar conclusion holds even if the $bm_S S^3$ term is included and dominates; the parametrics changes slightly and we find instead

$$\delta Z_H \gtrsim 4 \left(\frac{\sqrt{|\lambda|}}{4\pi} \right)^{3/2} = 0.03, \quad m_S \lesssim 2\pi v \left(\frac{4\pi}{\sqrt{|\lambda|}} \right)^{1/4} = 3.4 \text{ TeV}. \quad (18)$$

Note that the bounds correspond to extreme limits of strong coupling, and it is most reasonable for the new couplings to be perturbative, so m_S is most plausibly in the range of a few hundred GeV.

These estimates quantify the intuitive expectation that any new physics giving a first-order phase transition cannot be too heavy and too weakly coupled to the Higgs.

We also get an associated $O(1)$ deviation in the Higgs triple coupling, and a singlet mass in the range of at most a few TeV, both of which are easily accessible to a 100 TeV pp collider. Since the singlet mixes significantly with the Higgs, the singlet is produced just as heavy Higgs bosons would be, and the significant decays are $S \rightarrow HH, ZZ, W^+W^-$ and $t\bar{t}$. A rough estimate of the 100 TeV reach for $pp \rightarrow S \rightarrow HH$ in these modes is shown in Fig. 9. Here c is a measure of the mixing between the singlet S and the Higgs boson. We have $c \sim (av)/m_S \sim (m_H/m_S)$, so this mixing is expected to be sizable.

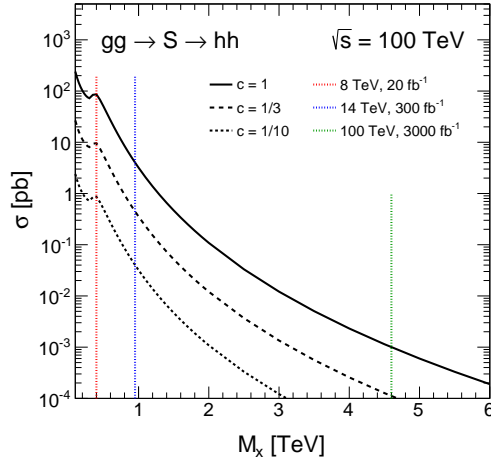


Figure 9: Estimate of reach in the $gg \rightarrow S \rightarrow HH$ channel at HL-LHC and a 100 TeV collider extrapolating from an ATLAS search [25]. The reach for the S scalar mass, shown by the vertical lines for different pp CM energies, assume that one Higgs decays to $b\bar{b}$ and the other to $\gamma\gamma$, and refer to the case $c = 1$.

In the above analysis we have assumed that $m_S^2 > 0$, so that the singlet is localized to the origin throughout the phase transition. There is also a qualitatively different possibility with $m_S^2 < 0$. Here, we can imagine that

it is really the phase transition for S that dominates the physics, and drags the Higgs along with it, since the effective Higgs mass term depends on $\langle S \rangle$ as $m_{h,eff}^2 = m_h^2 + am_S \langle S \rangle + \kappa \langle S \rangle^2$. The dynamics in the S -sector can make the S phase transition strongly first-order, at a temperature $T_c \sim \langle S \rangle$. Thus if we wish to have $\langle h \rangle / T_c \sim 1$, we should have $\langle h \rangle \sim \langle S \rangle$. This again gives us the obvious upper bound to the mass m_S , $m_S < 4\pi \langle S \rangle \sim 4\pi v \sim 2$ TeV, and S accessible to direct production at a 100 TeV collider.

Having discussed the “easy” cases for new physics giving a first-order electroweak phase transition, let us consider what appears to be the most difficult possible case, where a first-order electroweak phase transition is driven entirely by radiative effects, coupling the Higgs to SM singlet fields. This case is realized in our singlet model, if we further impose a Z_2 symmetry so that $a, b = 0$. This makes S exactly stable, and it could indeed be a component of Dark Matter. However this aspect is not relevant to our discussion; we may always assume a minuscule amount of Z_2 breaking giving a small a, b which allow S to decay on cosmological timescales.

As with our tree-level example, there are two qualitatively different cases to consider. When $m_S^2 > 0$, the role of the singlet is to give a large deformation to the Higgs potential at 1-loop, enabling a first-order phase transition directly in the Higgs direction. This will require κ to be large, which can be accomplished within a consistent weak-coupling approximation. In this case we expect a large correction to the zero-temperature Higgs potential and so an $O(1)$ deviation in the Higgs triple coupling. On the other hand, if $m_S^2 < 0$, we can have a two-step phase transition, where a first-order transition in S forces a first-order transition for h .

A detailed analysis of the model parameter space allowing a strong first-order phase transition has recently been given in [26], as shown in Fig. 10. The two-step transition operates for smaller values of the singlet masses and couplings, while larger masses and couplings can give rise to the modified Higgs potential giving the one-step transition along the Higgs direction.

In all cases, the singlet S is lighter than ~ 1 TeV, and so certainly kinematically accessible to a 100 TeV collider. In this worst-case scenario, since S only couples in pairs to the SM via the Higgs, as long as $m_S > m_H/2$ we must produce it via off-shell Higgses. Furthermore, if S is collider-stable, we are looking for missing energy signals very much like standard invisible Higgs decay searches, the main difference being the much smaller, non-resonant SS production cross-section. The dominant channels for SS production are in Vector-Boson-Fusion (VBF) $qq \rightarrow qqSS$, as well as in associated production

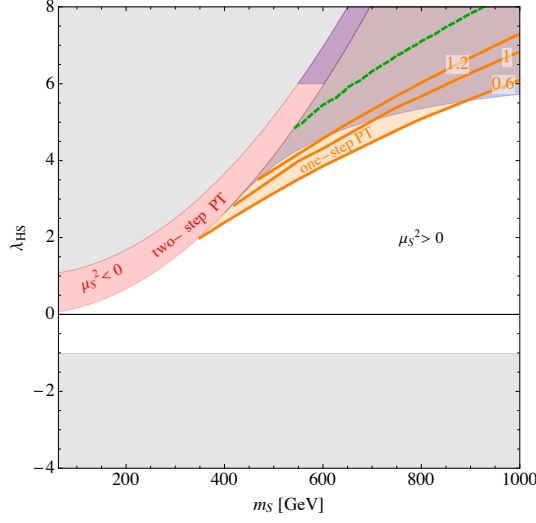


Figure 10: Parameter space with first order phase transition in the Z_2 model [26]. Red shaded region: for $m_S^2 < 0$ (m_S^2 is denoted as μ_S^2 in this figure [26]), it is possible to choose $\lambda_S = \kappa/2$ (in Eq. (12)) to get tree-induced two-step first-order electroweak phase transition. Orange contours: value of v_c/T_c for $m_S^2 > 0$. The orange shaded region indicates $v_c/T_c > 0.6$, where a one-step transition can be sufficiently first-order for electroweak baryogenesis. Above the green dashed line, singlet loop corrections generate a barrier between $h = 0$ and $h = v$ even at zero temperature, but results in the dark shaded region might not be reliable.

$qq \rightarrow VSS$ for $V = W^\pm, Z$. The cross sections for these processes at a 100 TeV collider are shown in the right panel of Fig. 11. These cross sections are very small, between $10^{-2} \rightarrow 10^{-4}$ pb. There is also a large background, in the VBF production of $Z \rightarrow \nu\bar{\nu}$, which is $\sim 10^3$ pb at 100 TeV. The authors of [26] imposed a simple set of cuts to isolate the signal, demanding exactly two forward jets with $p_{1,2}^T > 40$ GeV and $\eta_{1,2} < 5$, a missing energy cut $\cancel{E}_T > 150$ GeV, jet separation $|\eta_1 - \eta_2| > 3.5$ and $|\eta_{1,2}| > 1.8$, and $M_{jj} > 800$ GeV, while rejecting leptons with $|\eta| < 2.5$ and $p_T > 15$ GeV. The contours for S/\sqrt{B} in the (m_S, κ) plane resulting from their analysis are shown in the right panel of Fig. 11.

Already this simple analysis suggests that the entire region of the two-step transition can be probed by direct SS production at a 100 TeV collider. Note that this is a rough first pass at studying this signal, and one may expect to do significantly better. The main limiting factor is the huge $Z \rightarrow \nu\bar{\nu}$

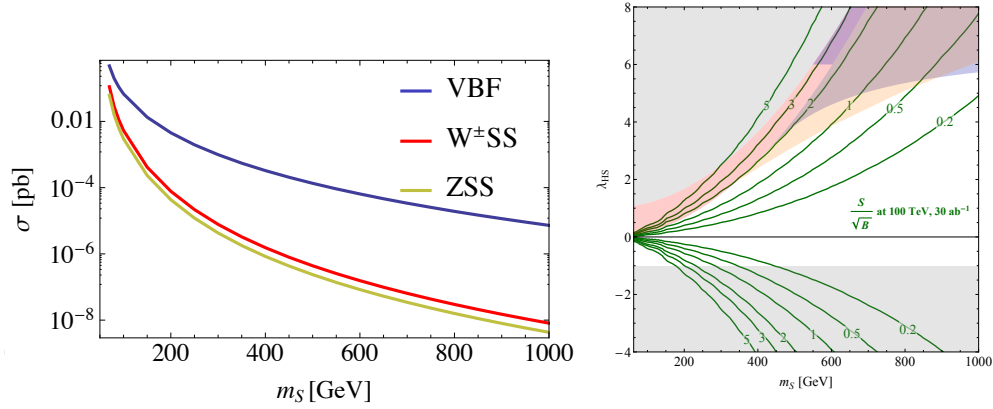


Figure 11: Left: Production rate for the VBF process at a 100 TeV collider. Right: S/\sqrt{B} of VBF process at the 100 TeV pp collider for an integrated luminosity of 30 ab^{-1} [26].

background, but this may be measured directly from the data in the familiar way, from the kinematically identical $Z \rightarrow \ell^+ \ell^-$ process, which should give a sharp handle on the systematics. In the part of parameter space giving the one-step transition, the direct production of SS is swamped by the $Z \rightarrow \nu \bar{\nu}$ background. However, this is exactly the case in which we expect an $O(1)$ deviation to the Higgs cubic coupling, as shown in the left panel of Fig. 12. We see that even pushing to the limit of $\langle h \rangle / T_c \sim 0.6$, we must have a deviation in the triple Higgs coupling of at least 20%, which is visible at a 100 TeV collider.

We conclude that, even in this very worst case scenario, a 100 TeV pp collider allows us to probe the physics giving us a first-order phase transition. Needless to say, even small modifications from this worst-case scenario can make detection much easier. For instance, if the Z_2 symmetry is broken by an even tiny amount so that $a > 10^{-10}$, then S will decay as $S \rightarrow HH$ inside the detector. Direct S production will be much easier to see, giving a spectacular signal $pp \rightarrow SS \rightarrow HHHH$. This should allow a 100 TeV pp collider to cover the allowed range of m_S up to 1 TeV. While a detailed study is left for future work, an estimate of the reach for producing 100 events is shown in Fig. 13. Note that, while at fixed mass the cross section at 100 TeV is at least ~ 100 times larger than at the LHC, the mass reach is ~ 2.5 times greater, compared to the typical factor of ~ 5 we are accustomed to. This is because both the production and decay vertices of the off-shell Higgs are

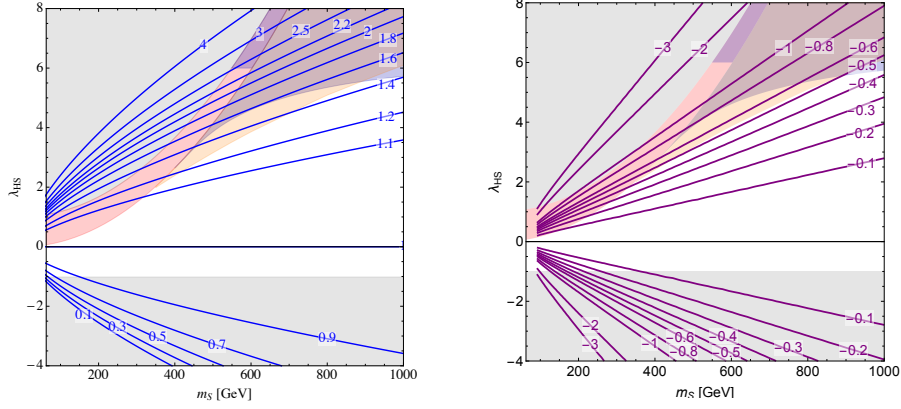


Figure 12: Left: Shift in triple Higgs coupling in the Z_2 singlet model. Right: Percentage shift in the $e^+e^- \rightarrow ZH$ cross section, which is directly proportional to δZ_H .

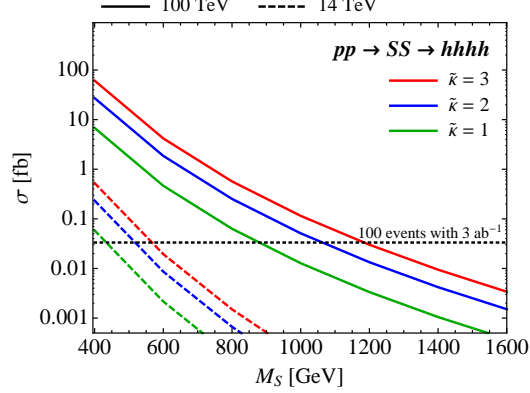


Figure 13: Rate of process $pp \rightarrow SS \rightarrow HHHH$ at the LHC and an 100 TeV pp collider.

suppressed by factors of (v/E) at high energies, and the cross-section scales as v^4/E^6 rather than the usual $1/E^2$. These suppressions would be absent with more physical Higgses in the final state. It would be interesting to see whether such final states with large Higgs multiplicity can be seen at a 100 TeV pp collider.

We have seen in our simple examples something we expect to hold more generally for models that drive a first-order phase transition: there should be large signals at a 100 TeV collider, either through the direct production of

new states, or via an $O(1)$ deviation in the cubic Higgs self-coupling. Probing the electroweak transition does not need a 10^3 TeV pp collider; 100 TeV pp collisions are just right to robustly probe this physics.

3. Naturalness of the Electroweak Scale

The notion of naturalness, as introduced by Ken Wilson and Gerard 't Hooft in the late 1970's, is deeply connected to our understanding of the structure of effective field theory, strongly supported by analogies with condensed matter physics. Naturalness has been the dominant force driving our thinking about physics beyond the Standard Model for the past four decades, suggesting a rich spectrum of new physics at the weak scale.

However, there have also been reasons to question this doctrine throughout this period. Most glaringly, naturalness seems to fail spectacularly for the cosmological constant, though this involves mysteries of gravity and cosmology that may not be relevant for particle physics. Within particle physics, there have also been a number of counter-indications to naturalness, from the lack of indirect signals that might have been induced by new physics at the weak scale in low energy flavor and CP violation to the absence of new states going back to LEP and the Tevatron. The absence of new physics at LHC Run 1 continues this trend and appears to put naturalness under further pressure. Settling the ultimate fate of naturalness is perhaps the most profound theoretical question of our time that is amenable to experimental tests, and will largely dictate the future development of fundamental physics in this century.

We will begin with a brief overview of this set of ideas to put them in context and elucidate their importance. As we will see, on top of what we learn from LHC14, a 100 TeV collider is certain to play a decisive role in unraveling this physics.

3.1. On the Mass of the Higgs Boson

A good place to begin a discussion of naturalness is to look at the name of the Standard Model itself, which has an apt moniker, since it gives us a *model*, rather than a deeper *theory*, for electroweak symmetry breaking. This is most obviously seen by the fact that m_h^2 is a parameter of the theory; its value is not predicted, but must be taken from experiment. Even the most qualitative property of the Higgs potential — the negative sign of m_h^2 , leading to symmetry breaking — is not predicted. The SM allows us to *model*

and *parametrize* symmetry breaking, but it certainly does not give us a real *understanding* of its origin.

The famous quadratically divergent radiative corrections to the Higgs mass, dominantly from the top quark at 1-loop

$$\delta m_h^2 \sim \frac{3y_t^2}{8\pi^2} \Lambda_{\text{UV}}^2 \sim (0.3 \Lambda_{\text{UV}})^2 \quad (19)$$

is one indication of the fact that the Higgs mass parameter cannot be computed in the SM. Note that purely within the SM, nothing obliges us to think about “UV sensitivity”, “fine-tuning” or the “hierarchy problem” — since there is no computation of the Higgs mass in the SM, these notions are not precise. There is no well-defined computation of the Higgs mass to complain about “fine-tuning”, and there is certainly no theoretical inconsistency with taking the value of the weak scale from experiment. However, we will immediately confront these issues in attempting to find a real theory where we can actually *calculate* the Higgs mass.

What should such a theory look like? Especially over the past century, we have been driven by the reductionist paradigm, in which explanations for mysterious low energy phenomena are to be found in a more fundamental high energy theory. Following this tradition, there should be an UV scale Λ_h , above which we find the theory in which the Higgs mass becomes calculable. Unlike the SM, in this theory there will be a concrete formula for the Higgs mass, which should take the form

$$m_h^2 = a\Lambda_h^2 + b\frac{3\lambda_t^2}{8\pi^2}\Lambda_h^2 + \dots \quad (20)$$

with a, b, \dots dimensionless constants that are calculable in the theory.

There are then two possibilities: (A) $\Lambda_h \sim m_h$ with a, b, \dots of $O(1)$. In this case we say the physics is “natural”, and the physics at the scale Λ_h gives a complete account of electroweak symmetry breaking. Otherwise (B) $\Lambda_h \gg m_h$; this entails an extreme correlation between deep UV and IR physics. While such a correlation is a logical possibility, we have never seen anything like this before, anywhere else in physics.

Let us illustrate these possibilities with a concrete example, to show how the naturalness issues are forced upon us as soon as we find a theory in which the Higgs mass becomes calculable. Let us start with a toy model of a light scalar Φ with mass m_Φ^2 , which is in the adjoint representation of an $SU(2)$ gauge group with coupling g . This mass m_Φ^2 is incalculable just as the Higgs

mass is incalculable in the SM. But there is a simple UV completion where it can be unambiguously computed: consider a five-dimensional gauge theory with gauge coupling g_5 compactified on a circle of radius R . The gauge field is obviously massless in the UV, but at energies much smaller than $1/R$ and at tree-level, we have a massless four-dimensional gauge field with coupling $g^2 = g_5^2/R$, and a massless scalar in the adjoint representation. The scalar will pick up a mass at 1-loop, and the radiative corrections in the full theory are calculable:

$$m_\Phi^2 = \frac{3\zeta(3)}{\pi^2} \times \frac{3g_4^2}{4\pi^2} \times \frac{1}{R^2}. \quad (21)$$

Now, $1/R$ also sets the mass of the new states in the theory — the Kaluza-Klein excitation of the gauge boson. Thus, in this UV completion where the scalar mass becomes calculable, it is simply impossible to keep the scalar much lighter than the new KK states: there must be “new physics” in the model, parametrically at exactly the energy scale predicted from the classic back-of-the-envelope estimates following from the quadratic divergence in the low energy theory, cut-off at the scale $1/R$.

Simple variants of this model, where the extra dimension is an interval, are used in various guises of realistic theories for the Higgs as a pseudo-Nambu-Goldstone boson, interpreted in either extra-dimensional or four-dimensional terms. Of course the realistic theories include a top quark with an adjustable Yukawa coupling y_t . Once again, the Higgs mass can be completely calculated as

$$m_h^2 = [a(g^2/8\pi^2) - b(3y_t^2/8\pi^2)] \times 1/R^2, \quad (22)$$

where $a, b > 0$ are calculable, and the masses of the KK excitations of the gauge fields and fermions are also calculable multiples of $1/R$. Even the signs of these contributions are fixed; remarkably, one can compute that when the top Yukawa is large, electroweak symmetry is necessarily broken. This beautifully explains one qualitative fact — why is electroweak symmetry broken? — as a consequence of the seemingly unrelated qualitative fact that the top Yukawa is larger than gauge couplings.

Note that, in this UV completion, it is possible to make the Higgs much lighter than the KK excitation set by $1/R$, but only if the couplings g and y_t happen to be adjusted to be extremely close to a particular ratio. Absent supersymmetry, there is nothing relating these couplings, and indeed they vary with scale, so the needed coincidence at just the right scale would be completely accidental. To say this more vividly, if as theorists we wished to

simulate this model on a computer, we would have to very delicately move around in parameter space in order to make the scalar very light, giving an operational meaning to “fine-tuning” in a concrete calculation. Of course it is logically possible that if such a model were realized in nature, the couplings would happen to be arranged in just a way as to yield a light scalar. But then the explanation for the generation of the weak scale would be deferred to the higher-energy theory, which predicts the seemingly random choices of y_t and g needed to make this happen, entailing the extreme correlation between UV and IR physics we alluded to.

If we discount the possibility of extreme UV/IR correlations, this logic predicts that light scalars with non-derivative gauge and Yukawa interactions can never be “lonely” — they must always be within a weak-coupling loop factor of heavier new physics. This conclusion has been borne out in all examples we have seen in Nature to date. For instance the charged pion is just an electromagnetic loop factor lighter than the ρ meson. And we have a nice understanding for the striking absence of non-derivatively coupled scalars in condensed matter systems.

There is of course a famous example from condensed matter physics, however, where we do see light scalars, and where the word “fine-tuning” has direct experimental relevance. This is the Landau-Ginzburg description of a system very close to a second-order phase transition, say in a metal. Within the reductionist paradigm, one might naively imagine that the detailed microphysics of the material would provide the explanation for the lightness of the scalar field in this system. However, this assumption is incorrect, because, in this system, it is not the physics of the material itself that controls the mass of the scalar, but rather the fact that the system is coupled to an external heat bath with a temperature that can be dialed by an experimentalist. In this example, the experimentalist must “fine-tune” the temperature to make the scalar very light. However, from the point of view of an observer within the material itself, the reductionist paradigm breaks down, since the explanation for macroscopic phenomena is not simply given by specifying the microphysics of the system, but also crucially depends on the presence of a “multiverse” outside it. The much discussed picture of an enormous landscape of vacua, populated by eternal inflation, is one possible analog of this scenario for particle physics.

Given the experimental observation of a light elementary Higgs scalar, we are confronted with three qualitatively different possibilities: if the reductionist paradigm continues to be the correct guide—as it has been for

centuries—we must either discover physics to make the Higgs mass natural, or we must allow a possibility we have never seen before, that of an extreme correlation between the physics of the deep UV and IR. Alternatively, we must acknowledge the failure of the reductionist paradigm altogether, and admit that the explanation for the lightness of the Higgs is not to be found in our microphysics. *Any* of these three conclusions would have monumental implications for the future of fundamental physics.

3.2. Natural Theories and the Tests at the 100 TeV pp Collider

The most conservative possibility is that naturalness holds. Even this conservative possibility involves major extensions to our picture of physics. Only a few theoretical possibilities for solving the hierarchy problem have emerged over the past few decades, starting from the early proposals of technicolor [27, 28] and variants with the Higgs as a pseudo-Goldstone boson [29, 30, 31]; the supersymmetric SM [32]; and the proposals of large [33] and warped [34] extra dimensions, the latter of which are in fact holographically dual [35] to versions of technicolor and composite Higgs models. Technicolor was in many ways the most conservative, simplest and most beautiful of these possibilities, but has been conclusively ruled out by the discovery of a light Higgs. Supersymmetry remains the best studied and most attractive possibility, especially given the striking success of supersymmetric gauge-coupling unification, precise at the percent level [32, 36].

However, with the continued absence of both indirect and direct evidence for new physics to date, it is also conceivable that we will come to see that naturalness is not a good guide to TeV scale physics, as it has perhaps already been seen to fail for the cosmological constant. The two alternatives to naturalness represent much more radical paradigm changes; it is true that without further positive clues from experiment we will not know which of the options is correct, but being forced into either of these directions would be an epochal shift, akin to the move away from the aether triggered by the null result of aether-drift experiments over a century ago.

Given the magnitude of the stakes involved, it is vital to get a clear verdict on naturalness from experiment, and a 100 TeV collider will be necessary to make this happen. To this end, we will be maximally conservative, and with a few exceptions will operate under the assumption that LHC14 sees no evidence for physics beyond the SM. Let us recall why this would be surprising from the usual perspective of naturalness. Consider the top-loop

contribution to the Higgs mass

$$\delta m_h^2 \sim (3\lambda_t^2/8\pi^2)\Lambda_{UV}^2 \sim (0.3\Lambda_{UV})^2. \quad (23)$$

Asking for δm_h^2 not to be larger than m_h^2 tells us that there must be some new state lighter than ~ 400 GeV, related to the top by some new symmetry that allows it to cancel the UV sensitivity. The couplings of this new state must be determined by λ_t ; in addition, since the “3” in the expression for m_h^2 arises from the number of colors, the simplest possibility is that the “top-partner” is also colored. This is what happens in most well-studied natural theories. The top partner in supersymmetric theories is the (colored) stop, while the fermionic top-partners in Little Higgs and composite Higgs theories are also colored. This is the way in which naturalness predicted a bonanza of new physics for the LHC, since *colored* 400 GeV particles could have been copiously produced even at LHC8.

Of course this has not happened, and if the LHC continues to see nothing but the Higgs, any colored top partners will be pushed to being heavier than ~ 1 TeV, indicating a level of fine-tuning of typically a few percent for electroweak symmetry breaking. As a canonical example, consider the case of supersymmetric theories, in which stop loops generate a contribution to the Higgs mass, logarithmically enhanced starting from the scale Λ_X where supersymmetry (SUSY) breaking is first communicated to the minimal supersymmetric SM (MSSM). This leads to a rough measure for the degree of fine-tuning, Δ^{-1} [37], as

$$\Delta^{-1} \sim 10^{-2} \left(\frac{1 \text{ TeV}}{m_{\tilde{t}}} \right)^2 \left(\frac{5}{\log(\Lambda_X/\text{TeV})} \right), \quad (24)$$

and $m_{\tilde{t}} \sim 1$ TeV is tuned at the percent level.

The question then becomes, how bad is percent-level tuning? Certainly it seems qualitatively different than the 10^{-30} levels of tuning usually discussed if Λ_{UV} is close to the Planck scale. Furthermore, we have seen accidents of order a few percent elsewhere in physics, ranging from the surprisingly large nucleon-nucleon scattering length, to the accident that the moon can nearly perfectly eclipse the sun! We do not tend to associate deep significance with these accidents at this level. Thus, while a failure to discover colored top-partners would be a major blow to the most popular natural theories of the weak scale, given the relative ubiquity of percent-level tunings in physics, it would perhaps not be a completely decisive blow. It is logically possible

that the LHC might have just been a bit unlucky, and the new states could be a little heavier, slightly beyond its reach. The 100 TeV collider will then play a critical role to settle the issue. If the new particles are indeed “just around the corner”, then 100 TeV collisions will produce them in enormous abundance. On the other hand, the 100 TeV reach for colored top partners will be able to discover them up to masses about 5 times higher than the LHC, pushing the fine-tuning to the $10^{-3} - 10^{-4}$ level, a degree we have never seen before anywhere else in particle physics.

But one may justifiably ask: if the LHC sees nothing beyond the Higgs, does not this already kill the possibility of a completely natural theory for electroweak symmetry breaking? Would the only role of future colliders be to further clinch an already clear case? The answer to this question is an emphatic “No”. What is true is that in all the natural theories for the weak scale developed over twenty years ago, we might have already expected to see new colored top-partners at the LHC. However this does not prove that the idea of naturalness itself is wrong, only that the particular natural scenarios theorists invented through the 1990’s are not realized in Nature. As we have emphasized already, this is not a new surprise delivered to us by the LHC, since there were already indirect indications that these theories could not be fully natural going back to the absence of indirect signals for new physics in low energy experiments and at LEP. Motivated by these considerations, in the mid 2000’s new classes of natural theories of EWSB were developed, where the top partners are not colored, but are charged under mirror gauge groups. These includes variations on the “Twin Higgs” [38], which realizes this idea with the Higgs as a pseudo-Goldstone boson, and “Folded SUSY” [39], where supersymmetry is ultimately responsible for the naturally light scalars. These “color-neutral natural” theories are much less constrained by LHC searches, and indeed, *completely natural* regions of parameter space for these theories could be completely missed by the LHC. They provide an existence proof that the idea of naturalness can survive the LHC era entirely unscathed, and there may be further ideas along these lines that have yet to be unearthed. Thus no new physics at the LHC will not decide the fate of naturalness, the final verdict awaits pp collisions at 100 TeV.

We begin with a discussion of more conventional theories with colored top partners, and, for concreteness, we will discuss these issues mostly in the context of supersymmetric theories; a detailed investigation of other scenarios is left for future studies.

If the MSSM is just mildly tuned we should be able to produce all the

superpartners at a 100 TeV collider. The reach for stops in particular will be critical; any gain in mass reach relative to the LHC is squared in the measure of tuning. Another interesting possibility is minimally split supersymmetry [40, 41, 42, 43, 44, 45]. Here, the spectrum has one-loop splitting between the gauginos (and perhaps higgsinos) compared to the scalars, as typically happens in the simplest models of SUSY breaking. The gauginos/higgsinos are at the TeV scale for reasons of dark matter, while the scalars have a mass $m_S \sim 10^2 - 10^3$ TeV, entailing a “meso-tuning” of $O(10^{-6})$ for electroweak symmetry breaking, while preserving gauge coupling unification and removing all flavor and CP difficulties of the MSSM. The usual SUSY boundary conditions for the Higgs quartic coupling is then easily compatible with the observed $m_h = 125$ GeV for heavy scalar masses in this range. Interestingly, this tells us that the gluino cannot get heavier than ~ 20 TeV, quite apart from any constraints on the electroweak part of the spectrum from dark matter. So for mini-split SUSY, a 100 TeV collider should be able to produce the gluino, and the electroweak-inos as well.

At a 100 TeV pp collider, we expect an significant improvement of the mass reach of the superpartners beyond those of the LHC. This is a direct consequence of the large increase of the production rates, shown in Fig. 14, resulting from the increase of the center of mass energy.

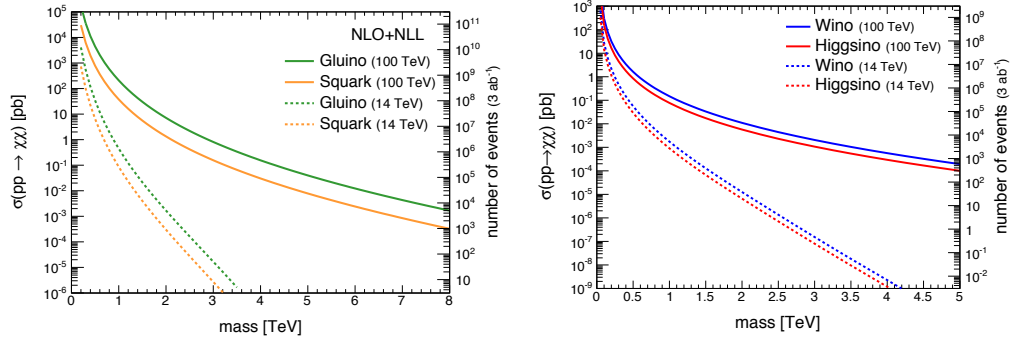


Figure 14: Pair production of SUSY particles for (a) gluino and squark, and (b) higgsino and wino at 14 and 100 TeV, see also Ref. [46]

An investigation of the SUSY reach for 100 TeV colliders was carried out in [47] for a number simplified models of SUSY production and decay, covering most of the qualitatively interesting scenarios. We summarize their

findings here, referring to [47] for details of their analysis.

The first simplified model is that of gluino pair production, with gluinos decaying to neutralino + light flavors, $\tilde{g} \rightarrow q\bar{q}\tilde{\chi}^0$. This process will dominate if the squarks are heavier than the gluino, and is particularly well-motivated in the case of split SUSY. The reach is obviously most powerful if there is a large splitting between the gluino and neutralino masses, and is shown in the left panel of Fig. 15, comparing also to a 33 TeV pp collider and to the LHC at 14 TeV. The 100 TeV discovery reach goes up to $m_{\tilde{g}} = 11$ TeV, about 5 times the reach of LHC at 14 TeV. If the gluino and neutralino are

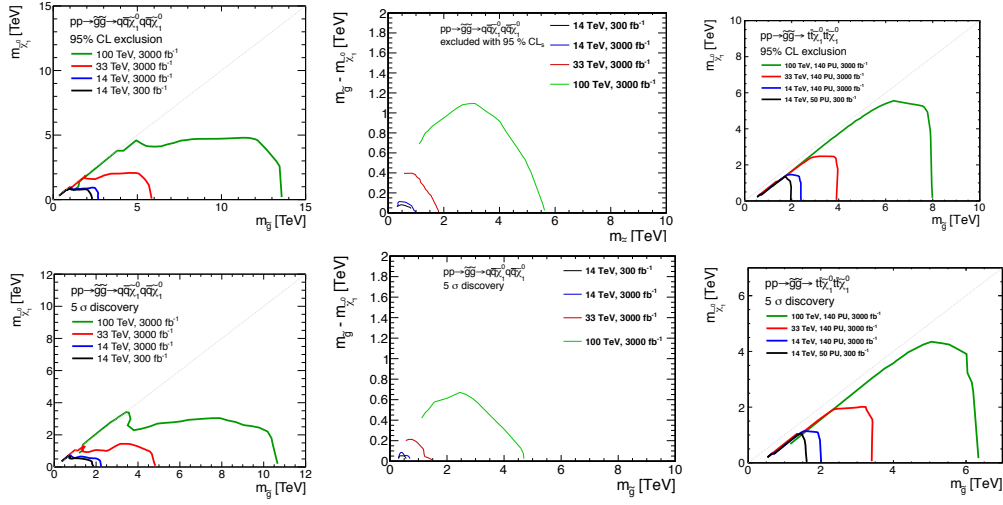


Figure 15: Reach for gluino at 100 TeV pp collider for separated (left column) and compressed (center column) spectrum. The reach for gluino decay dominated by $\tilde{g} \rightarrow t\bar{t}\tilde{\chi}_0^0$ is shown in the right column. The 95% exclusion reach and 5 σ discovery potential are shown in the top and bottom rows, respectively.

instead relatively degenerate, the decay products will be too soft to see and one will have to rely on the emission of initial or final state radiation to tag the events. The mass reach still goes up to an impressive ~ 5 TeV in this case, as shown in the middle panel of Fig. 15. It is also interesting to consider that gluinos decay dominantly to top quarks and the neutralino: $\tilde{g} \rightarrow t\bar{t}\tilde{\chi}_0^0$. This can easily arise from top-down theories, since stops are typically driven to be lighter than the first two generations of squarks, under RG evolution, and is again particularly well-motivated in split SUSY. In this case, the reach is shown in the right panel of Fig. 15.

A much more challenging case with smallest production cross-section for colored particles, is the pair production of the first-two generation squarks, which are taken to be degenerate, followed by the decay to the lightest neutralino as $\tilde{q} \rightarrow q\tilde{\chi}^0$. The gluino is taken to be much heavier than the scalars. It is not easy to realize such a scenario from a top-down point of view, since a heavy gluino will quickly drag up the squarks under RG evolution. The reach for the case with the squarks significantly split from the neutralino is shown in the left panel of Fig. 16, while the case with more nearly degenerate squarks and neutralino is shown in the middle panel of Fig. 16.

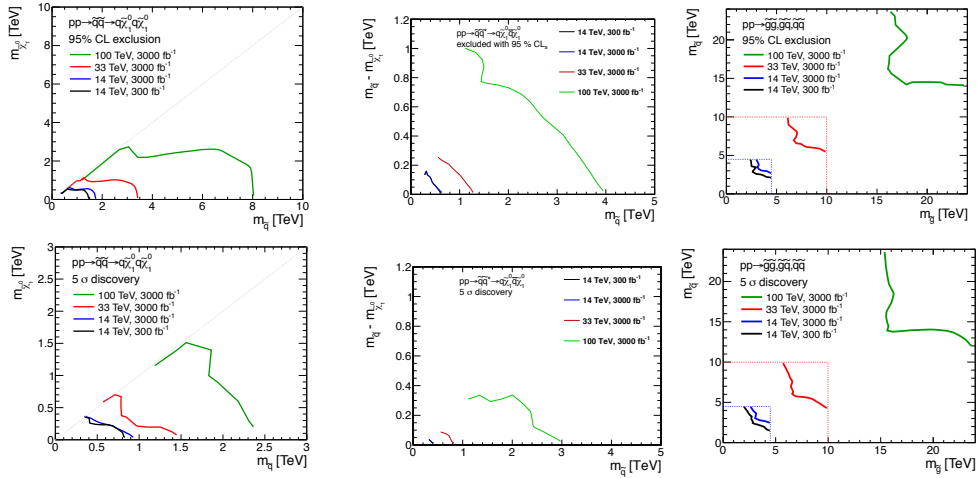


Figure 16: Reach of squark with separated (left column) and compressed (middle column) spectrum. The reach in the case of gluino and squark with comparable mass is shown in the right column. The 95% exclusion reach and 5σ discovery potential are shown in the top and bottom rows, respectively.

Since the production cross-section is so small, it is difficult to see the signal over the background, so the improvement of the discovery reach at a 100 TeV collider relative to the LHC is not as pronounced here as in the previous examples. Nonetheless the exclusion reach is very impressive in both cases, again representing a factor ~ 5 improvement relative to the LHC.

The final simplified model is closest to a “typical” supersymmetric spectrum, where both the gluino and first-two generation squarks are light enough to be produced at a 100 TeV collider, via pair-production of $\tilde{g}\tilde{g}$, $\tilde{q}\tilde{q}$, and also associated production $\tilde{g}\tilde{q}$. If the gluino is heavier than the squark, it decays to the squark and neutralino as $\tilde{g} \rightarrow \tilde{q}\tilde{\chi}^0$, while if the gluino is lighter than

the squark, it decays to light flavors + neutralino as $\tilde{g} \rightarrow q\bar{q}\tilde{\chi}^0$, and similarly for the squark, which decays as $\tilde{q} \rightarrow q\tilde{g}$ if heavier than the gluino, and $\tilde{q} \rightarrow q\tilde{\chi}^0$ if lighter than the gluino. The neutralino is taken to be much lighter than the gluinos and squarks. The 100 TeV reach is shown in right panel of Fig. 16. This shows an amazing reach up to $m_{\tilde{g}}, m_{\tilde{q}} \sim 15$ TeV.

We now turn to the 100 TeV reach for stops, which will probe masses up to the 5 – 10 TeV range, pushing the fine-tuning measure to the 10^{-4} level. It is interesting to note that with moderately large $\tan\beta$, stops in the 5 – 10 TeV range can also be easily responsible for pushing the Higgs mass up to 125 GeV. To be conservative, we look at the simplified model with all particles but the stop and the lightest neutralino decoupled, considering the QCD production of $t\bar{t}^*$, followed by $\tilde{t} \rightarrow t\tilde{\chi}^0$. The same search is of course being carried out at the LHC, but an interesting novelty arises in 100 TeV collisions. With heavy enough stops, the top quarks produced in the decay are so highly boosted, that it becomes more difficult to identify the individual top decay products as compared to the LHC. Thus simply scaling up the LHC analysis to 100 TeV is suboptimal, and identifying highly boosted tops becomes an important challenge for 100 TeV detectors. It is possible to use a strategy less dependent on unknown detector response: when a highly boosted top decays hadronically, the muons from the resulting b decays will be collinear with the top jet; thus requiring a lepton inside a jet can be used to effectively tag the boosted tops [48, 49].

The 100 TeV reach for direct stop production is shown in the left panel of Fig. 17, for the two usual cases of a separated and compressed spectrum: The gain from using the boosted top tagging can be clearly seen. Stops can be discovered (excluded) up to ~ 6 (8) TeV with this method.

Similar reaches are possible for non-supersymmetric theories. For instance, in composite Higgs models, we have fermionic top partners T' . Depending on whether we have the “T-parity” analog of R-parity, these may decay to tops + missing energy, or via $T' \rightarrow tZ, T' \rightarrow th$. A dedicated projection to the reach for these models at 100 TeV collider has not yet been done. However, in the case with T-parity, the signal is very similar to that of the stop. Therefore, we can use the stop reach and get a rough estimate of the reach of T' by matching the production rate and mass splitting. The result is shown in the right panel of Fig. 17.

All of this discussion has assumed no signals for new physics at the LHC. In the more optimistic case that LHC *does* produce, e.g., superpartners, the need to proceed to the higher energies of 100 TeV collisions is even more

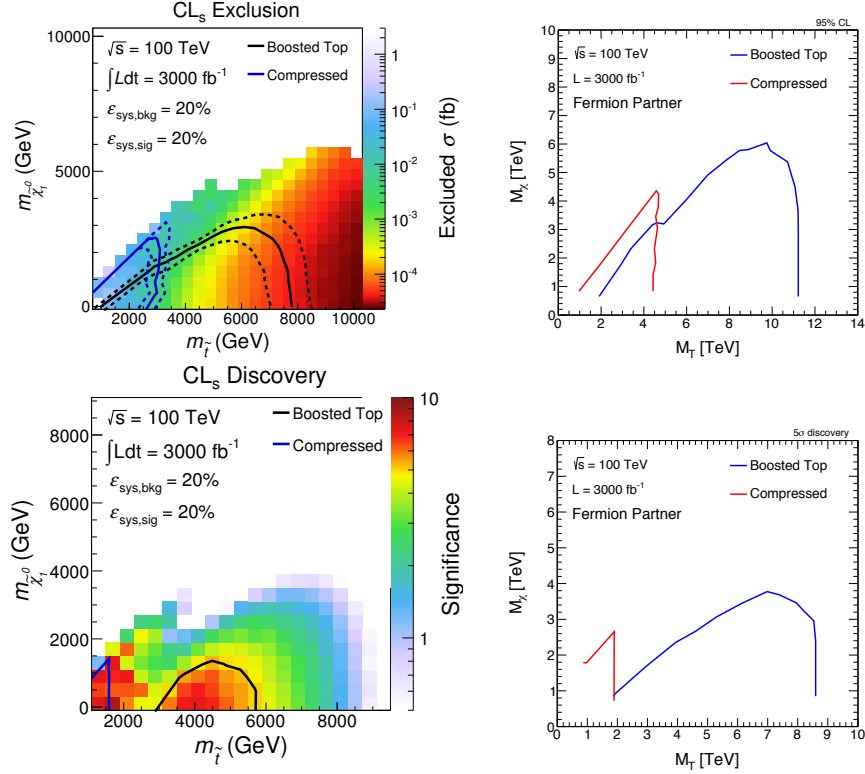


Figure 17: Reach for stops (left column) and fermionic top partners (right column) at a 100 TeV pp collider.

urgent, for two obvious reasons. First, given that we have not seen any superpartners at LHC8, while LHC14 could be powerful enough to discover them, it is unlikely to produce them in high enough numbers for the more detailed study needed to ascertain what the particles are trying to tell us about TeV scale physics. As a simple example, consider a gluino with mass of 1.5 TeV, just at the LHC Run 1 limit. Roughly 10^4 of these particles will be produced through the LHC14 program, certainly enough to be able to claim a discovery, but not much else. The careful examination of its properties, necessary to even hope for a zeroth order claim that supersymmetry has been discovered, will need a 100 TeV collider, producing $\sim 10^7 - 10^8$ gluinos of the same mass. Second, the fact that we have not seen any new physics at LHC Run 1 also makes it very unlikely that the entire spectrum of new states will be produced at LHC14. Consider the example of “natural SUSY”, where the

stops and gluinos are light. At the same time, the first two generations should plausibly be heavier than ~ 5 TeV, enough to eliminate their dangerous contribution to electric dipole moments. But they cannot get too heavy, as they induce a logarithmically enhanced negative mass for the (light) third-generation squarks [50, 51], and so cannot be pushed higher than at most ~ 30 TeV. Finding these heavier scalars will be critical for a zeroth-order understanding of the spectrum, which entangles the physics of flavor and supersymmetry breaking in a fascinating way. While these scalars are well outside the reach of the LHC, they will be accessible to a 100 TeV collider. The most powerful production channel is the associated production of the gluino and first-two generation squarks, as shown in Fig. 18. The reach for

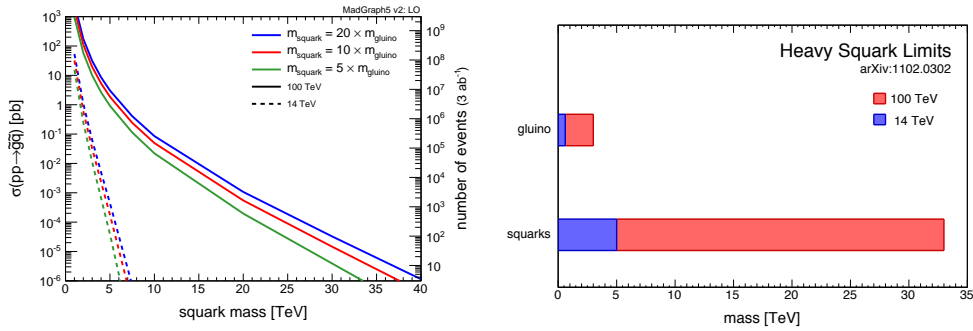


Figure 18: Cross section (left panel) and reach (right panel) for a heavy squark produced in association with a light gluino at the 100 TeV pp collider.

squarks goes up to an incredible ~ 35 TeV, covering the entire range of masses for the first-two generation scalars of natural SUSY.

The supersymmetric implementations of neutral naturalness do not generate this large oblique Higgs operator at tree-level. In the simplest cases, the top partners are scalars like the stop, but charged under a mirror $SU(3)$, with six states in total. We can parametrize all the interesting possibilities from the bottom up: we imagine that there is some number N_ϕ of new scalars ϕ_I , and a quartic interaction with the Higgs

$$\frac{1}{2}c_\phi(\phi_I\phi_I)h^\dagger h. \quad (25)$$

Some or all of the global symmetries acting on the ϕ_I might be gauged, either by the SM electroweak interactions, or mirror interactions. There must be

an underlying symmetry that relates c_ϕ to the top Yukawa coupling, so as to guarantee

$$c_\phi \times N = \lambda_t^2 \times 6 \rightarrow c_\phi = \frac{6\lambda_t^2}{N}. \quad (26)$$

It is also possible to directly produce the ϕ_I at the 100 TeV pp collider, again the discussion is analogous to the production of the S singlets in our discussion of the electroweak phase transition. There, the phase-transition requirement forced S to be light enough and sufficiently strongly coupled, for the ϕ_I naturalness plays the same role. For simplicity the ϕ_I are taken to be degenerate. The signals is just as we had before, vector-boson fusion production of the ϕ_I , which escape the detector (or decay invisibly). The 100 TeV reach is shown in Fig. 19, along with the effective $|c_\phi|$ associated with the case $N = 6$.

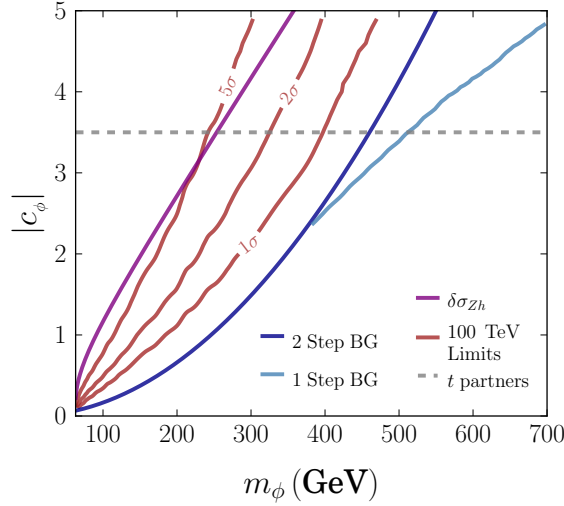


Figure 19: The reach for neutral top partners produced through Higgs portal at a 100 TeV pp collider [52]. The lines labelled as “1 Step BG” and “2 Step BG” correspond to two scenarios in which the Higgs portal interactions with top partners can make the electroweak physics transition first order. The horizontal dashed line denotes the coupling needed to cancel top quadratic divergence.

Thus a 100 TeV collider has a reach for 5σ discovery up to ~ 250 GeV, and a 2σ exclusion up to ~ 350 GeV, pushing to the boundaries of the natural

region.

In all examples studied so far, we have seen that a 100 TeV collider can decisively settle whether fully natural theories of electroweak symmetry breaking are realized in Nature. While we have avoided using the language of “no-lose theorems” to discuss the physics opportunities of this machine, it is possible that more detailed future studies can actually formulate a sensible “no-lose theorem” for probing naturalness at a 100 TeV collider; preliminary examples along these lines can be found in the recent works [53].

4. Dark Matter

The existence of cold dark matter is one of the most direct and powerful pieces of evidence for physics beyond the Standard Model. There are a huge range of possibilities for what the dark matter might be, since for any mass we can simply adjust the number density to get the needed energy density today, with $\Omega_{DM}h^2 \sim 0.1$. Even if the new particle physics is completely specified, the main uncertainty is cosmological: what determines the abundance of the new particles in the early universe?

4.1. WIMP Dark Matter

Weakly Interacting Massive Particles (WIMPs) remain the best motivated and well-studied possibility for dark matter by giving a clear answer to this question: the dark matter particles interact with the SM and are thermalized in the early universe. Assuming a standard cosmological history, the present abundance of dark matter can be unambiguously computed once the underlying particle physics is fixed, in much the same way as the abundance of light elements is predicted in big bang nucleosynthesis.

The relic abundance of dark matter particles is set by their annihilation cross section in the early universe [54, 55, 56]

$$\Omega h^2 = 0.11 \times \left(\frac{\langle \sigma v \rangle_{\text{freeze}}}{2.2 \times 10^{-26} \text{ cm}^3/\text{s}} \right)^{-1}, \quad (27)$$

with $\sigma \propto g_{\text{eff}}^4/M_{\text{DM}}^2$. Therefore, to avoid overclosure, the limit on the dark matter mass is

$$M_{\text{DM}} < 1.8 \text{ TeV} \left(\frac{g_{\text{eff}}^2}{0.3} \right). \quad (28)$$

As has been long appreciated, it is quite remarkable that the TeV scale emerges so naturally in this way, assuming dark matter couplings comparable

in strength to the electroweak gauge interactions. This gives a strong, direct argument for new physics at the TeV scale, independent of any theoretical notions of naturalness.

Compellingly, dark matter often falls out of theories of physics beyond the SM without being put in by hand. Indeed, if the SM is augmented by new physics, not even necessarily close to the weak scale, but far beneath the GUT scale, the interactions with new states should respect baryon and lepton number to a very high degree. Since all SM particles are neutral under the discrete symmetry $(-1)^{B+L+2S}$, any new particles that are odd under this symmetry will be exactly stable. This is the reason for the ubiquitous presence of dark matter candidates in BSM physics. It is thus quite plausible that the dark matter is just one part of a more complete sector of TeV-scale physics; this has long been a canonical expectation, with the dark matter identified as e.g. the lightest neutralino in a theory with TeV-scale supersymmetry. The dominant SUSY processes at hadron colliders are of course the production of colored particles—the squarks and gluinos—which then decay, often in a long cascade of processes, to SM particles and the lightest supersymmetric particle (LSP), resulting in the well known missing energy signals at hadron colliders. This indirect production of dark matter dominates, by far, the direct production of dark matter particles through electroweak processes.

However, as emphasized in our discussion of naturalness, it is also worth preparing for the possibility of a much more sparse spectrum of new particles at the TeV scale. Indeed, if the idea of naturalness fails even slightly, the motivation for a very rich set of new states at the hundreds-of-GeV scale evaporates, while the motivation for WIMP dark matter at the TeV scale still remains. This is for instance part of the philosophy leading to models of split SUSY: in the minimal incarnation, the scalars and the second Higgs doublet of the MSSM are pushed to $\sim 10^2 - 10^3$ TeV, but the gauginos (and perhaps the higgsinos) are much lighter, protected by an R -symmetry. The scalars are not so heavy as to obviate the need for R -parity, so the LSP is still stable, and must be set at the TeV scale in order not to overclose the universe, thereby making up some or perhaps all of the dark matter.

In exploring dark matter at colliders, therefore, it is most prudent to first look for direct production of dark matter, rather than dark matter arising in the decay products of other states that may not be accessible. We will therefore explore the reach of a 100 TeV collider for the production of new states with only electroweak quantum numbers, which also certainly give the

simplest possible picture for what the dark matter could be. The simplest case of all would be a single new state: a real triplet or vector-like doublet adds the fewest possible number of degrees of freedom to the SM, and no new interactions, so the only free parameters are the particle masses. We can be slightly more general and allow for the presence of additional singlet states. Including just singlets, doublets, and triplets gives a minimal “module” for dark matter, which we will consider, described by the Lagrangian

$$\begin{aligned} \Delta L = & M_1 \tilde{B} \tilde{B} + M_2 \tilde{W} \tilde{W} + \mu \tilde{H}_u \tilde{H}_d \\ & + \sqrt{2} \kappa_1 h^\dagger \tilde{W} \tilde{H}_u + \sqrt{2} \kappa_2 h \tilde{W} \tilde{H}_d + \frac{\kappa'_1}{\sqrt{2}} h^\dagger \tilde{B} \tilde{H}_u + \frac{\kappa'_2}{\sqrt{2}} h \tilde{B} \tilde{H}_d. \end{aligned} \quad (29)$$

Since the quantum numbers are the same as binos (\tilde{B}), winos (\tilde{W}), and higgsinos ($\tilde{H}_{u,d}$) of supersymmetric theories, we will use this notation and language in referring to these states, as “charginos”, “neutralinos”, “the LSP”, and so on. Much of our analysis is, however, free of supersymmetric assumptions: supersymmetry only relates the new Yukawa couplings to the SM gauge couplings as $\kappa \sim g$ and $\kappa' \sim g'$, but this won’t play an essential role in most of our discussion.

Given this spectrum of electroweak states, we can consider two obvious limits. One of these states can be significantly lighter than the others; if it is also significantly heavier than M_Z , then the dark matter is close to being a “pure” electroweak state, so we can have a “pure wino” or “pure higgsino” (a “pure bino” has no interactions at leading order and so is not relevant to our discussion). Alternately, the lightest state can be a significant admixture of different electroweak states.

For both the higgsino and wino, the electroweak multiplet contains charged and neutral states that would be degenerate in the absence of electroweak symmetry breaking; however, a small splitting between these states arises after electroweak symmetry is broken. There is a calculable radiative correction to the splitting, that can be thought of as the difference between the “electrostatic” energy of the photon and Z fields for the charged and neutral components, giving

$$\Delta m \sim \alpha_{\text{EM}} M_Z. \quad (30)$$

This irreducible splitting is $\Delta m = 166$ MeV for winos [57] and $\Delta m = 355$ MeV for higgsinos [58]. Further splittings can also arise from UV effects, by integrating out heavier particles (for instance the heavier electroweak states).

For the higgsino, the leading dimension-5 operator generates a splitting between the charged and neutral states as

$$(\kappa^2/M)(h^\dagger \tilde{H}_u)(h \tilde{H}_d) \Rightarrow \Delta m \sim M_Z^2/M. \quad (31)$$

For the wino, the leading dimension-5 operator does not split the two states, and we have to go to the dimension-7 operator, which generates an even smaller splitting as

$$(\kappa^4/M^3)(h^\dagger \tilde{W} h)^2 \Rightarrow \Delta m \sim M_Z^4/M^3. \quad (32)$$

Comparing the radiative and UV splittings, if there is just an $\mathcal{O}(1)$ difference in mass between the wino and the rest of the states, the UV splittings become much smaller than the radiative splitting.

Since the wino and higgsino have sizable electroweak gauge interactions, they annihilate very efficiently; this is why their masses have to be pushed to 1 – 3 TeV to be thermal relics. By contrast, the bino has no electroweak couplings at all. Therefore it is interesting to consider the dark matter as having a sizable admixture of bino together with wino or higgsino. Since the mixing between the states arises through electroweak symmetry breaking, in the limit where the masses M_1, M_2, μ are large compared to M_Z , the mixing angles will be very small, suppressed by powers of (M_Z/M) , unless some pair of the diagonal masses are close to degenerate, as with the case of “well-tempered” neutralinos [43]. For the case where the bino/higgsino are nearly degenerate, the mixing terms are parametrically $\sim M_Z$, and this also sets the size of the splitting between the charged and neutral states, which can be typically $\sim 20 - 50$ GeV. For the bino/wino case, the mixing terms are parametrically $\sim M_Z^2/M$, and we expect somewhat smaller splittings.

Thermal relic pure winos and higgsinos must have a mass of 3.1 TeV and 1.1 TeV respectively to account for all the dark matter. At smaller masses they can still account for a significant fraction of the dark matter, for instance a 2 TeV wino can account for half of the dark matter. Mixed dark matter can be lighter but masses around ~ 500 GeV are typical.

The direct detection of pure winos and higgsinos is extremely challenging. The leading dark matter-nucleon interaction arises at 1-loop, and gives rise to a tiny spin-independent cross section [59, 60]

$$\sigma_{\text{SI}} \begin{cases} \approx 10^{-47} \text{ cm}^2 & \text{for winos,} \\ \leq 10^{-48} \text{ cm}^2 & \text{for higgsinos.} \end{cases}$$

These cross sections are just at the border of the irreducible neutrino scattering floor for direct detection experiments, and with TeV masses the rates are also too low to be seen in any of the planned experiments. Mixed dark matter is a much more promising target for direct detection, and is already tested by current limits, but a sizable region of parameter space continues to be viable.

We can also consider indirect detection of high energy particles resulting from dark matter annihilation near the center of our galaxy. Of course predictions for indirect detection rates are fraught with astrophysical uncertainties, and it is difficult to get robust limits in this way. Nonetheless, pure winos are constrained in an interesting way, since their annihilation cross section has a significant Sommerfeld enhancement [61]. The absence of any signals in the HESS experiment for high energy gamma photons from the galactic center [62] sets limits on the fraction of dark matter a wino of a given mass can comprise. A 3 TeV wino making up all the dark matter is excluded for a standard NFW dark matter distribution, though it is allowed for more “cored” profiles [63, 64, 65, 66, 67]. The current limits are summarized in Fig. 20.

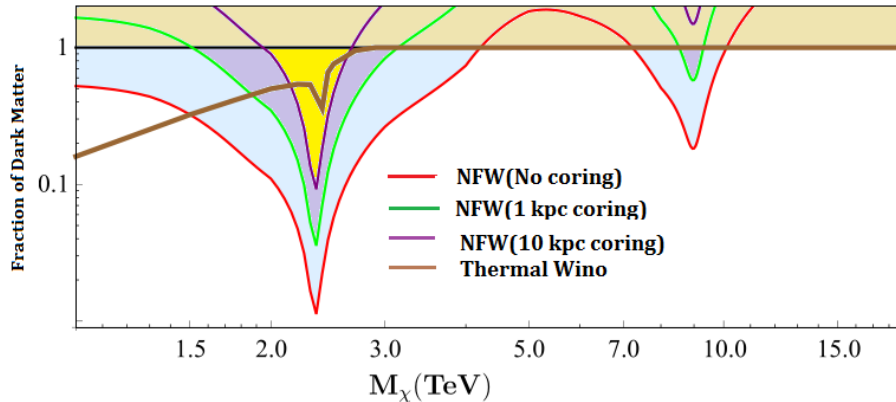


Figure 20: Exclusion plot for an NFW profile with the wino making up only some fraction of the dark matter [67].

Future indirect detection experiments, such as CTA, could move the wino bounds down to 1 TeV, subject to the same astrophysical uncertainties. But we can see that thermal relic winos making up an $\mathcal{O}(1)$ fraction of dark matter are certainly still consistent. For both pure higgsinos as well as mixed dark

matter, the annihilation is not significantly Sommerfeld enhanced, and there are no interesting limits from indirect detection,

It is striking that the very simplest models of dark matter—pure winos and higgsinos—could be completely inaccessible to direct detection experiments, while astrophysical uncertainties make it hard to interpret indirect detection limits. We are left with directly producing the dark matter at accelerators. Relic winos and higgsinos forming a significant component of dark matter, which have masses in few TeV scale, are hopelessly out of reach for direct production at the LHC, which has an ultimate reach up to $\sim 300 - 400$ GeV for pure wino and ~ 200 GeV for pure higgsino production. Moreover, only a fraction of the parameter space for mixed dark matter is accessible to direct production at the LHC.

4.2. WIMP Dark Matter at the 100 TeV pp Collider

As we will see shortly, however, the huge increase of rate at 100 TeV will allow a much larger range of the relevant parameter space to be explored. The most basic process we will first consider is dark matter pair production. Since the dark matter escapes the detector without leaving a trace, we need to look for additional hard radiation of SM particles from the process—quarks or gluons, photons, W/Z ’s, and Higgses. Of these, the “monojet” channel where a quark or gluon is radiated typically gives the best sensitivity. For mixed states we can have a mass splitting $m_{\chi^\pm} - m_{\chi^0} \sim 20 - 50$ GeV between the chargino and neutralino states. In this case, in addition to a hard jet, it is possible to search for low p_T leptons resulting from a chargino or neutralino, which decay to the LSP and leptons. We call this the soft lepton channel. On the other hand, when the lightest state is pure, the radiative mass splitting is tiny and the decay length is long, leaving a striking signature of a high- p_T charged track abruptly ending when the chargino decays to the LSP and very soft, likely undetected, SM particles. We include this disappearing-tracks search in our considerations as well.

Monojets: Our first analysis looks for a single hard jet produced in association with a pair of dark matter particles, the classic monojet plus missing energy search. Monojet searches for dark matter and large extra dimensions have been carried out both at the Tevatron and the LHC. The backgrounds for this channel include SM processes with a hard jet and neutrinos. Processes with leptons also comprise part of the background because leptons can fail to be tagged if they are outside the detector acceptance, not isolated, or

too soft. This is a very challenging channel with the uncertainty dominated by the background’s systematics.

Soft Leptons: of mixed dark matter, where we have splittings of $\Delta m \sim 20 - 50$ GeV, the heavier states can also be pair produced, and decay to the dark matter via off-shell gauge bosons, which then decay hadronically or into low- p_T leptons. The hadronic decays are difficult to extricate from the noisy hadronic environment, but it is possible to tag the soft leptons. This is different from the standard multilepton searches where there are both more and harder leptons. It has been noted that triggering on a hard jet, as in the monojet search, is advantageous in a soft lepton search.

Disappearing Tracks: The third analysis leverages the near degeneracy of charginos and the LSP for pure electroweak states. Due to the tiny mass splitting, the dominant decay $\chi^\pm \rightarrow \pi^\pm \chi^0$ can have a long enough lifetime – $c\tau \sim 6$ cm for winos – to leave a track in the inner detector. This chargino track disappears within the inner detector when it decays to a neutralino and soft pion. This is a promising search channel with no obvious physics background. Searches can also be done when the charginos have a shorter or longer lifetime and look for displaced vertices and stable charged massive particles, respectively.

Multi-Lepton Finally when one moves away from the compressed region of parameter space, any mass splitting between the next-to-lightest supersymmetric particle (NLSP) and the LSP can be generated and it is most natural to cast limits in the NLSP-LSP mass plane. For these searches, there are multiple leptons from the NLSP-to-LSP decays whose energies scale with the NLSP-LSP splitting. They are energetic enough that the hard jet required for triggering in the soft lepton search is unnecessary. These searches can be categorized by the particular combination of leptons for which they are looking. Here we consider the three lepton (3ℓ), the opposite-sign dilepton (OSDL), and the same-sign di-lepton (SSDL) signatures, although the 3ℓ is always the most sensitive. Multi-lepton searches are based on the observation that while the signal has large mass splittings and heavy invisible particles, the background has neither and so has harder back-to-back jets, with leptons, than the signal.

As the optimal search strategy strongly depends on the splittings, it would be interesting to look at the overlap and transitions between the approaches discussed above. This more detailed analysis deserves focus in future studies.

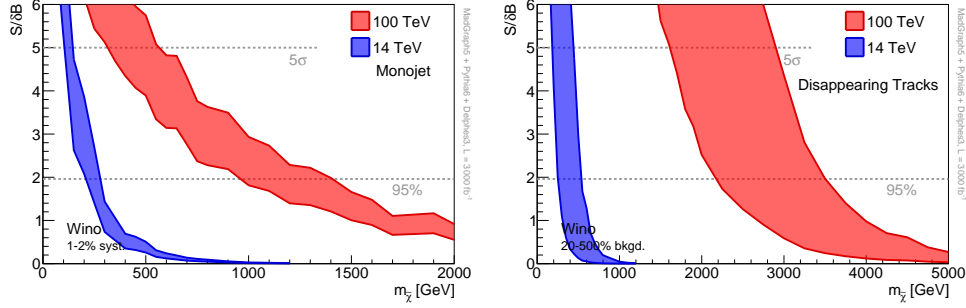


Figure 21: Left: The mass reach for the pure wino in the monojet channel with $\mathcal{L} = 3 \text{ ab}^{-1}$ for the 14 TeV LHC (blue) and at 100 TeV (red). The bands are generated by varying the background systematics between 1 – 2% and the signal systematic uncertainty is set to 10% [68]. Right: The mass reach in the pure wino scenario in the disappearing track channel with $\mathcal{L} = 3 \text{ ab}^{-1}$ for the 14 TeV LHC (blue) and at 100 TeV (red). The bands are generated by varying the background normalization between 20 – 500% [68].

4.2.1. Pure Wino

The pure wino has nearly degenerate charged and neutral states. The pair production of the chargino proceeds via Drell-Yan production through an s -channel Z/γ^* , while the production of a chargino/neutralino proceeds through an s -channel W . The charginos decay to the neutralino and a soft pion.

The mass reach in the monojet channel for a pure wino is shown in Fig. 21. The dominant uncertainty in the reach comes from the systematics of the background, which is varied between 1 – 2%, generating the bands in the plot. Naively scaling by total event rates the systematics from current ATLAS studies [69] (see Ref. [70] for the CMS study) would yield 0.5% for 3 ab^{-1} , but this is clearly overly optimistic. Choosing the systematic error $\sim 1 - 2\%$ as we have done may also be optimistic, but it sets a reasonable benchmark, and underscores that minimizing these systematics should be a crucial factor taken into account in the design of the 100 TeV detectors. Given the same integrated luminosity, the monojet search increases the reach relative to the LHC by nearly a factor of 5, as shown in the left panel of Fig. 21.

Due to the tiny mass splitting $\Delta m = 166 \text{ MeV}$ between the chargino and the neutralino, the decay lifetime can be long. The resulting disappearing track is a very distinctive signal in this case. Since the dominant background for a disappearing track search would be mis-measured low- p_T tracks, we

cannot accurately predict the backgrounds in the not-yet-designed 100 TeV detectors. Nonetheless, we can calibrate against the present ATLAS searches for disappearing tracks [71] (see Ref. [72] for the CMS search). For example, we can require that $d^{\text{track}} > 30$ cm, with tens of signal events passing all cuts. The resulting mass reach is shown in the right panel of Fig. 21, and the bands result from varying the background normalization upwards and downwards by a factor of 5. The disappearing tracks could be extremely powerful, with the potential to both convincingly rule out, or discover, thermal wino dark matter.

4.2.2. Pure Higgsino

Pure higgsinos are also produced through s -channel Z 's and W 's, and the analysis is similar to the pure wino case. The reach of the monojet search is shown in the left panel of Fig. 22. As for winos, the search improves by nearly

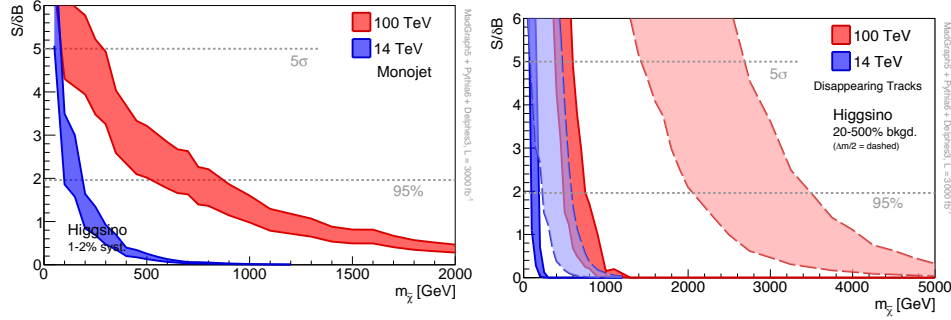


Figure 22: Left: The mass reach for the pure higgsino in the monojet channel with $\mathcal{L} = 3 \text{ ab}^{-1}$ for the 14 TeV LHC (blue) and at 100 TeV (red). The bands are generated by varying the background systematics between 1 – 2% and the signal systematic uncertainty is set to 10% [68]. Right: The mass reach for the pure higgsino in the disappearing-track channel with $\mathcal{L} = 3 \text{ ab}^{-1}$ for the 14 TeV LHC (blue) and at 100 TeV (red). The bands are generated by varying the background normalization between 20 – 500% [68].

a factor of 5 in mass relative to the LHC; the weaker reach relative to winos is due to the smaller production cross section. With optimistic systematics, higgsinos can be excluded up to 800 GeV.

We can next look at the disappearing-tracks search. If the splitting between the states is purely radiative, the lifetime for the higgsino is much shorter than for the wino, since the lifetime scales as $\tau \propto \Delta m^{-5}$. This

makes the disappearing-track search less effective than the monojet search for higgsinos; the reach is shown in the right panel (solid contour) of Fig. 22.

However it is worth recalling that unlike for the pure wino, the splitting for the higgsino states can more easily be affected by the presence of heavier states, which can generate $\Delta m \sim M_Z^2/M$ — which could be comparable to the radiative splittings if the heavier electroweak states are near $M \sim 5$ TeV. If these splittings are comparable, resulting in a reduction of the width by a factor of 2, the decay length increases by a factor of $\sim 10 - 30$, and the higgsino reach becomes comparable to that for winos as shown in the right panel (dashed contour) of Fig. 22. This could be extremely exciting — not only discovering the higgsino, but giving direct evidence for new multi-TeV electroweak states needed to reduce the higgsino mass-splittings in order to account for its anomalously long lifetime.

4.2.3. Mixed dark matter

In the case of mixed dark matter we can expect mass splittings of tens of GeV, and so the search is dominated by looking for the soft leptons from chargino decays via off-shell W 's and Z 's. This will give us a more powerful reach than with the monojet alone. On the other hand, with these splittings the decays are prompt and we lose the advantages of the disappearing-tracks search. We will focus on two representative examples, with mass splittings of 20 GeV. The first is a bino/higgsino mixture and the second is a bino/wino(/higgsino) mixture, obtained by dialing all three of $|M_1|$, $|M_2|$, $|\mu|$ close to each other. The mass reach for these scenarios is shown in Fig. 23.

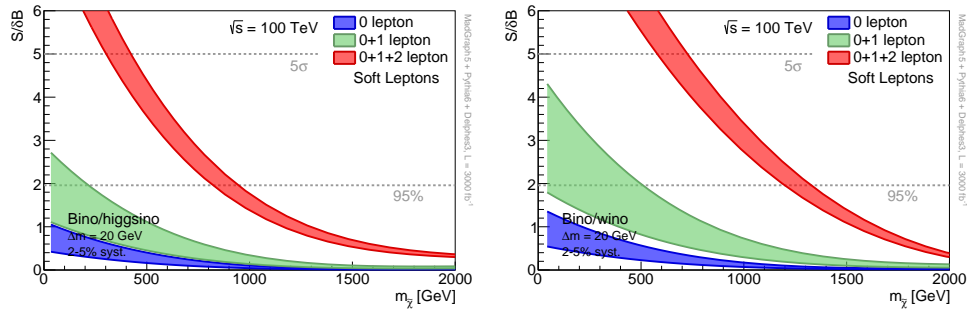


Figure 23: The mass reach in the mixed bino/higgsino ($\Delta = 20$ GeV) scenario in the soft lepton channel at 100 TeV with $\mathcal{L} = 3 \text{ ab}^{-1}$, looking for 0 leptons (blue), 0 or 1 leptons (green), and 0, 1, or 2 leptons (red). The bands are generated by varying the background systematics between 2 – 5% and the signal systematic uncertainty is set to 10% [68].

Note that in all cases the tagging of soft leptons is very important to maximize the mass reach. The 2-lepton bin is most important: while the 0 and 1 lepton bin backgrounds are dominated by single gauge-bosons, the 2-lepton backgrounds are controlled by diboson production with a much smaller cross section. We find exclusions reaching up to ~ 1 TeV masses, and discovery up to several hundred GeV.

4.2.4. Electroweak cascades

We have so far focused on the most difficult cases for dark matter production, where the lightest electroweak states are produced and their decays contain only soft particles. The mass reach can be considerably higher if there is an electroweak spectrum with sizable splittings. If the heavier states can be produced, they will decay to the dark matter state, emitting hard W 's, Z 's, and Higgses. This leads to the familiar signals of multi-lepton plus missing energy, and searches for events with leptons, such as 4 leptons, opposite- and same-sign di-leptons. A study of the reach at 100 TeV for electroweak cascades has recently been carried out in [73], for four representative cases of the production of NLSP's decaying to the LSP:

- Wino NLSP and higgsino LSP ($M_1 \gg M_2 > \mu$)
- Higgsino NLSP and wino LSP ($M_1 \gg \mu > M_2$)
- Higgsino NLSP and bino LSP ($M_2 \gg \mu > M_1$)
- Wino NLSP and bino LSP ($\mu \gg M_2 > M_1$)

The heaviest electroweakino in all cases is fixed to 5 TeV. Bino NLSP's have too small a production cross section to be relevant, so they are never considered as the NLSP.

The reach for the final case, with wino NLSP and bino LSP, depends importantly on the wino branching ratios: for very heavy higgsinos, the decay $\tilde{W} \rightarrow \tilde{B}h$ dominates, but it is also possible to have sizable branching ratios for emitting W 's, Z 's as well. The 100 TeV reach for these four scenarios is summarized in Fig. 24.

This represents a major gain over the reach of the LHC. Most notably, the entire interesting range for higgsino masses can be probed in this way, provided the wino is lighter than 3 TeV, and not too degenerate with the higgsino.

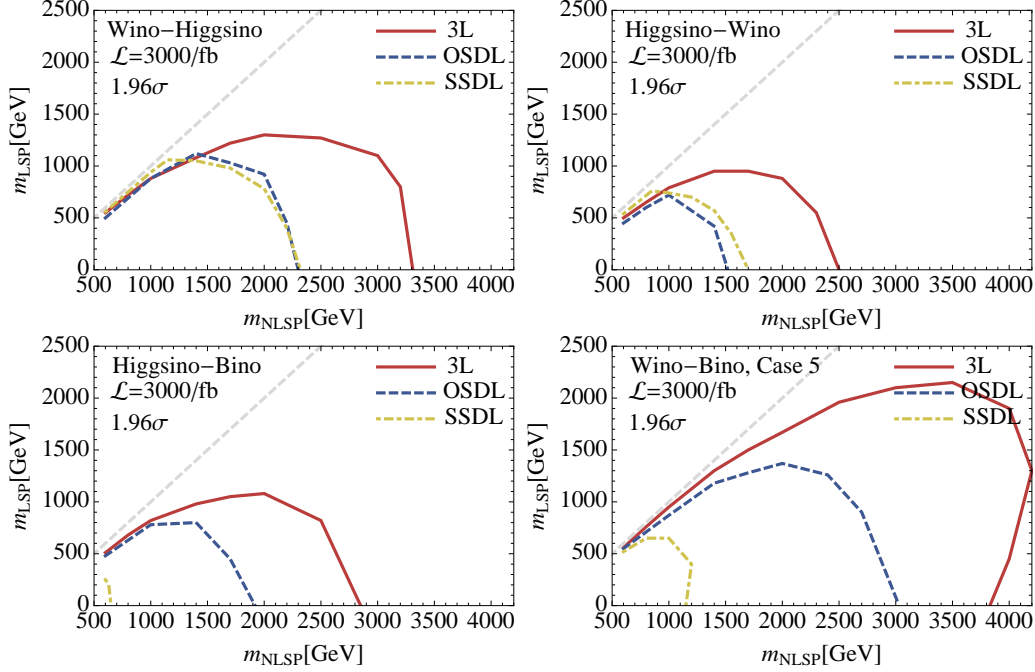


Figure 24: 95 % CL limits for wino-NLSP and higgsino-LSP (top left), higgsino-NLSP and wino-LSP (top right), higgsino-NLSP and bino LSP (bottom left) and wino-NLSP and bino-LSP (bottom right) [73].

4.2.5. Co-annihilation with Bino dark matter

So far we have only briefly considered the case of bino dark matter. Due to its small couplings, the bino does not annihilate efficiently as it freezes out, and typically overcloses the universe unless it is extremely light. Bino dark matter can be made viable in a supersymmetric context, if there are other superpartners with a mass nearly degenerate with it. Their presence can enhance the bino annihilation rate and give the correct relic abundance for heavier bino masses. If the co-annihilators are gluinos, stops, or squarks, the bino masses giving the correct relic abundance are in the multi TeV region, ~ 7 TeV for gluino co-annihilation, and ~ 2 TeV for stop or squark co-annihilation. Since the colored states are very close in mass to the bino, they can have large production rates at a 100 TeV collider. They will then decay to the bino and soft SM particles, resulting in the monojet signal. Due to the colored production, however, these rates will be much higher than with electroweakino monojet signals.

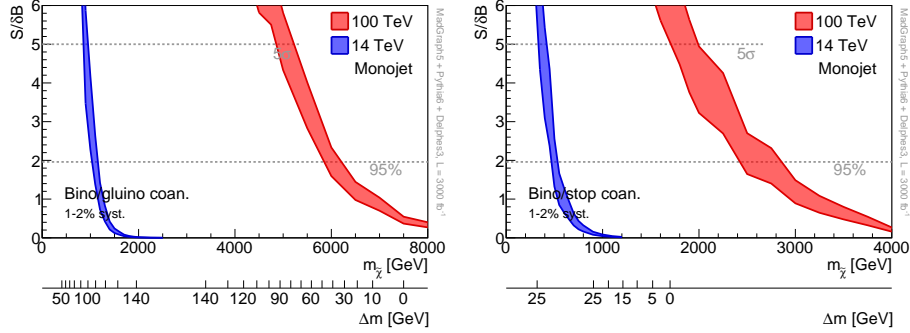


Figure 25: Left: The mass reach in the gluino coannihilation scenario in the monojet channel with $\mathcal{L} = 3 \text{ ab}^{-1}$ for the 14 TeV LHC (blue) and at 100 TeV (red). The bands are generated by varying the background systematics between 1–2% and the signal systematic uncertainty is set to 10%. The lower x -axis displays the gluino-bino mass splitting Δm for a given bino mass that is required to saturate the relic density [74, 75]. A tick is placed every 10 GeV with the exception of the consecutive $\Delta m = 140$ GeV ticks [68]. Right: The mass reach in the stop coannihilation scenario in the monojet channel with $\mathcal{L} = 3 \text{ fb}^{-1}$ for the 14 TeV LHC (blue) and at 100 TeV (red). The bands are generated by varying the background systematics between 1–2% and the signal systematic uncertainty is set to 10%. The lower x -axis displays the stop-bino mass splitting Δm for a given bino mass that is required to satisfy the relic density [75]. A tick is placed every 5 GeV with the exception of the consecutive $\Delta m = 25$ GeV ticks [68].

The reach at 100 TeV for gluino and stop annihilations, as obtained by [68], is shown in the left and right panels of Figs. 25, respectively. For gluino co-annihilation the gluino-bino splitting required to get the right relic abundance is shown on the bottom x -axis of the left panel of Fig. 25. We see that a 100 TeV collider covers most of this parameter space. It is also worth recalling, that we have presented the most conservative search as we assume that whatever accompanies the LSP from the co-annihilator decay is undetectable. In practice, the searches can be augmented by looking for the possibly soft decay products.

The mass splitting for the correct relic abundance in stop co-annihilation has also been computed and is displayed on the bottom x -axis of the right panel of Fig. 25. Here, a 100 TeV collider can make strong statements about this spectrum. Both exclusion and discovery are possible even in the degenerate stop-bino limit.

Summary

A broad summary of the dark matter reaches we have discussed is given in Fig. 26. While the LHC can look for electroweak states up to a few hundred

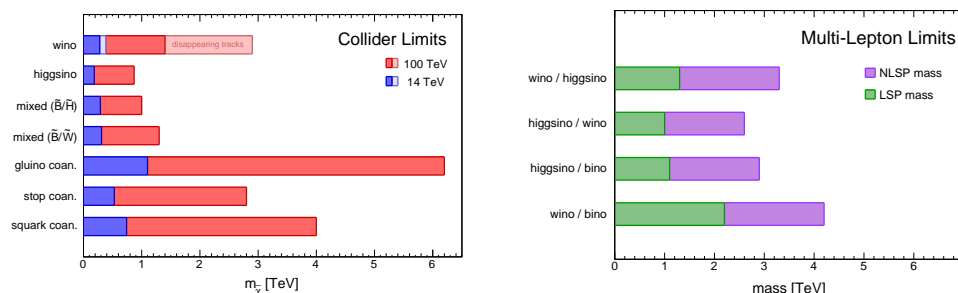


Figure 26: Summary of colliders' reach for neutralino dark matter [68] and in electroweakino cascades [73].

GeV, it will not probe the TeV mass range that is most natural for thermally saturating dark matter. By contrast, the jump to 100 TeV extends the LSP mass reach from the LHC roughly by a factor of 5, and thus allows us to go deep into this territory, with a great potential to discover WIMP dark matter.

5. Other New Physics Searches

As the next exploration facility at the energy frontier, the 100 TeV pp collider will lead us into completely new territory. In this section, we present the projections of a variety of new particles and phenomena that could show up. We show the cross section increases with respect to the LHC, and provide qualitative estimates of the observability in experiments at 100 TeV.

5.1. New Color Resonances

A high energy hadron collider is a QCD machine. Any new states with QCD interactions would be copiously produced via quark and gluon partons. Some such exotic states have been systematically classified in Ref. [76], and the LHC experiments have been actively searching for them [77, 78]. The non-observation at the LHC sets bounds on their mass, bounds that will extend well beyond a few TeV after the LHC energy increase to 13 – 14 TeV. This mass reach would be substantially extended by the 100 TeV collider.

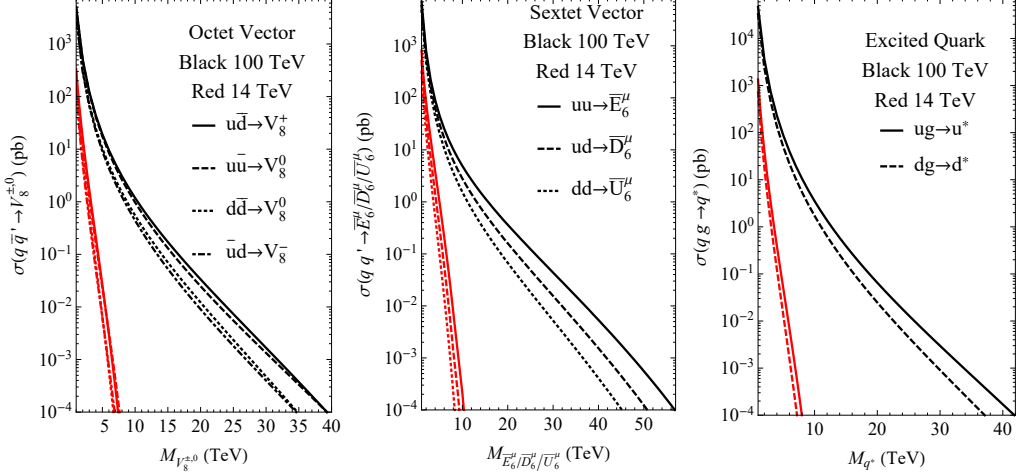


Figure 27: Production cross sections for exotic colored resonances at 14 TeV and 100 TeV, for (a) charged and neutral color-octet vector states, (b) fractionally charged color-sextet vector states (di-quark-like), and (c) spin-3/2 excited quark states.

We show the total production cross sections for a representative set of new resonant states in Fig. 27, considering (a) charged or neutral color-octet vector states (techni- ρ -like), (b) fractionally charged color-sextet vector states (di-quark-like), and (c) excited quark states (spin-3/2 for quark compositeness). We see that the cross sections² for these exotic colored states' production can reach 0.1–1 fb for the mass range of 25–55 TeV, a rate which is expected to be easily observable given the planned several ab^{-1} . The color-octet vector states in Fig. 27(a) are produced via the Drell-Yan process from $q\bar{q}$ annihilation, which results in a lower reach by about 10 TeV than the colored di-quark states in Fig. 27(b), produced through the valence quark pair annihilation. In contrast, the excited quark states in Fig. 27(c) are produced via dimension-5 operators³ with qg fusion and have a sensitivity reach in between the above two. The exotic colored states will typically decay back to two jets, leading to di-jet resonances. One will thus expect that the 100 TeV experiments would be able to significantly extend the LHC coverage of the exotic colored states, reach a broad mass range beyond about 25–55 TeV.

²There is a model-dependent dimensionless coupling constant for each of the couplings. We have set it to be unity for illustration [76].

³We set the cutoff scale to be equal to the resonance mass for simplicity [76].

5.2. New Gauge Bosons and Vector Resonances

One of the most striking signals would be the new electroweak gauge boson resonant production with the subsequent decay to leptonic final states — the typical Drell-Yan mechanism. New charged W' and neutral Z' gauge bosons exist in many theories with gauge extensions beyond the SM. We illustrate the typical cross sections for W' and Z' production for various well-motivated models [79, 80] in Fig. 28 at both 14 and 100 TeV. As expected, the LHC may be able to uncover a W' , Z' signal up to a mass of about 5 TeV with a cross section of the order 0.1 fb. At 100 TeV, one will extend the mass reach to about 25 TeV for a $(B - L)$ Z' (the smallest in rate), and to about 35 TeV for a left-right symmetric model W' (the largest in rate). Somewhere in between, a sequential SM Z' may be observable to about 30 TeV. Similarly, the production rate of a color-singlet ρ -like vector state in the minimal version of composite Higgs models is shown in Fig. 29. The production rate is roughly comparable to that of the $(B - L)$ Z' .

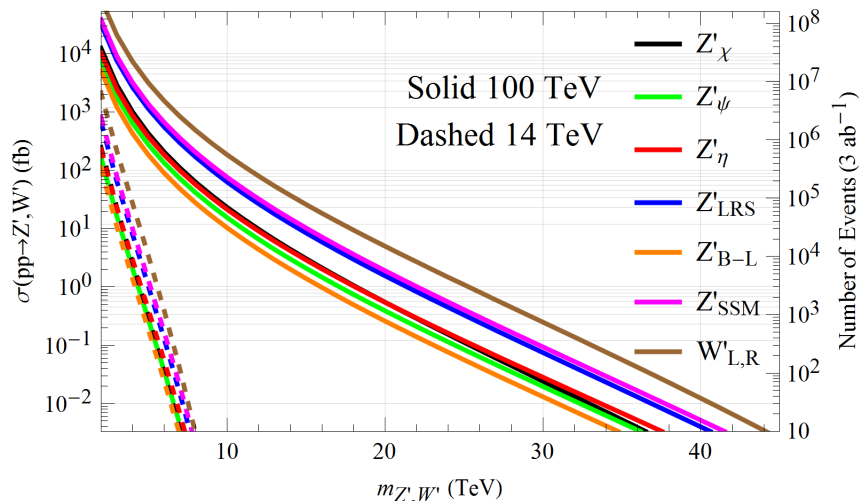


Figure 28: Production cross section of new heavy electroweak gauge bosons W' and Z' in various models [79, 80] at 14 and 100 TeV.

5.3. Heavy Higgs Bosons in Doublet and Triplet Models

Many theories beyond the SM need the extension of the Higgs sector, resulting in the prediction of new Higgs bosons, some of the commonly considered examples are denoted as H^0 , A^0 , H^\pm , and $H^{\pm\pm}$. Searching for the

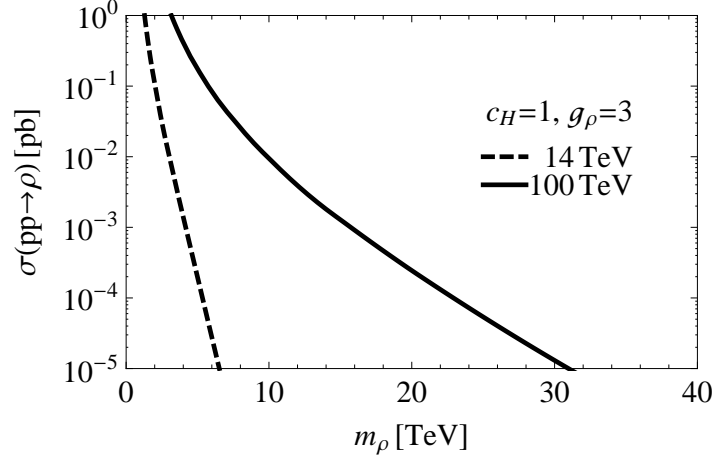


Figure 29: Production cross section of color-singlet vector resonances ρ at 14 and 100 TeV.

heavy Higgs bosons will be extremely important from the point of view of both understanding the full electroweak sector, and exploring the naturalness paradigm. Indeed, the mere existence of additional Higgs bosons at the TeV scale would unambiguously reveal new principles in the construction of the EW sector, and presenting new challenges in comprehending the naturalness problem with multiple scalars. However, it would be very challenging to discover those states at the LHC because of the rather small production cross section and the large SM backgrounds to their decay products in the final state, perhaps limited to a mass scale around 1 TeV [81, 82]. It is thus expected that the significant increase of the CM energy to 100 TeV would allow us to extend the coverage for heavy Higgs boson searches.

The leading production channels for heavy Higgs bosons are the single Higgs boson associated with heavy quarks (b and t). Figure 30 shows the total cross section for H^0 (A^0) and H^\pm processes. The calculations include $gg \rightarrow t\bar{t}H^0$, $t\bar{t}H^\pm$ and $gt \rightarrow tH^0$, $gb \rightarrow tH^\pm$ and with proper treatment for the collinear subtraction of the massive quark partons in the ACOT scheme [84, 83], for $\tan\beta = 10$. We see the orders of magnitude increase of the cross section going from 14 TeV to 100 TeV, and the relative enhancement becomes more substantial at higher masses. The typical experimental signatures of the heavy Higgs doublet are the decays of the Higgs bosons to heavy fermions $H^\pm \rightarrow tb$, $\tau\nu$; $H^0, A^0 \rightarrow t\bar{t}$, $b\bar{b}$, $\tau\tau$. While having to face the challenge of the highly boosted objects from the heavy Higgs decays, one can expect the

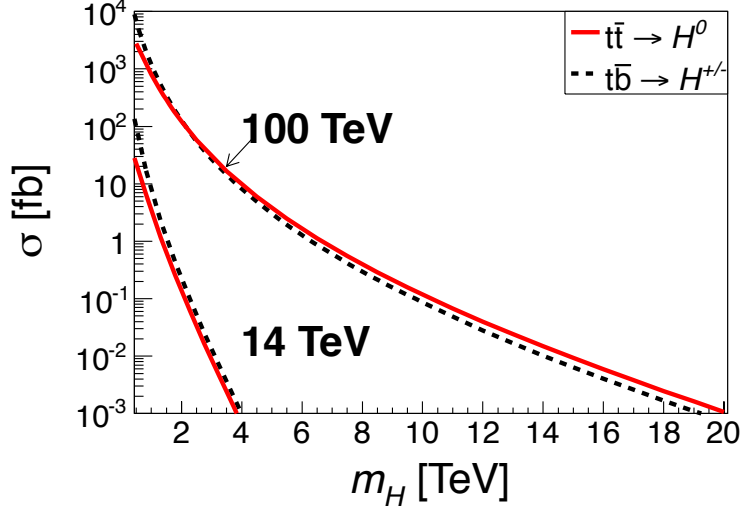


Figure 30: Single heavy Higgs boson production (H^0 , A^0 and H^\pm) associated with a heavy quark (t and b) at 14 and 100 TeV for $\tan\beta = 10$. The calculations include the gluon initial as well as the heavy quark initial processes with proper collinear subtraction [83] in the ACOT scheme.

100 TeV collider to extend the LHC coverage substantially. Depending on the value of $\tan\beta$, it is conceivable to reach the heavy Higgs mass up to 10 TeV [82] with a cross section of the order 0.1 fb at the 100 TeV collider.

It is important to note that the cross sections for Higgs pair production $\gamma^*, Z^* \rightarrow H^+H^-$, $H^{++}H^{--}$ and $W^{\pm*} \rightarrow H^\pm A^0$, $H^{++}H^-$ depend only on the electroweak gauge interactions. In contrast, the complementary processes $Z^* \rightarrow A^0 H^0$, $A^0 h^0$ and $W^{\pm*} \rightarrow H^\pm H^0$, $H^\pm h^0$, are sensitive to the model parameter of the neutral scalar mixing $\cos(\beta - \alpha)$ (here assumed to be close to 1). In Fig. 31, we present those cross sections for (a) a generic two-Higgs doublet model (2HDM), and (b) a $Y = 1$ triplet model. The results are shown for the Higgs pair production at 14 and 100 TeV, versus the heavy Higgs mass (assumed to be degenerate). Because of the heavy mass and the electroweak coupling, the pair production cross sections are lower than the heavy-quark associated production by about three orders of magnitude. It is nevertheless conceivable to reach the sensitivity of the Higgs pair production with a mass scale of about a few TeV.

The striking feature for the $Y = 1$ triplet Higgs (Φ) is the existence of

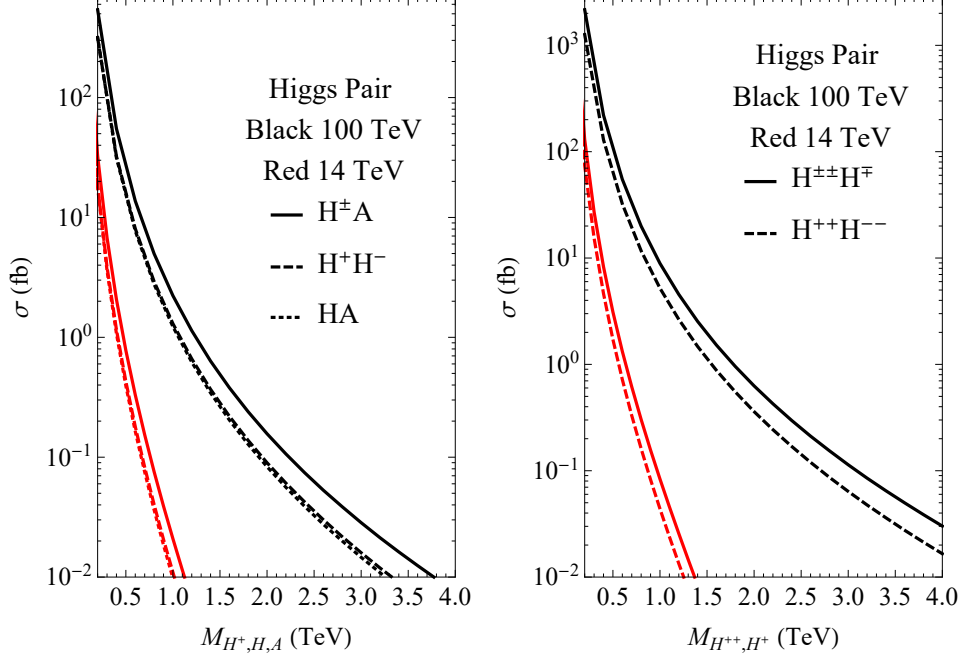


Figure 31: Pair production of heavy Higgs bosons via pure EW gauge interactions at 14 and 100 TeV.

the doubly-charged Higgs boson $H^{\pm\pm}$. The severe constraint from the SU(2) custodial symmetry bounds the triplet vev to be smaller than about a GeV. The co-existence of the couplings to the lepton doublet and to the Higgs doublet

$$-y_\nu \bar{L} \Phi i \sigma_2 L^c + \mu H^T i \sigma_2 \Phi H$$

features the Type-II seesaw mechanism for the Majorana neutrino mass generation [85, 86]. The model breaks the lepton number by two units and leads to a neutrino Majorana mass $m_\nu \sim y_\nu v' \sim y_\nu \mu v^2 / M_\Phi^2$. An interesting borderline is $v' \sim 10^{-4}$ GeV, above which $H^{\pm\pm} \rightarrow W^\pm W^\pm$ dominates, and below which $H^{\pm\pm} \rightarrow \ell_i^\pm \ell_j^\pm$ takes over. This is an extremely attractive scenario because not only it leads to very clean like-sign di-lepton signals at hadron colliders with unambiguous lepton-number violation, but also the flavor combinations of the lepton pairs $\ell_i \ell_j$ would correlate with the low-energy neutrino mixing patterns and thus could help probe the neutrino mass hierarchy [87]. The LHC will probe the doubly charged Higgs to about a TeV in

mass and a 100 TeV collider would be able to extend the coverage to about 5 TeV.

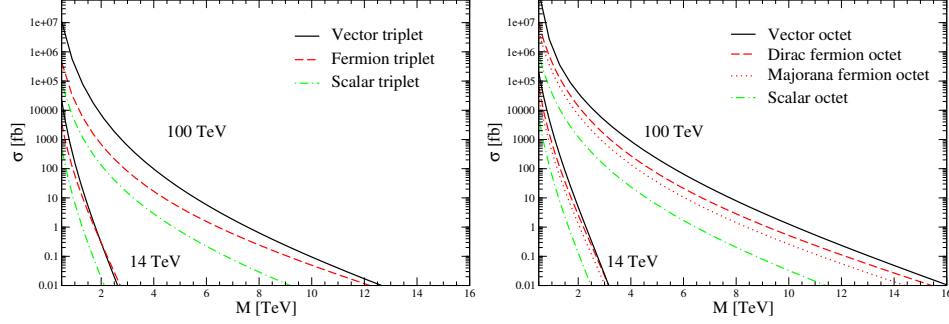


Figure 32: Pair production of new states of color-triplets (left panel) and color-octets (right panel) for spin-1 (solid curves), 1/2 (dashed), and 0 (dot-dashed) at 14 and 100 TeV.

5.4. Pair Production of Exotic Color States

Because of the large top-quark Yukawa coupling, the key ingredient for naturalness requires the existence of a top-quark partner at or below the TeV scale, most commonly a scalar partner in SUSY (stop \tilde{t}) or a fermionic partner in composite theories (T'). They are arguably the “most wanted” new particles in a natural theory of the Higgs sector, and the discovery sensitivity of them has been presented in an earlier section Sec. 3. On the other hand, there are other possible colored states that may be directly or indirectly associated with the top partners, such as the gluinos, massive gluons, and even spin-1 top partners [88]. As a QCD machine, a 100 TeV collider would certainly open up a new perspective for the discovery of the exotic colored states.

In Fig. 32, we show the typical production cross sections at 14 and 100 TeV, for color-triplets [89] (upper panel) and color-octets [90] (lower panel), for the possible states of spin-0, 1/2, and 1. Among those color-triplet states, a scalar is obviously stop-like (dot-dashed lines), a fermion is T' -like (dashed lines), and a color-triplet vector can be a spin-1 top-quark partner in an extended gauge theory [88]. Among the color-octets, a spin-0 state could be a colored Higgs or a techni-meson (dot-dashed), a fermion is obvious gluino-like, that could be either a Dirac or Majorana state (two close-by dotted lines), and a color-octet vector can be KK-gluon-like (solid line).

Once the color and spin quantum numbers are specified, the pair production cross sections are completely determined by the QCD dynamics. As expected, the production rate for the fermionic states is larger than that of the scalar by about a factor of 8, largely due to the spin-state counting and the threshold behavior. For the same reason, the vector states yield even a larger cross section. Because of the color factors, the octet states lead to a higher production cross section than that of the triplets. Given the substantial production rates as seen in Fig. 32, as long as the decay channels are not too disfavored for the signal identification, it would be quite conceivable that the mass coverage for those states would be extended to about 5, 10 and 15 TeV, respectively.

5.5. Pair Production of Heavy Leptons

To complete our overview of new particle production at the future hadron colliders, we discuss the case of new heavy leptons. While the existence of a purely sequential SM-like 4th generation is disfavored by existing data on the production of the 125 GeV Higgs boson, there are good motivations to consider new heavy leptons, both neutral and charged, for example in connection with possible models of neutrino mass generation.

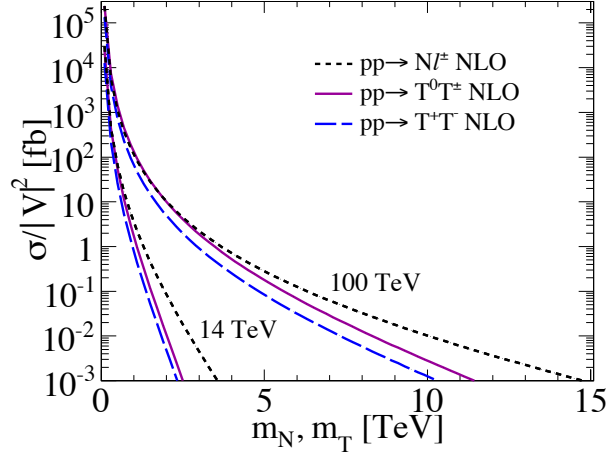


Figure 33: Pair production of new heavy leptons at 14 and 100 TeV, for an SU(2) triplet ($T^{\pm,0}$) and for a singlet state $N\ell^{\pm}$ via mixing.

We present the production cross sections for heavy lepton pairs at 14 and 100 TeV in Fig. 33. The states T^{\pm}, T^0 form an SU(2) triplet (representa-

tive in the Type-III seesaw model [91]) and the production cross sections, $q\bar{q}' \rightarrow W^* \rightarrow T^0 T^\pm$ (solid curves) and $q\bar{q} \rightarrow \gamma^*, Z^* \rightarrow T^+ T^-$ (dashed), are fully determined by their SU(2) gauge quantum numbers [92, 93], as they should be the same as any other pure SU(2) triplet production. For heavy leptons of a TeV mass, the cross section increase from 14 TeV to 100 TeV may reach a factor 4 – 5. The triplet components are nearly degenerate in mass. Although their mixing with the SM leptons may be small, the leading decay channels will still be $T^\pm \rightarrow W^\pm \nu, Z\ell^\pm, h\ell^\pm$ and $T^0 \rightarrow W^\pm \ell^\mp, Z\nu, h\nu$, leading to distinctive and reconstructable final states. It is conceivable that a 100 TeV collider will be able to extend the heavy lepton mass coverage to about 6 – 8 TeV.

For illustration, we have also included the cross section for the production of a heavy neutral lepton N (a heavy neutrino) in association with a SM charged lepton ℓ^\pm . This production rate, however, is governed by the mixing matrix V between N and the charged leptons ℓ^\pm . This may be a representative for variations of Type-I seesaw models. The dotted curves are for the $N\ell^\pm$ production normalized to $V^2 = 1$, which would correspond to the production of an SU(2) fermion doublet.

6. Benchmark Standard Model processes

Standard Model particles play multiple roles in the 100 TeV collider environment. In the context of BSM phenomena, and for most scenarios, new BSM particles eventually decay to the lighter SM states, which therefore provide the signatures for their production. BSM interactions, furthermore, can influence the production properties of SM particles, and the observation of SM final states can probe the existence of an underlying BSM dynamics. SM processes therefore provide both signatures and potential backgrounds for any exploration of BSM phenomena. SM backgrounds have an impact on BSM studies in different ways: on one side they dilute, and can hide, potential BSM signals; on the other, SM processes influence the trigger strategies, since they determine the irreducible contributions to trigger rates and may affect the ability to record data samples of interest to the BSM searches.

The observation of SM processes has also an interest per se. The huge rates available at 100 TeV allow, in principle, to push to new limits the exploration of rare phenomena (e.g. rare decays of top quarks or Higgs bosons), the precision in the determination of SM parameters, and the test of possible deviations from SM dynamics. The extremely high energy kinematical

configurations probe the shortest distances, and provide an independent sensitivity to such deviations.

Finally, SM processes provide a necessary reference to benchmark the performance of the detectors, whether in the context of SM measurements, or in the context of background mitigation for the BSM searches.

In this Chapter we review the key properties of SM processes at 100 TeV, having in mind the above considerations. This will serve as a reference for future studies, and to stimulate new ideas on how to best exploit the immense potential of this collider. We shall focus on the production of key SM objects, such as jets, heavy quarks, gauge bosons and the Higgs boson. We shall not address issues like the current or expected precision relative to given processes. On one side, and with some well understood exceptions notwithstanding, leading-order calculations are typically sufficient to give a reliable estimate of the production rates, and assess possible implications for trigger rates, background contributions, and detector specifications. On the other, any statement about the precision of theoretical calculations today will be totally obsolete by the time this collider will operate, and assumptions about the accuracy reach cannot but be overly conservative.

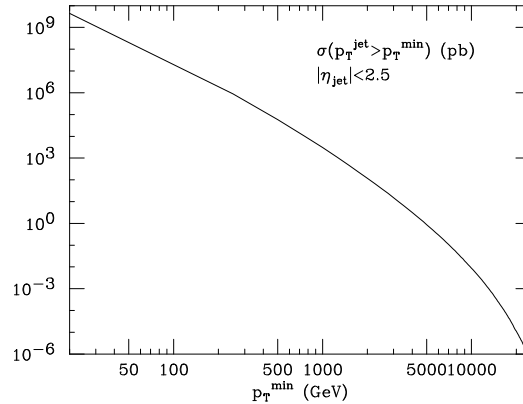


Figure 34: Rates of 1-jet inclusive events with $|\eta| < 2.5$ and $p_T > p_T^{min}$.

6.1. Jets

The production of jets is the process that by far dominates, at all distance scales, the final states emerging from hard collisions among the proton constituents. Figure 34 shows the integrated rates for the production of events with at least one jet of transverse momentum p_T larger than a given threshold.

The distribution refers to jets with pseudorapidity η in the range $|\eta| < 2.5$. Figure 35 shows the probability that events with jets above certain p_T threshold be contained inside certain η ranges. Notice the huge η extension, even for jets with p_T in the TeV range. Assuming integrated luminosities in excess of 1 ab^{-1} , the reach in p_T extends well above 20 TeV. Fully containing and accurately measuring these jet energies sets important constraints on the design of calorimeters, e.g. requiring big depth and therefore large transverse size, with a big impact on the overall dimensions and weight of the detectors.

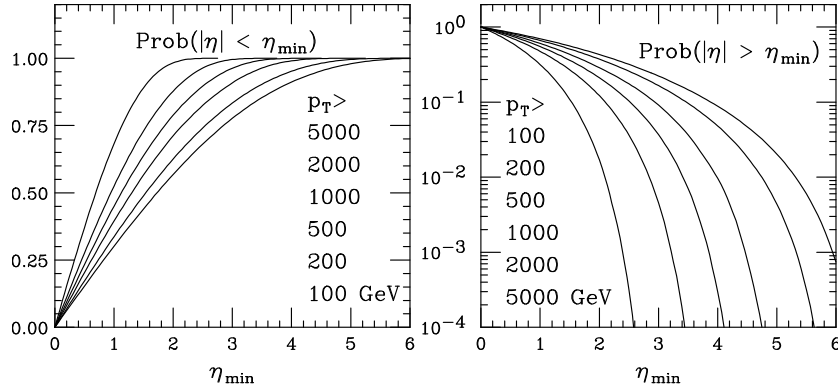


Figure 35: Left: acceptance, for jets above various p_T thresholds, to be contained within $|\eta_j| < \eta_{\min}$. Right: probability to be outside the η_{\min} acceptance.

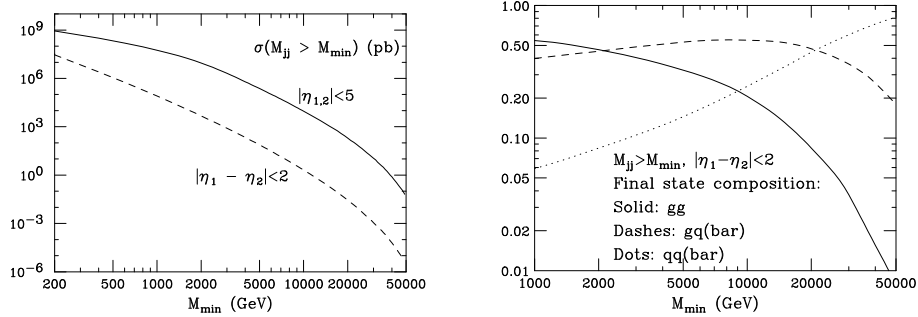


Figure 36: Left: dijet mass spectra, for different η constraints. Right: partonic composition of dijet final states, as a function of the dijet mass.

These choices become particularly relevant in the context of searches for high-mass resonances in dijet final states, where the separation from the continuum background of possibly narrow states requires good energy resolution.

Figure 36 shows the rates for QCD production of final states with a dijet of invariant mass above a given threshold. We consider two cases: the dijet mass spectrum of all pairs with jets within $|\eta| < 5$, and the spectrum limited to jets produced at large angle in the dijet center of mass ($|\eta_1 - \eta_2| < 2$), a configuration which is more typical of the production and decay of a possible resonance. Notice that, particularly at the largest masses, the former rates are several orders of magnitude larger than the latter ones. This is because one is dominated there by the low-angle scattering. But even for central production we have rates in excess of 1 event/ab^{-1} for masses above 50 TeV. The relative partonic composition of central dijet events, as a function of the dijet mass, is shown in the right plot of Fig. 36. In the region $2 \text{ TeV} \lesssim M_{jj} \lesssim 20 \text{ TeV}$ the final states are dominated by $q\bar{q}$ pairs. Above 20 TeV, we find mostly $q\bar{q}$ pairs (the $q\bar{q}$ component is greatly suppressed throughout).

The ability to tag the nature of the partons that originate the jets at these energies could be crucial to understand the properties of possible signals of new physics, such as a decaying resonance with a multi-TeV mass. Some general features of multi-TeV jets from the QCD background processes, or from the evolution and hadronic decay of bottom, top or W bosons, are shown in Figs. 37-39.

Figure 37 plots the multiplicity distribution of particles (both charged and neutral, assuming stable π^0 's) contained within a cone of radius $R = 0.4$ around the jet axis. The three columns of plots refer to jets of $p_T > 1, 5$ and 10 TeV, respectively (jets are defined here by the anti- k_T algorithm [94], with a wide cone of $R = 1$). The three rows contain the distributions relative to hadronically-decaying top jets (upper row), bottom jets and inclusive jets (light quarks and gluons, according to the QCD-predicted fraction), and hadronically-decaying W bosons (lower row). For W bosons, the multiplicity is practically independent of p_T , and reflects the multiplicity of a W decay at rest, with a negligible contamination from initial-state radiation. The other objects show a clear evolution with p_T , and tend asymptotically to very similar spectra, as expected since at large p_T the differences induced by the bottom and top masses, and by the top decay products, are reduced. Notice of course that the multiplicity of top jets has a sharp onset at about $N_{part} \sim 40$, because of the presence of the W decay products. Similar features are observed in the distribution of the jet energy fraction contained in a subcone of radius R_0 , shown in Fig. 38, and in the distribution of the jet mass within a cone of $R = 0.4$, shown in Fig. 39. Figure 38, in particular,

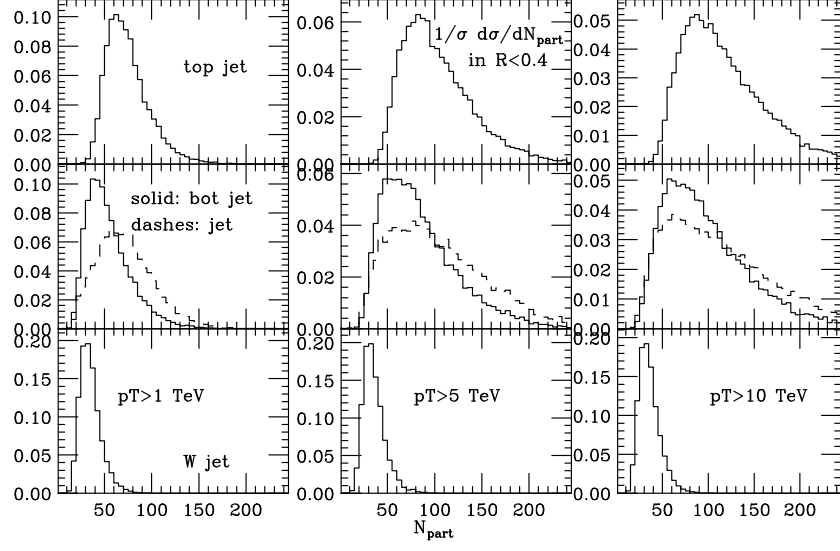


Figure 37: Multiplicity distribution in high- p_T jets originating from hadronically decaying top quarks (upper rows), bottom quarks and light partons (central rows) and hadronic decays of W bosons (lower rows).

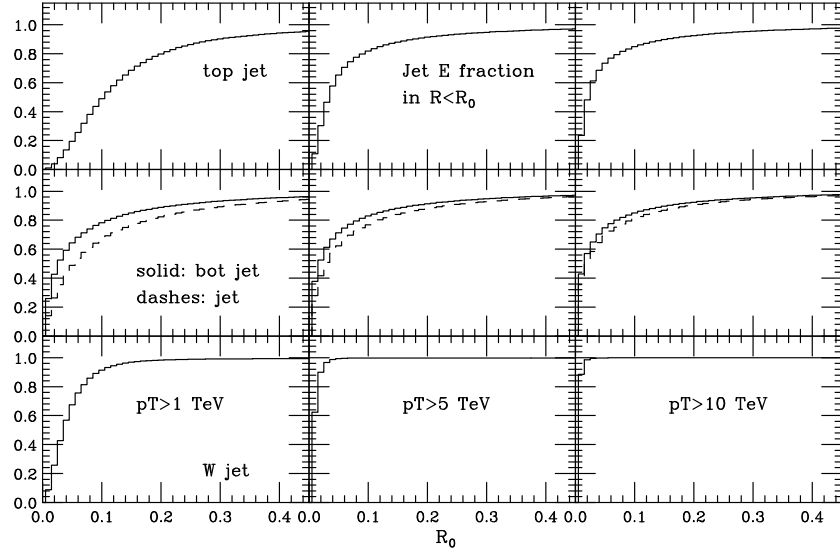


Figure 38: Fraction of the total energy for $R = 1$ jets, contained within smaller radii R_0 .

shows that practically all the energy from a 10 TeV W jet is contained within a cone of radius $R \lesssim 0.02$; this means an average of 40 particles all inside

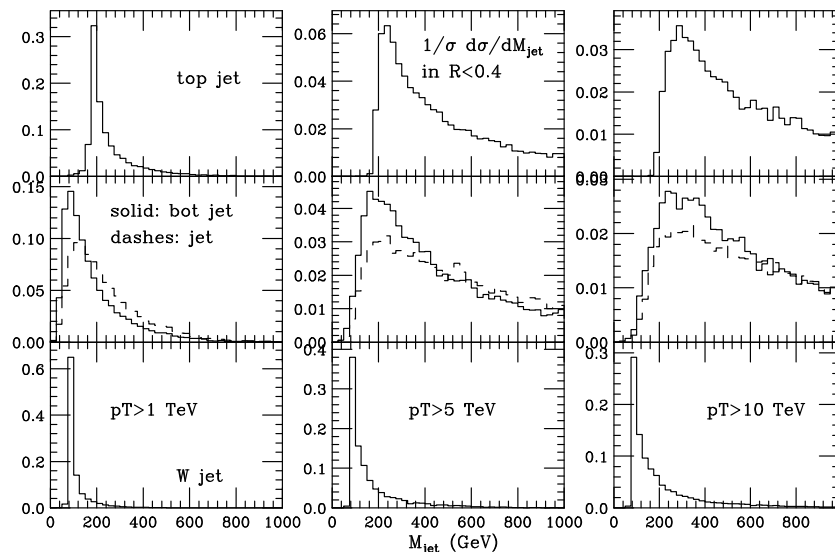


Figure 39: Distribution of the jet invariant mass contained with a cone of radius $R = 0.4$ around the jet axis.

this tiny radius, making their individual reconstruction experimentally very challenging. Efforts are ongoing to exploit the small differences observed in distributions such as those shown here, in order to statistically separate with good efficiency objects such as top quarks or gauge bosons from each other, and from light jets. Such techniques, developed for the $p_T \sim \text{TeV}$ range of relevance to LHC physics, are being extended to the more challenging multi-TeV regime relevant to the future physics of a 100 TeV collider. See for example the study in Ref. [95], dedicated to top quarks.

6.2. W/Z Production

The production of W and Z bosons is a valuable probe of both EW and QCD dynamics. The production properties are known today up to next-to-next-to-leading order (NNLO) in QCD, leading to a precision of the order of the percent. A detailed discussion of the implications of this precision, and of the possible measurements possible with W and Z final states at 100 TeV, is outside the scope of this review, also because the LHC has only started exploiting the full potential of what can be done with them. We shall therefore focus here on documenting some basic distributions, to show the extreme kinematical configurations that may be accessed at 100 TeV, and to

highlight some of the novel features of EW interactions that will emerge at these energies.

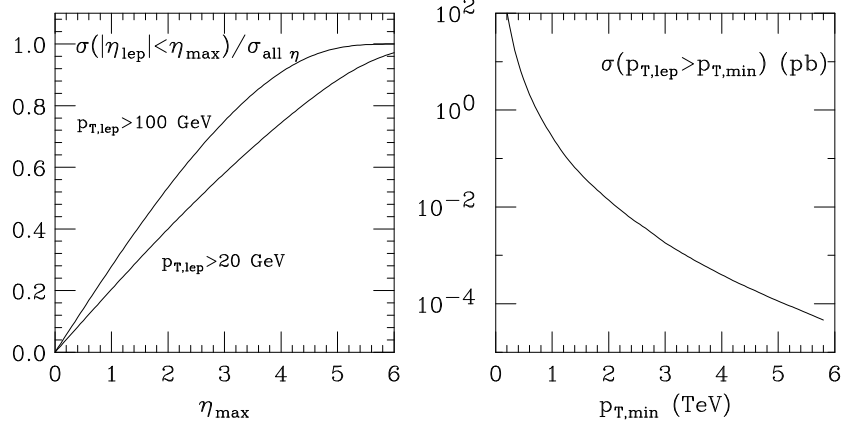


Figure 40: Left: rapidity acceptance for leptons from inclusive W production and decay, for p_T thresholds of 20 and 100 GeV. Right: inclusive lepton p_T spectrum.

The total production rate of W^\pm (Z^0) bosons at 100 TeV is about 1.3 (0.4) μb . This corresponds to samples of $O(10^{11})$ leptonic (e, μ) decays per ab^{-1} . At 100 TeV, gauge bosons will have a rather broad rapidity distribution and, as shown in the left plot of Fig. 40, more than 50% of the leptons with $p_T > 20 \text{ GeV}$ will be produced at $|\eta| > 2.5$ (w.r.t. $\sim 30\%$ at 14 TeV). Even leptons with $p_T > 100 \text{ GeV}$ will have a large forward rate, with about 40% of them at $|\eta| > 2.5$ ($\sim 10\%$ at 14 TeV). Their p_T spectrum will also extend to large values, as shown in the right plot of Fig. 40. The largest fraction of these high- p_T leptons will arise from W 's produced at large p_T , in association with jets.

6.2.1. Multiple gauge boson production

Table 1 shows the rates of associated production of multiple gauge bosons from full NLO calculations [97, 96]. Production of each additional EW gauge boson brings the cross section down roughly by the order of α , as naively expected in perturbation theory. Even including the branching ratios for the best visible leptonic decays, the rates are sufficient in principle to observe the production of up to four gauge bosons. This will lead to unprecedented precision in the measurement of anomalous triple gauge couplings, and to the detection of quartic couplings, furthermore providing a probe of anomalous higher-dimension operators involving multiple gauge bosons.

Proc	WWW	WWZ	WZZ	ZZZ
$\sigma(\text{fb})$	4.3×10^3	4.0×10^3	1.4×10^3	2.6×10^2

Proc	WWWW	WWWZ	WWZZ	WZZZ	ZZZZ
$\sigma(\text{fb})$	41	60	33	7.1	0.8

Table 1: NLO cross sections for production of multiple gauge bosons, at 100 TeV [96].

6.2.2. FSR effects of the gauge bosons and initial state partons

The left plot in Fig. 41 shows the integrated p_T spectrum of W bosons.⁴ With luminosities in excess of 1 ab^{-1} , data will extend well beyond 15 TeV. For processes involving gauge bosons and jets at such large energies, however, a very interesting new phenomenon emerges, namely the growth of the gauge boson emission probability from high- p_T jets. If we ask what is the most likely mechanism to produce gauge bosons in final states with at least one multi-TeV jet, it turns out that this is not the LO QCD process where the gauge boson simply recoils against the jet, but the higher-order process where it is a second jet that absorbs the leading jet recoil, and the gauge boson is radiated off some of the quarks [99], the effect of “final state radiation” (FSR). In other words, the parton-level scattering $qq \rightarrow qqV$ dominates over $qq \rightarrow qV$ (for simplicity, we do not show explicitly the possibly different quark flavour types involved in the processes). The emission probability of gauge bosons in this case is enhanced by large logarithms of $p_{T,jet}/M_V$, and can reach values in the range of 10% and more, as shown in the right plot of Fig. 41. This gives the emission probability for one or more W bosons in events in which there is at least one jet above a given p_T threshold. The kinematical properties of these events are illustrated in Fig. 42, in the case of final states with a jet above 1 TeV, and above 10 TeV, to highlight the kinematical evolution with jet p_T . In the case of largest p_T , we see the dominance of events in which the two jets balance each other in transverse momentum, while the W carries a very small fraction of the leading jet momentum. One third of the W ’s are

⁴This calculation only includes the QCD effects. For p_T beyond the TeV scale, the effects of virtual EW corrections are known to lead to important corrections [98].

emitted within $\Delta R < 1$ from the subleading jet, with a large tail of emission at larger angles, due in part to W radiation from the initial state.

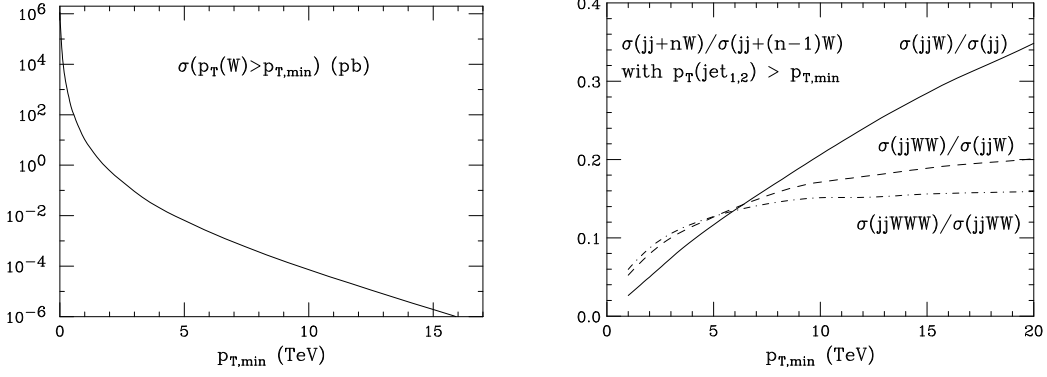


Figure 41: Left: inclusive p_T spectrum of W bosons. Right: emission probability for additional W bosons in dijet events at large p_T .

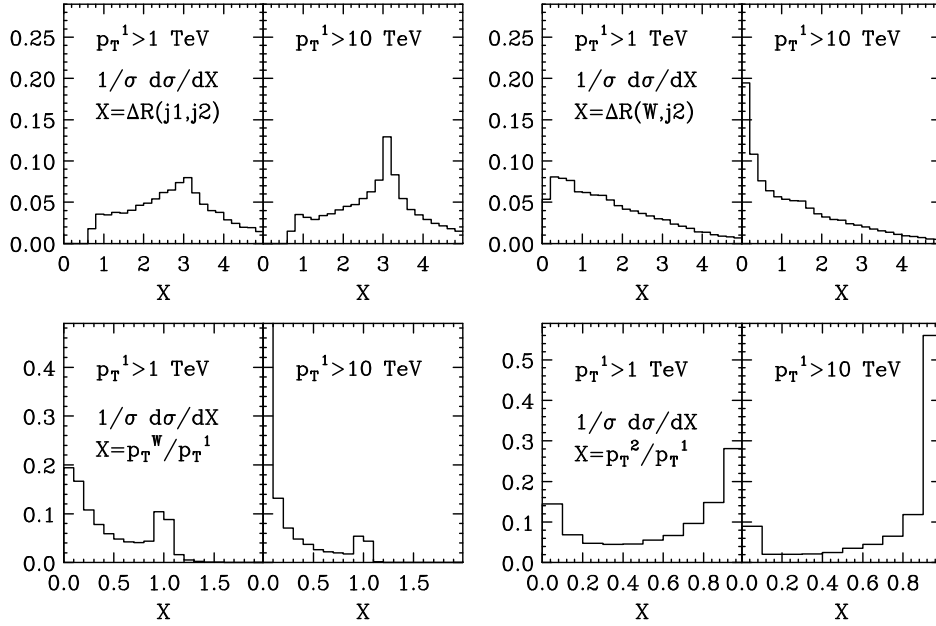


Figure 42: Kinematical correlations in high- p_T jet events with W radiation, for values of the leading jet $p_T > 1$ and 10 TeV.

The process considered above is just one manifestation of the general fact that, in hard electroweak interactions at multi-TeV energies, the soft/collinear

structure of almost *any* multi-TeV process can become significantly altered, as the logarithmic enhancements familiar from QED and QCD will become active for electroweak emissions (see, e.g., [100, 101, 102, 103, 10]). Obtaining correct descriptions of the complete event structure when $\sqrt{\hat{s}} \gg M_W$ can be then greatly facilitated by incorporating factorization and resummation, such as that provided by parton showering and parton distribution functions. In effect, we will begin to see weak bosons (including the Higgs boson) behaving as nearly-massless partons, in stark contrast to the conventional perspective in which they are viewed as “heavy” particles. Jets, whether initiated by QCD processes, electroweak process, or new physics processes, will be found to contain electroweak splittings with probabilities at the $O(10\%)$ level. Similarly, weak bosons can usefully be thought of as collinear components of the protons, at the same level as gluons and photons.

To develop some intuition of the collinear splitting behavior of electroweak “partons,” it is useful to first consider a conceptual limit with an unbroken $SU(2) \times U(1)$ gauge symmetry with massless gauge bosons and fermions, supplemented by a massless scalar doublet field ϕ without a VEV (the would-be Higgs doublet). In this limit, many processes are direct analogs of those in QED and QCD. Fermions with appropriate quantum numbers may emit (transverse) $SU(2)$ and $U(1)$ gauge bosons with both soft and collinear enhancements. The $SU(2)$ bosons couple to one another via their non-abelian gauge interactions, and undergo soft/collinear splittings of the schematic form $W \rightarrow WW$, similar to $g \rightarrow gg$. All of the electroweak gauge bosons may also undergo collinear-enhanced splittings into fermion pairs, similar to $g \rightarrow q\bar{q}$ or $\gamma \rightarrow f\bar{f}$. Beyond these, the major novelty is the introduction of the scalar degrees of freedom. First, the scalars may themselves radiate $SU(2)$ and $U(1)$ gauge bosons, with soft/collinear limits identical to their counterparts with fermionic sources. Second, the electroweak gauge bosons can split into a pair of scalars, again in close analog with splittings to fermion pairs. Third, fermions with appreciable Yukawa couplings to the scalar doublet can emit a scalar and undergo a chirality flip. Finally, the scalars can split into collinear fermion pairs.

In the realistic case of spontaneously-broken symmetry, several important changes take place. Primarily, all of the soft and collinear divergences associated with the above splittings become physically regulated, effectively shutting off at $p_T \lesssim M_W$ (or m_H, m_t where appropriate). Roughly speaking, M_W plays a role similar to Λ_{QCD} in the QCD parton shower, albeit with far less ambiguity of the detailed IR structure since this regulation occurs at

Process	$\mathcal{P}(p_T)$	$\mathcal{P}(1 \text{ TeV})$	$\mathcal{P}(10 \text{ TeV})$
$f \rightarrow V_T f$	$(5 \times 10^{-3}) \log^2 \frac{p_T}{m_{\text{EW}}}$	3%	12%
$f \rightarrow V_L f$	$(2 \times 10^{-3}) \log \frac{p_T}{m_{\text{EW}}}$	0.6%	1%
$V_T \rightarrow V_T V_T$	$(0.01) \log^2 \frac{p_T}{m_{\text{EW}}}$	6%	25%
$V_T \rightarrow V_L V_T$	$(0.01) \log \frac{p_T}{m_{\text{EW}}}$	2%	4%
$V_T \rightarrow f \bar{f}$	$(0.01) \log \frac{p_T}{m_{\text{EW}}}$	2%	4%
$V_T \rightarrow V_L h$	$(2 \times 10^{-3}) \log \frac{p_T}{m_{\text{EW}}}$	0.6%	1%
$V_L \rightarrow V_T h$	$(5 \times 10^{-3}) \log^2 \frac{p_T}{m_{\text{EW}}}$	3%	12%
$V_L \rightarrow V_L h$	$(2 \times 10^{-3}) \log \frac{p_T}{m_{\text{EW}}}$	0.6%	1%

Table 2: An illustrative set of approximate total electroweak splitting rates in final-state showers at two representative energies [108].

weak coupling. Another major difference is the mixing of the scalar doublet’s Goldstone degrees of freedom into the W and Z gauge bosons, allowing for the appearance of longitudinal modes. In many cases, the longitudinal gauge bosons behave identically to the original scalars, as dictated by the Goldstone equivalence theorem [104, 105]. For example the splitting $W_T^+ \rightarrow W_L^+ Z_L$ is, up to finite mass effects, an exact analog of $W_T^+ \rightarrow \phi^+ \text{Im}(\phi^0)$ in the unbroken theory. Similarly for longitudinal gauge boson emissions from heavy fermions, such as the equivalence between $t_L \rightarrow Z_L t_R$ and $t_L \rightarrow \text{Im}(\phi^0) t_R$.

But important exceptional cases now also occur for emissions near $p_T \sim M_W$. Most well known, even a massless fermion exhibits a kind of soft/collinear-enhanced emission of W_L and Z_L [106, 107]. These emissions have no Goldstone equivalent analog, and are highly power-suppressed for $p_T \gtrsim M_W$. But the overall population of emissions at the boundary between “broken” and “unbroken” behavior nonetheless grows logarithmically with the fermion energy. This is formally subdominant to the double-logarithmic growth of transverse emissions, but remains numerically important at multi-TeV energy scales. Emissions from massless quarks also cause the energetic initial-state protons to act as sources of longitudinal boson beams, allowing for studies of the high-energy interactions of the effective Goldstone bosons through weak boson scattering (discussed further below). Similar types of emissions occur in the splittings of transverse bosons, such as $W_T^+ \rightarrow Z_L W_T^+ / Z_T W_L^+$.

Table 2 provides a few estimates for total splitting rates of individual final-state particles [108], including approximate numerical values for particles

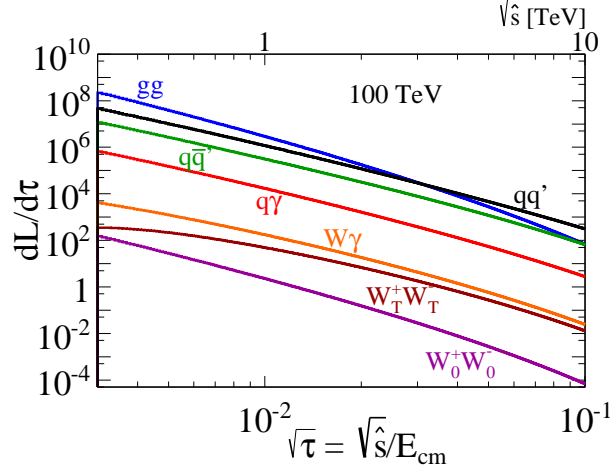


Figure 43: Partonic luminosities at 100 TeV, illustrating the relative contributions from weak bosons when treated as partons in the proton [108].

produced at $p_T = 1$ TeV and 10 TeV. The $SU(2)$ self-interactions amongst transverse gauge bosons tend to give the largest rates, quickly exceeding 10% as the energy is raised above 1 TeV (these rates are slightly lower than those extracted from Fig. 41, since there an important contribution to W emission came from initial state radiation). This has significant impact on processes with prompt transverse boson production such as $W/Z/\gamma$ +jets, and especially on multiboson production including transverse boson scattering. Generally, it is important to appreciate that *any* particle in an event, whether initial-state or final-state, or even itself produced inside of a parton shower, can act as a potential electroweak radiator. Consequently, the total rate for finding one or more electroweak splittings within a given event must be compounded, and can sometimes add up to $O(1)$.

In this regards, it would be interesting, both conceptually and technically, to consider the electroweak bosons as patrons in high-energy collisions. Fig. 43 summarizes the parton luminosities when electroweak bosons are included in the PDFs. One immediate observation from comparing the $W_T\gamma$ and W_TW_T luminosities is that transverse weak bosons begin to appear on the same footing as photons, as might have been anticipated. Ultimately, they must be folded into the full DGLAP evolution, though at 100 TeV energies the running effects are not yet sizable. The longitudinal bosons are

sourced from the quarks as described above at $p_T \sim M_W$, with individual splitting rates $O(3\text{--}10)$ times smaller than their transverse counterparts at multi-TeV energies. This leads to $O(10\text{--}100)$ times smaller luminosities. For VBF process initiated by the longitudinal bosons, the PDF approach effectively integrates out the usual forward tagging jets, treating them as part of the “beam.” This of course becomes a progressively more justifiable approach, as these jets with $p_T \sim M_W$ will appear at extremely high rapidities, and may anyway become a less distinctive feature to discriminate against backgrounds in the presence of copious QCD initial-state radiation at similar p_T . From a practical perspective, the ability to treat VBF as a $2 \rightarrow 2$ process rather than $2 \rightarrow 4$ would significantly reduce the computational burden for event simulation. The tagging jets can then be resolved using the usual initial-state radiation machinery, appropriately adapted for this unique electroweak splitting process.

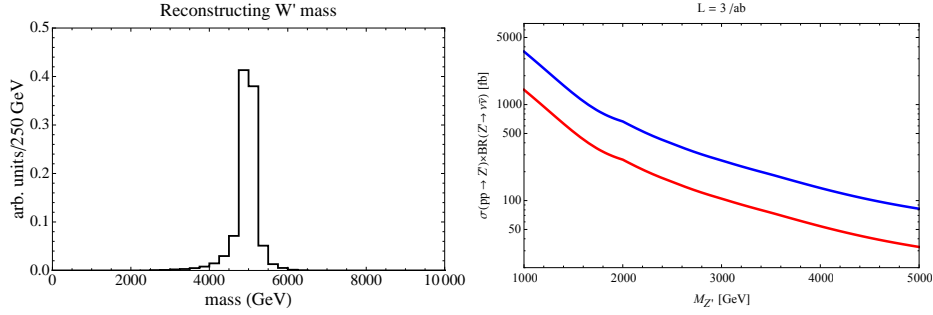


Figure 44: Under the assumption that the neutrino is collinear with the leptonic Z , the reconstructed neutrino allows one to guess the real missing energy in an event as well as reconstruct the full mass peak of a W' particle (plot on the LHS). The mass resolution is smeared since the Z is not always collinear with the neutrino, but the peak is very clearly at the W' mass of 5 TeV. On the right hand side, we plot the reach of a 100 TeV collider to a Z' decaying invisibly for a luminosity of 100 fb^{-1} and 3000 fb^{-1} . The blue and red lines are the 5 and 2 σ results respectively.

The enhanced W and Z radiation can also have interesting applications in new physics searches. We briefly mention a couple of examples here. The invisible and semi-invisible decays $Z' \rightarrow \nu\nu$ and $W' \rightarrow \ell\nu$ are difficult to probe directly. At large energies, neutrinos can emit W and Z bosons which can help tagging these processes.⁵ The Sudakov enhancement of this

⁵The importance of heavy Z' three-body decays was first mentioned in Ref. [109] in

process can make the three-body decays of a W' or Z' significant if the leptons are sufficiently boosted, e.g. $Z' \rightarrow \nu \bar{\nu} Z$ or $Z' \rightarrow \nu l^- W^+$. If a Z boson is radiated, the collinear enhancement results in a strong tendency for the Z boson to be emitted parallel to the neutrino. This allows one to reconstruct approximately the neutrino momentum. If a W boson is radiated and reconstructed (most likely in a hadronic decay mode), the small ΔR distance between it and the lepton allows one to tag the lepton as originating from a neutrino. These effects at an 100 TeV pp collider have been studied in Ref. [10]. The analysis is at parton level and Madgraph5 [111, 112, 113] was used to generate the events. The results are shown in Fig. 44.

This approach can be pursued further and help determine quantum numbers of new particles based on total EW gauge bosons emission. Particles which are not charged under $SU(2)_L \times U(1)_Y$ do not radiate W and Z bosons and can thus be distinguished from their charged counterparts.

We illustrate this effect in an example where we assume a “natural SUSY”-like spectrum at the TeV scale, namely a stop as an NLSP decaying into a neutralino LSP. SUSY with light third generation squarks is a well motivated [50, 114] and well studied scenario [115, 116, 117]. The left and right handed stops have different couplings to the Z . Due to electroweak symmetry breaking, they mix so that the NLSP is an admixture of the two. At large masses, the chirality of the stops can be measured by the additional radiation of a Z or W in the event. The Sudakov enhancement for the radiation of Z s and W s makes this measurement feasible at a 100 TeV machine. Note however that the radiation of the EW gauge bosons from the stop is only single log enhanced because the collinear singularity in this case is cut off by the mass of the emitting particle (the stop) and effectively does not lead to any enhancement. Meanwhile, both ISR and FSR have a Sudakov double log enhancement. Because both the decay products of the stop and the initial state quarks have the same chirality as the stop, the radiation strength provides a good measure of the chirality of the stop regardless of where the radiation came from.

Fig. 45 demonstrated such a measurement with two benchmark stop masses: $m_{\tilde{t}} = 0.7$ TeV and $m_{\tilde{t}} = 1.5$ TeV, all decaying into a massless bino-like neutralino. Note that the first benchmark point can be easily discovered by the LHC while the second one is inaccessible even for the LHC14.

the context of SSC and later in Ref. [110, 10] in context of a 100 TeV collider.

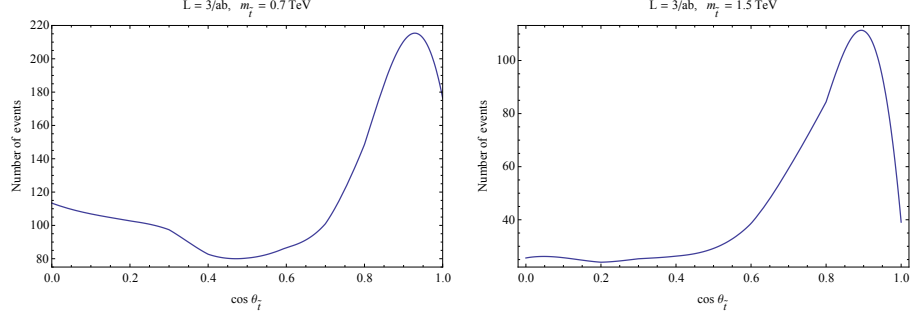


Figure 45: Number of signal events after imposing all selection cuts, detailed in Ref. [10], as a function of $\cos \theta_t$ for three mass points. $\cos \theta_t = 0$ is a right handed stop.

There is a clear difference between $\cos \theta_t = 0$ and 1. Thus purely left and purely right handed stops can be distinguished.

6.3. Heavy Quarks

6.3.1. Inclusive bottom production

Inclusive production of b hadrons in hadronic collisions offers unlimited opportunities for flavour studies in the b sector, as shown very well by the Tevatron and LHC experiments. The long-term interest in these studies will

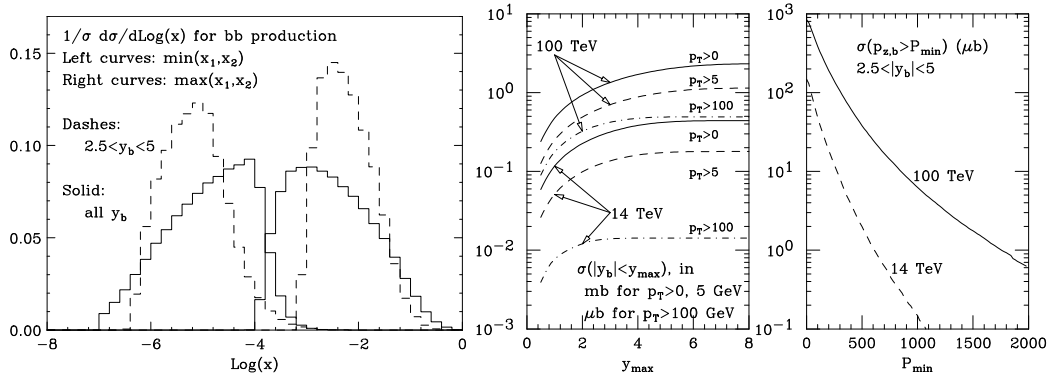


Figure 46: Left: distribution of the smaller and larger values of the initial partons momentum fractions in inclusive $b\bar{b}$ events (solid) and in events with at least one b in the rapidity range $2.5 < |y| < 5$ (dashes). Center: production rates for b quarks as a function of detection acceptance in y , for various p_T thresholds (rates in μb for $p_T > 100$ GeV, in mb otherwise). Right: forward b production rates, as a function of the b longitudinal momentum.

depend on what future LHCb and Belle2 data will tell us, and on the flavour

implications of possible LHC discoveries in the high- Q^2 region. But it is likely that heavy flavour studies will remain a pillar of the physics programme at 100 TeV. The total $b\bar{b}$ production cross section at 100 TeV is about 2.5mb, and increase of ~ 5 relative to the LHC, and it is more than a 1% fraction of the total pp cross section. This rate comes with a large uncertainty, due to the contribution of gluons at very small x values, where the knowledge of PDFs is today extremely poor and mostly dictated, at best, by reasonably guessed extrapolations. The left plot of Fig. 46 shows that, for a detector like LHCb, covering the rapidity region $2.5 < y < 5$, about 50% of the b events would originate from gluons with momentum $x < 10^{-5}$, i.e. in a domain totally unexplored so far! The following two plots of Fig. 46 provide the rapidity distributions for b quarks produced above some thresholds of p_T and, for b quarks produced in the region $2.5 < |y| < 5$, the integrated spectrum in longitudinal momentum p_z , comparing results at 14 and 100 TeV. We note that, while the total production rate grows only by a factor of ~ 5 from 14 to 100 TeV, the rate increase can be much greater once kinematic cuts are imposed on the final state. For example, at 100 TeV b quarks are produced in the forward region $2.5 < |y| < 5$ with $p_z > 1$ TeV at the astounding rate of $10\mu\text{b}$, 100 times more than at the LHC. To which extent this opens concrete opportunities for new interesting measurements, to be exploited by the future generation of detectors, remains to be studied.

6.3.2. Inclusive top production

Table 3 shows the NLO cross sections for the inclusive production of top quark pairs, and for production in association with one and two gauge bosons. The ~ 30 nb inclusive rate is more than 30 times larger than at 14 TeV. For the planned total integrated luminosity, two experiments would produce of the order of 10^{12} (anti)top quarks. The possible applications emerging from this huge statistics have yet to be explored in detail. It would be interesting to consider the potential of experiments capable of recording all these events (only a small fraction of top quarks produced at the LHC survives for the analyses). Triggering on one of the tops, would allow for unbiased studies of the properties of the other top and of its decay products: studies of inclusive W decays [118] (which are impossible using the W 's produced via the Drell-Yan process), of charm and τ leptons produced from those W decays, of flavour-tagged b 's from the top decay itself [119].

Comparing the rates for associated production, in Table 3, with those in Table 1 for multiple gauge boson production, and considering that each top

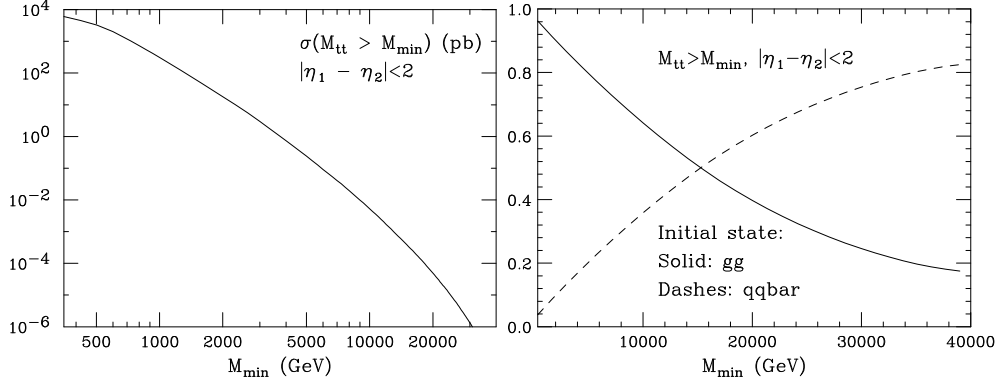


Figure 47: Left: integrated invariant mass distribution for production of central $t\bar{t}$ quark pairs. Right: initial state composition as a function of the $t\bar{t}$ invariant mass.

	$t\bar{t}$	$t\bar{t}t\bar{t}$	$t\bar{t}W^\pm$	$t\bar{t}Z^0$	$t\bar{t}WW$	$t\bar{t}W^\pm Z$	$t\bar{t}ZZ$
$\sigma(\text{pb})$	$3.2 \cdot 10^4$	4.9	16.8	56.3	1.1	0.17	0.16

Table 3: NLO cross sections for associated production of (multiple) top quark pairs and gauge bosons [96, 121].

quark gives rise to a W through its decay, we remark that top quark processes at 100 TeV will provide the dominant source of final states with multiple W bosons, and thus with multiple leptons. This will have important implications for the search of new physics signals characterized by the presence of many gauge bosons or leptons from the decay of the new heavy particles.

Notice also that $t\bar{t}Z^0$ production is more abundant than $t\bar{t}W^\pm$, contrary to the usual rule that W bosons are produced more frequently than Z^0 's in hadronic collisions. This is because the $t\bar{t}Z^0$ process is driven by the gg initial state, which for these values of \hat{s}/s has a much larger luminosity than the $q\bar{q}'$ initial state that produces $t\bar{t}W$. This also implies that studies of top production via initial state light quarks (e.g. in the context of t vs \bar{t} production asymmetries) will benefit from a higher purity of the $q\bar{q}$ initial state w.r.t. gg if one requires the presence of a W boson (see e.g. Ref. [120]).

6.3.3. Bottom and top production at large Q^2

Production of bottom and top quarks at large Q^2 is characterized by two regimes. On one side we have final states where the heavy quark and

antiquark (Q and \bar{Q}) give rise to separate jets, with a very large dijet invariant mass $M_{Q\bar{Q}}$. These are the configurations of relevance when, for example, we search for the $Q\bar{Q}$ decay of massive resonances. In the case of top quarks, the left-hand side of Fig. 47 shows the production rate for central $t\bar{t}$ pairs above a given invariant mass threshold. At 100 TeV there will be events well above $M_{t\bar{t}} > 30$ TeV. The right plot in Fig. 47 furthermore shows that, due to the absence at LO of contributions from qq or qg initial states, gg initial states remain dominant up to very large mass, $M_{t\bar{t}} \sim 15$ TeV. Well above $M_{Q\bar{Q}} \sim \text{TeV}$, the results for $b\bar{b}$ pair production are similar to those of the top.

The second regime occurs when we request only one jet to be tagged as containing a heavy quark. This could be of interest, for example, in the context of high- p_T studies of single top production. In this regime, configurations in which the heavy quark pair arises from the splitting of a large- p_T gluon are enhanced. The final state will then contain a jet formed by the heavy-quark pair, recoiling against a gluon jet. An example of the role of these processes is shown in Fig. 48, where we compare the p_T spectrum of b jets in events where the $b\bar{b}$ pair is produced back to back (as in the first case we discussed above), and the spectrum of jets containing the b pair (here jets are defined by a cone size $R = 0.4$). The latter is larger by approximately one order of magnitude at the highest p_T values, leading to rates in excess of 1 event/ab $^{-1}$ for $p_T > 15$ TeV. Similar considerations apply to the case of top quark production in this multi-TeV regime, as shown in the right plot of Fig. 48. In this case the rate for $t\bar{t}$ jets is only slightly larger than that for single-top jets, due to the much larger mass of the top quark, which leads to a smaller probability of $g \rightarrow t\bar{t}$ splitting.

6.3.4. Heavy quark partons

At 100 TeV, particles with masses around the electroweak scale appear as light as the bottom quark at the Tevatron collision energy of $\sqrt{s} = 2$ TeV. When a very heavy scale is involved in the process, the gluon splitting into a top-antitop pair may present a large logarithmic enhancement. For $Q \sim 10$ TeV, for instance, $\alpha_s(Q) \log(Q^2/m_t^2) \sim 0.6$, which makes a perturbative expansion of the hard process questionable. Defining a parton distribution function (PDF) for the top-quark inside the proton allows us to resum large collinear logarithms $\alpha_s^n(Q) \log^n(Q^2/m_t^2)$ to all orders in perturbation theory. Initial heavy quarks have been studied in detail in the context of bottom-initiated processes [122, 123], and the main concepts can be adopted for the

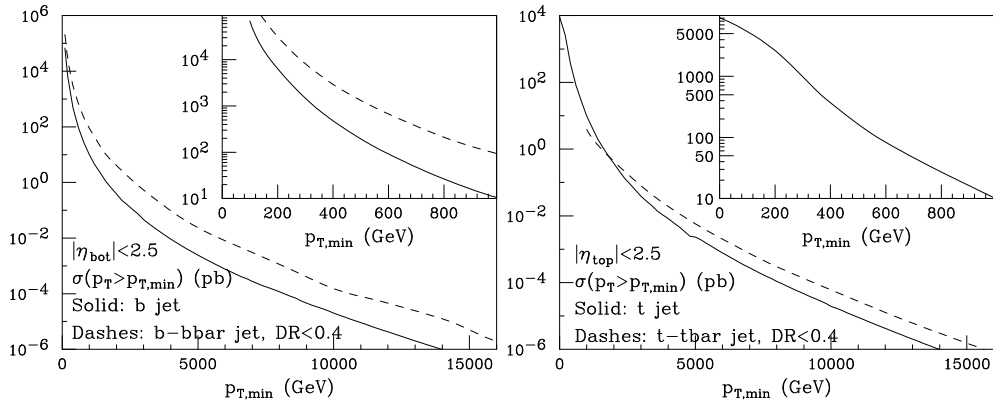


Figure 48: Left: production rates for b jets (solid), and for jets containing a $b\bar{b}$ pair within $\Delta R < 0.4$ (dashes). Right: same, for top-quark jets (top treated as stable).

top-quark. The NNPDF collaboration has released a top-quark PDF as part of their NNPDF2.3 set [124], which facilitates the implementation.

Figure 49 shows a comparison of calculations in the 5-flavor, massless 6-flavor, and ACOT schemes [84, 125] for the inclusive production of a hypothetical heavy scalar (H^0) at a 100 TeV pp collider [83]. The ACOT scheme with proper treatment of collinear subtraction shows the desired behavior of interpolating between the region near the top threshold and the very high energy limit. We point out that the simplest LO 6-flavor calculation is unreliable for masses below 10 TeV, indicating that the minimum scale above which a parton interpretation for the top quark becomes justified is much larger than the top mass itself.

6.4. Higgs Production Rates

We collect here, for reference, the production rates at 100 TeV of SM Higgs bosons, including both the canonical production channels, as well as more rare channels of associated production. Associated production of Higgs bosons with other objects could allow independent tests of the Higgs boson properties, and might provide channels with improved signal over background, with possibly reduced systematic uncertainties.

Table 4, extracted from the compilation produced by the LHC Higgs Cross Section working group [126], shows the rates for channels that will already be accessible and used at the LHC. The rates are typically a factor of 10-20 larger than at the LHC, except for the associate $t\bar{t}H$ production, where the gg initial state and the large mass of the final state benefit more

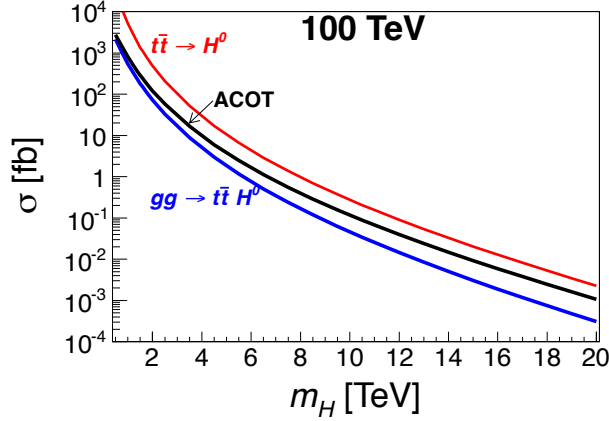


Figure 49: Inclusive cross section for a heavy scalar H^0 production with Yukawa coupling $y = 1$ at 100 TeV versus its mass m_H , in the 5-flavor scheme (bottom blue), the 6-flavor scheme (upper red), and the ACOT scheme with proper subtraction (middle black).

	$gg \rightarrow H$	VBF	HW^\pm	HZ	$t\bar{t}H$
$\sigma(\text{pb})$	740	82	15.9	11.3	37.9
$\sigma(100 \text{ TeV})/\sigma(14 \text{ TeV})$	14.7	18.6	9.7	12.5	61

Table 4: Upper row: cross sections [126] for production of a SM Higgs boson in gg fusion, vector boson fusion, associated production with W and Z bosons, and associated production with a $t\bar{t}$ pair. Lower row: rate increase relative to 14 TeV. All results are NNLO, except $t\bar{t}H$ (NLO), with the central PDF from the MSTW2008(N)NLO set.

significantly from the higher energy, leading to a rate growth by a factor of 60. The samples obtained with a luminosity of 10 ab^{-1} will therefore be a factor of 30-200 larger than what available after the completion of the HL-LHC programme. The statistical uncertainties for the extraction of the Higgs couplings to the third generation fermions, to the charm and the muon, and to the EW gauge bosons, will become smaller than the percent level. It is difficult today to estimate how the theoretical progress will improve the theoretical systematics, and the determination of experimental systematics will require detailed simulation studies, based on realistic detector concepts. The large statistics for both signals and backgrounds will certainly help in

	HH	$HHjj$ (VBF)	HHW^\pm	HHZ	$HHt\bar{t}$	$HHtj$
$\sigma(\text{fb})$	$1.2 \cdot 10^3$	81	8.1	5.5	86	4.6

Table 5: NLO cross sections for production of a SM Higgs boson pair, including associated production channels, at 100 TeV [97].

improving the modeling systematics, which in many cases are a limitation to the precision foreseen for the HL-LHC. It is therefore not excluded that the final uncertainties, at least in some channels, may reach the percent level.

An example is the extraction of the top Yukawa coupling y_{top} from the $t\bar{t}H$ process [9]. The large cross section at 100 TeV allows to consider boosted topologies for the hadronic decays of both the top quarks and the Higgs boson ($H \rightarrow b\bar{b}$), placing tight cuts on the emerging jets, and drastically reducing the various sources of backgrounds, while maintaining a statistical sensitivity on the production rate at the percent level. This matches the theoretical systematics, which, already today, is at the percent level [9], if one considers the ratio $\sigma(t\bar{t}H)/\sigma(t\bar{t}Z)$, which is very stable with respect to PDF and scale uncertainties. The branching ratio for the $H \rightarrow b\bar{b}$ decay, needed to extract the top Yukawa coupling from this measurement, will be known with sufficient accuracy if an e^+e^- Higgs factory (at a linear or circular collider) will be operating. Otherwise, a percent-level measurement of $y_{top} * \text{BR}(H \rightarrow b\bar{b})$ will still be one of the most precise determinations of a combination of Higgs couplings, with direct sensitivity on y_{top} .

Studies are also available [5, 6, 7, 8] of the determination of the Higgs self-coupling in the $HH \rightarrow b\bar{b}\gamma\gamma$ decay channel⁶, with a projected uncertainty on the measurement of the SM coupling in the range of 5 – 10% with a total of 30 ab^{-1} .

Table 5, extracted from the NLO results of Ref. [97], reports the rates for SM Higgs pair production, including channels of associated production with jets, gauge bosons and top quarks. Once again, the possible implications of the measurement and study of these exotic Higgs production channels are under study.

Table 6, extracted from the NLO results of the aMC@NLO code [97, 96],

⁶For a study of more rare decay modes, see Ref. [127].

	HW^+W^-	$HW^\pm Z$	HZZ	$HW^\pm\gamma$	$HZ\gamma$
$\sigma(\text{fb})$	170	100	42	78	43

Table 6: NLO cross sections for associated production of a SM Higgs boson with multiple gauge bosons [97].

reports the rates for associated production of a SM Higgs with gauge boson pairs. Theoretical systematics, including scale and PDF uncertainties, are typically below 10%.

6.5. Sources of Missing Transverse Energy

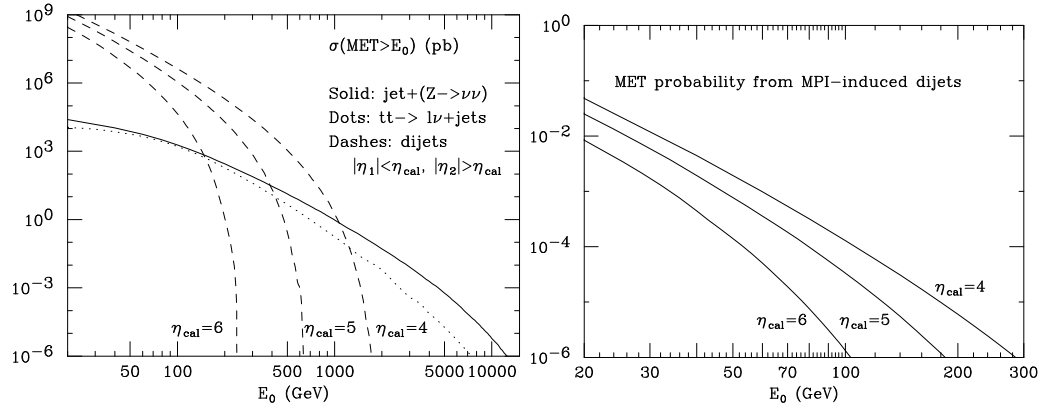


Figure 50: Left: Missing transverse energy rates, from jet+($Z \rightarrow \nu\bar{\nu}$) events and from dijets, with a jet escaping undetected at large rapidity. Right: Missing transverse energy probability induced by multiple-parton interactions, for different values of the jet rapidity acceptance.

Missing transverse energy (\cancel{E}_T) is an important signature for many BSM processes. At 100 TeV, SM sources of \cancel{E}_T can contribute with very large rates of irreducible backgrounds. We consider here, for illustration, the effect of three of the leading sources of irreducible \cancel{E}_T : the associated production of jets and a Z^0 boson decaying to neutrinos, the semileptonic decay of top quarks, and the production of jets outside the calorimeter acceptance. The latter channel is important, since the high energy available in the CM allows for the production of large p_T jets at very forward rapidities. This is shown in Fig. 50, where the dashed lines correspond to the rate of dijet events in which

one jet is within the calorimeter acceptance (defined by the η_{cal} label), and the other is outside. With the standard LHC calorimeter coverage, $\eta_{cal} = 5$, dijets would give a \cancel{E}_T signal larger than Z +jets for \cancel{E}_T up to ~ 400 GeV. This is reduced to ~ 150 GeV with a calorimeter extending out to $\eta_{cal} = 6$.

It must be noticed that the limited calorimeter acceptance can induce a \cancel{E}_T signal in any hard process, due to the finite probability of the coincidence of a multiparton interaction. Multiparton interactions are hard scatterings taking place among the partons not engaged in the primary hard process, and cannot be separated experimentally since the resulting particles emerge from exactly the same vertex as the primary scattering. The probability that a multiparton interaction leads to a secondary hard process X in addition to the primary one is parameterized as $\sigma(X)/\sigma_0$, where σ_0 is a process-independent parameter. The right plot of Fig. 50 shows the probability of multiparton interactions leading to dijet final states, with one jet inside the calorimeter and the other outside. For this example we chose $\sigma_0 = 30$ mb, a number consistent with the direct experimental determinations from Tevatron and LHC data. \cancel{E}_T signals in the range of 30-70 GeV are induced with probability of about 10^{-3} if η_{cal} is in the range 4 to 6, stressing once again the need to instrument the detectors with a calorimetric coverage more extended than at the LHC.

7. Directions for Further Exploration

Many years will go by before a 100 TeV pp collider becomes a reality. The technological, financial and political challenges—which we have not even alluded to in this report—are immense, and far from being trivially surmountable. But the physics opportunities are even more compelling, and have motivated ongoing efforts taking place worldwide to define more precisely the tasks required to give substance to this dream.

In this report we just scratched the surface of the vast array of contributions that the 100 TeV collider could give to physics. New ideas and proposals appear in the literature almost on a daily basis, and the overall picture will continue to evolve, not least in view of what will emerge from the future LHC runs. In this report we presented some examples of concrete and central theoretical issues that are unlikely to be settled conclusively by the LHC, and will require exploration at much higher energies. Discoveries at the LHC may of course change the theoretical priorities, and give higher weight to alternative future avenues. For example, discoveries at the edge

of the LHC mass reach can be studied in detail with good statistics even by just doubling the LHC energy, to 28 TeV. The discovery of new weakly interacting particles well below the TeV would strengthen the case of a lepton collider in the TeV range. It is clear, therefore, that, while the physics case of a 100 TeV collider is strong and clear as a long-term goal for the field—no other proposed or foreseeable project can have direct sensitivity to such large mass scales—the precise route used to get there must take account of the fuller picture to emerge from the LHC as well as other current and future experiments in areas ranging from flavour physics to dark matter searches.

In the meantime, several directions are open for continued studies of the physics capabilities of the 100 TeV collider. To start with, it is essential to assess the progress that can be anticipated in detector and data acquisition technologies, and how these might impact the ultimate experimental performance and systematics. This is critical to give more realistic estimates of the physics reach. The prospects in areas such as precise measurements of the Higgs properties, or searches and studies of signatures that today are elusive because of trigger or background limitations, will be strongly affected by the detector performance. In this report, we gave some examples of projected performance for Higgs studies where the impact of a 100 TeV collider will certainly be comparable, if not superior, to any sub-TeV e^+e^- collider (the measurement of the Higgs self-coupling and of the top Yukawa coupling). But it may happen that future studies, in the context of ambitious detector concepts, could expose important complementarity, if not superiority, also in areas that typically represent golden channels for the e^+e^- colliders. Future theoretical improvements in the precision of calculation and modeling of hard processes in pp collisions will also play a key role. Important inputs for these calculations include the determination of α_S and of the PDFs. Whether the LHC, or the 100 TeV collider itself, can provide sufficient inputs to reach the needed precision, is a further relevant question. Scrupulous studies of the complementarity and synergy of the pp and e^+e^- approaches, as well as the role of a possible future ep collider, are therefore a pressing priority for future work.

We discussed here some landmark issues that might lie in the exclusive domain of the 100 TeV collider, such as the understanding of the nature of the EW phase transition and the observation of dark matter, should this be due to a WIMP thermal relic. More work is needed to explore all possible scenarios, and to support more firmly the statement that this facility could give conclusive answers to those questions. With these clear goals in

mind, phenomenological analyses of the most important processes will ideally provide useful benchmarks for the detector performance.

The infrastructure of a 100 TeV collider enables in principle a broader range of studies than we discussed: from higher-energy and higher-intensity fixed target experiments, to higher-energy heavy ion collisions, to dedicated collider experiments focused on flavour physics or further explorations of the properties of SM particles (the top quark, gauge bosons, etc). In the case of flavour physics, for example, the importance of these studies may be enhanced by future findings, at the LHC, at Belle2, in rare kaon decay experiments, or in the lepton sector. Thus, even in these areas, more comprehensive studies of the physics opportunities and of the complementarity of a 100 TeV collider with other experimental approaches is desirable.

The process of consolidating the physics case of a 100 TeV collider will certainly be rich and fruitful, no matter what: it will prompt theorists to consider possible new ideas – which may not emerge if one just focused on what is measurable by today’s facilities – and will challenge experimentalists and detector experts to push further their creativity – opening new avenues to approach measurements considered impossible before. This progress on all fronts will likely bear fruits already during the LHC era, and will hopefully give confidence to the high-energy community to unite forces behind this fantastic project, which will push our knowledge of the fundamental laws of nature well beyond our current limited view of physics at the TeV scale.

Acknowledgments

We would like to thank the Institute for High Energy Physics in Beijing for hospitality during our visits. TH would like to thank Chien-Yi Chen, Junmou Chen, Zhen Liu, Richard Ruiz, Josh Sayre, Brock Tweedie, and Susanne Westhoff for collaboration and for providing some figures. LTW would like to thank Matthew Low for supplying some of the figures and results. The work of TH is supported in part by the U.S. Department of Energy under grant No. DE-FG02-95ER40896 and in part by PITT PACC. LTW’s research is supported in part by a DOE grant DE-SC0013642. The work of MLM is supported by the ERC grant 291377 *LHCtheory: Theoretical predictions and analyses of LHC physics: advancing the precision frontier*.

- [1] G. Aad, et al., Observation of a new particle in the search for the Standard Model Higgs boson with the ATLAS detector at the LHC, Phys.Lett. B716 (2012) 1–29. [arXiv:1207.7214](#), [doi:10.1016/j.physletb.2012.08.020](#).
- [2] S. Chatrchyan, et al., Observation of a new boson at a mass of 125 GeV with the CMS experiment at the LHC, Phys.Lett. B716 (2012) 30–61. [arXiv:1207.7235](#), [doi:10.1016/j.physletb.2012.08.021](#).
- [3] M. Endres, T. Fukuhara, D. Pekker, M. Cheneau, P. Schauss, et al., The ‘Higgs’ Amplitude Mode at the Two-Dimensional Superfluid-Mott Insulator Transition, Nature 487 (2012) 454–458. [arXiv:1204.5183](#), [doi:10.1038/nature11255](#).
- [4] J. Campbell, K. Hatakeyama, J. Huston, F. Petriello, J. R. Andersen, et al., Working Group Report: Quantum Chromodynamics [arXiv:1310.5189](#).
- [5] W. Yao, Studies of measuring Higgs self-coupling with $HH \rightarrow b\bar{b}\gamma\gamma$ at the future hadron colliders [arXiv:1308.6302](#).
- [6] H.-J. He, J. Ren, W. Yao, Probing New Physics of Cubic Higgs Interaction via Higgs Pair Production at Hadron Colliders [arXiv:1506.03302](#).
- [7] A. J. Barr, M. J. Dolan, C. Englert, D. E. F. de Lima, M. Spannowsky, Higgs Self-Coupling Measurements at a 100 TeV Hadron Collider [arXiv:1412.7154](#).
- [8] A. Azatov, R. Contino, G. Panico, M. Son, Effective field theory analysis of double Higgs production via gluon fusion [arXiv:1502.00539](#).
- [9] M. Mangano, T. Plehn, P. Reimitz, T. Schell, H.-S. Shao, Measuring the Top Yukawa Coupling at 100 TeV [arXiv:1507.08169](#).
- [10] A. Hook, A. Katz, Unbroken $SU(2)$ at a 100 TeV collider, JHEP 09 (2014) 175. [arXiv:1407.2607](#), [doi:10.1007/JHEP09\(2014\)175](#).
- [11] I. Hinchliffe, A. Kotwal, M. L. Mangano, C. Quigg, L.-T. Wang, Luminosity goals for a 100-TeV pp collider [arXiv:1504.06108](#).

- [12] T. G. Rizzo, Mass Reach Scaling for Future Hadron Colliders, *Eur. Phys. J. C* 75 (4) (2015) 161. [arXiv:1501.05583](#), [doi:10.1140/epjc/s10052-015-3381-1](#).
- [13] M. Benedikt, “FCC study overview and status”, talk at the FCC week 2015, Washington D.C., 23-29 March 2015, <http://indico.cern.ch/event/340703/session/108/contribution/186>.
- [14] X.-m. Zhang, Operators analysis for Higgs potential and cosmological bound on Higgs mass, *Phys.Rev. D* 47 (1993) 3065–3067. [arXiv:hep-ph/9301277](#), [doi:10.1103/PhysRevD.47.3065](#).
- [15] X. Zhang, B. Young, S. Lee, Electroweak sphaleron for effective theory in the limit of large Higgs boson mass, *Phys.Rev. D* 51 (1995) 5327–5330. [arXiv:hep-ph/9406322](#), [doi:10.1103/PhysRevD.51.5327](#).
- [16] C. Grojean, G. Servant, J. D. Wells, First-order electroweak phase transition in the standard model with a low cutoff, *Phys.Rev. D* 71 (2005) 036001. [arXiv:hep-ph/0407019](#), [doi:10.1103/PhysRevD.71.036001](#).
- [17] S. R. Coleman, E. J. Weinberg, Radiative Corrections as the Origin of Spontaneous Symmetry Breaking, *Phys.Rev. D* 7 (1973) 1888–1910. [doi:10.1103/PhysRevD.7.1888](#).
- [18] V. Kuzmin, V. Rubakov, M. Shaposhnikov, On the Anomalous Electroweak Baryon Number Nonconservation in the Early Universe, *Phys.Lett. B* 155 (1985) 36. [doi:10.1016/0370-2693\(85\)91028-7](#).
- [19] D. Bodeker, L. Fromme, S. J. Huber, M. Seniuch, The Baryon asymmetry in the standard model with a low cut-off, *JHEP* 0502 (2005) 026. [arXiv:hep-ph/0412366](#), [doi:10.1088/1126-6708/2005/02/026](#).
- [20] C. Delaunay, C. Grojean, J. D. Wells, Dynamics of Non-renormalizable Electroweak Symmetry Breaking, *JHEP* 0804 (2008) 029. [arXiv:0711.2511](#), [doi:10.1088/1126-6708/2008/04/029](#).
- [21] M. Bicer, et al., First Look at the Physics Case of TLEP, *JHEP* 01 (2014) 164. [arXiv:1308.6176](#), [doi:10.1007/JHEP01\(2014\)164](#).

- [22] CEPC project website. [link].
URL <http://cepc.ihep.ac.cn>
- [23] K. Fujii, et al., Physics Case for the International Linear Collider [arXiv:1506.05992](#).
- [24] L. Linssen, A. Miyamoto, M. Stanitzki, H. Weerts, Physics and Detectors at CLIC: CLIC Conceptual Design Report [arXiv:1202.5940](#), [doi:10.5170/CERN-2012-003](#).
- [25] G. Aad, et al., Search For Higgs Boson Pair Production in the $\gamma\gamma b\bar{b}$ Final State using pp Collision Data at $\sqrt{s} = 8$ TeV from the ATLAS Detector [arXiv:1406.5053](#).
- [26] D. Curtin, P. Meade, C.-T. Yu, Testing Electroweak Baryogenesis with Future Colliders, JHEP 1411 (2014) 127. [arXiv:1409.0005](#), [doi:10.1007/JHEP11\(2014\)127](#).
- [27] S. Weinberg, Implications of Dynamical Symmetry Breaking, Phys.Rev. D13 (1976) 974–996. [doi:10.1103/PhysRevD.13.974](#).
- [28] L. Susskind, Dynamics of Spontaneous Symmetry Breaking in the Weinberg-Salam Theory, Phys.Rev. D20 (1979) 2619–2625. [doi:10.1103/PhysRevD.20.2619](#).
- [29] D. B. Kaplan, H. Georgi, SU(2) x U(1) Breaking by Vacuum Misalignment, Phys.Lett. B136 (1984) 183. [doi:10.1016/0370-2693\(84\)91177-8](#).
- [30] N. Arkani-Hamed, A. G. Cohen, H. Georgi, Electroweak symmetry breaking from dimensional deconstruction, Phys.Lett. B513 (2001) 232–240. [arXiv:hep-ph/0105239](#), [doi:10.1016/S0370-2693\(01\)00741-9](#).
- [31] K. Agashe, R. Contino, A. Pomarol, The Minimal composite Higgs model, Nucl.Phys. B719 (2005) 165–187. [arXiv:hep-ph/0412089](#), [doi:10.1016/j.nuclphysb.2005.04.035](#).
- [32] S. Dimopoulos, H. Georgi, Softly Broken Supersymmetry and SU(5), Nucl.Phys. B193 (1981) 150. [doi:10.1016/0550-3213\(81\)90522-8](#).

- [33] N. Arkani-Hamed, S. Dimopoulos, G. Dvali, The Hierarchy problem and new dimensions at a millimeter, *Phys.Lett.* B429 (1998) 263–272. [arXiv:hep-ph/9803315](#), doi:10.1016/S0370-2693(98)00466-3.
- [34] L. Randall, R. Sundrum, A Large mass hierarchy from a small extra dimension, *Phys.Rev.Lett.* 83 (1999) 3370–3373. [arXiv:hep-ph/9905221](#), doi:10.1103/PhysRevLett.83.3370.
- [35] J. M. Maldacena, The Large N limit of superconformal field theories and supergravity, *Int.J.Theor.Phys.* 38 (1999) 1113–1133. [arXiv:hep-th/9711200](#), doi:10.1023/A:1026654312961.
- [36] P. Langacker, M.-x. Luo, Implications of precision electroweak experiments for M_t , ρ_0 , $\sin^2 \theta_W$ and grand unification, *Phys.Rev.* D44 (1991) 817–822. doi:10.1103/PhysRevD.44.817.
- [37] R. Barbieri, G. Giudice, Upper Bounds on Supersymmetric Particle Masses, *Nucl.Phys.* B306 (1988) 63. doi:10.1016/0550-3213(88)90171-X.
- [38] Z. Chacko, H.-S. Goh, R. Harnik, The Twin Higgs: Natural electroweak breaking from mirror symmetry, *Phys.Rev.Lett.* 96 (2006) 231802. [arXiv:hep-ph/0506256](#), doi:10.1103/PhysRevLett.96.231802.
- [39] G. Burdman, Z. Chacko, H.-S. Goh, R. Harnik, Folded supersymmetry and the LEP paradox, *JHEP* 0702 (2007) 009. [arXiv:hep-ph/0609152](#), doi:10.1088/1126-6708/2007/02/009.
- [40] J. D. Wells, Implications of supersymmetry breaking with a little hierarchy between gauginos and scalars [arXiv:hep-ph/0306127](#).
- [41] N. Arkani-Hamed, S. Dimopoulos, Supersymmetric unification without low energy supersymmetry and signatures for fine-tuning at the LHC, *JHEP* 0506 (2005) 073. [arXiv:hep-th/0405159](#), doi:10.1088/1126-6708/2005/06/073.
- [42] G. Giudice, A. Romanino, Split supersymmetry, *Nucl.Phys.* B699 (2004) 65–89. [arXiv:hep-ph/0406088](#), doi:10.1016/j.nuclphysb.2004.11.048.

- [43] N. Arkani-Hamed, A. Delgado, G. Giudice, The Well-tempered neutralino, Nucl.Phys. B741 (2006) 108–130. [arXiv:hep-ph/0601041](#), [doi:10.1016/j.nuclphysb.2006.02.010](#).
- [44] A. Arvanitaki, N. Craig, S. Dimopoulos, G. Villadoro, Mini-Split, JHEP 1302 (2013) 126. [arXiv:1210.0555](#), [doi:10.1007/JHEP02\(2013\)126](#).
- [45] N. Arkani-Hamed, A. Gupta, D. E. Kaplan, N. Weiner, T. Zorawski, Simply Unnatural Supersymmetry [arXiv:1212.6971](#).
- [46] C. Borschensky, M. Krmer, A. Kulesza, M. Mangano, S. Padhi, T. Plehn, X. Portell, Squark and gluino production cross sections in pp collisions at $\sqrt{s} = 13, 14, 33$ and 100 TeV, Eur. Phys. J. C74 (12) (2014) 3174. [arXiv:1407.5066](#), [doi:10.1140/epjc/s10052-014-3174-y](#).
- [47] T. Cohen, T. Golling, M. Hance, A. Henrichs, K. Howe, et al., SUSY Simplified Models at 14, 33, and 100 TeV Proton Colliders, JHEP 1404 (2014) 117. [arXiv:1311.6480](#), [doi:10.1007/JHEP04\(2014\)117](#).
- [48] T. Cohen, R. T. D’Agnolo, M. Hance, H. K. Lou, J. G. Wacker, Boosting Stop Searches with a 100 TeV Proton Collider, JHEP 1411 (2014) 021. [arXiv:1406.4512](#), [doi:10.1007/JHEP11\(2014\)021](#).
- [49] J. A. Aguilar-Saavedra, B. Fuks, M. L. Mangano, Pinning down top dipole moments with ultra-boosted tops, Phys. Rev. D91 (2015) 094021. [arXiv:1412.6654](#), [doi:10.1103/PhysRevD.91.094021](#).
- [50] S. Dimopoulos, G. Giudice, Naturalness constraints in supersymmetric theories with nonuniversal soft terms, Phys.Lett. B357 (1995) 573–578. [arXiv:hep-ph/9507282](#), [doi:10.1016/0370-2693\(95\)00961-J](#).
- [51] N. Arkani-Hamed, H. Murayama, Can the supersymmetric flavor problem decouple?, Phys.Rev. D56 (1997) 6733–6737. [arXiv:hep-ph/9703259](#), [doi:10.1103/PhysRevD.56.R6733](#).
- [52] N. Craig, H. K. Lou, M. McCullough, A. Thalapillil, The Higgs Portal Above Threshold [arXiv:1412.0258](#).
- [53] D. Curtin, P. Saraswat, Towards a No-Lose Theorem for Naturalness [arXiv:1509.04284](#).

- [54] B. W. Lee, S. Weinberg, Cosmological Lower Bound on Heavy Neutrino Masses, *Phys.Rev.Lett.* 39 (1977) 165–168. doi:10.1103/PhysRevLett.39.165.
- [55] H. Goldberg, Constraint on the Photino Mass from Cosmology, *Phys.Rev.Lett.* 50 (1983) 1419. doi:10.1103/PhysRevLett.50.1419.
- [56] G. Steigman, B. Dasgupta, J. F. Beacom, Precise Relic WIMP Abundance and its Impact on Searches for Dark Matter Annihilation, *Phys.Rev. D* 86 (2012) 023506. arXiv:1204.3622, doi:10.1103/PhysRevD.86.023506.
- [57] M. Ibe, S. Matsumoto, R. Sato, Mass Splitting between Charged and Neutral Winos at Two-Loop Level, *Phys.Lett. B* 721 (2013) 252–260. arXiv:1212.5989, doi:10.1016/j.physletb.2013.03.015.
- [58] S. D. Thomas, J. D. Wells, Phenomenology of Massive Vectorlike Doublet Leptons, *Phys.Rev.Lett.* 81 (1998) 34–37. arXiv:hep-ph/9804359, doi:10.1103/PhysRevLett.81.34.
- [59] J. Hisano, K. Ishiwata, N. Nagata, A complete calculation for direct detection of Wino dark matter, *Phys.Lett. B* 690 (2010) 311–315. arXiv:1004.4090, doi:10.1016/j.physletb.2010.05.047.
- [60] R. J. Hill, M. P. Solon, WIMP-nucleon scattering with heavy WIMP effective theory, *Phys.Rev.Lett.* 112 (2014) 211602. arXiv:1309.4092, doi:10.1103/PhysRevLett.112.211602.
- [61] J. Hisano, S. Matsumoto, M. M. Nojiri, O. Saito, Non-perturbative effect on dark matter annihilation and gamma ray signature from galactic center, *Phys.Rev. D* 71 (2005) 063528. arXiv:hep-ph/0412403, doi:10.1103/PhysRevD.71.063528.
- [62] A. Abramowski, et al., Search for Photon-Linelike Signatures from Dark Matter Annihilations with H.E.S.S., *Phys.Rev.Lett.* 110 (2013) 041301. arXiv:1301.1173, doi:10.1103/PhysRevLett.110.041301.
- [63] T. Cohen, M. Lisanti, A. Pierce, T. R. Slatyer, Wino Dark Matter Under Siege, *JCAP* 1310 (2013) 061. arXiv:1307.4082, doi:10.1088/1475-7516/2013/10/061.

- [64] J. Fan, M. Reece, In Wino Veritas? Indirect Searches Shed Light on Neutralino Dark Matter, JHEP 1310 (2013) 124. [arXiv:1307.4400](#), [doi:10.1007/JHEP10\(2013\)124](#).
- [65] A. Hryczuk, I. Cholis, R. Iengo, M. Tavakoli, P. Ullio, Indirect Detection Analysis: Wino Dark Matter Case Study, JCAP 1407 (2014) 031. [arXiv:1401.6212](#), [doi:10.1088/1475-7516/2014/07/031](#).
- [66] G. Ovanessian, T. R. Slatyer, I. W. Stewart, Heavy Dark Matter Anihilation from Effective Field Theory [arXiv:1409.8294](#).
- [67] M. Baumgart, I. Z. Rothstein, V. Vaidya, Constraints on Galactic Wino Densities from Gamma Ray Lines [arXiv:1412.8698](#).
- [68] M. Low, L.-T. Wang, Neutralino dark matter at 14 TeV and 100 TeV, JHEP 1408 (2014) 161. [arXiv:1404.0682](#), [doi:10.1007/JHEP08\(2014\)161](#).
- [69] Search for New Phenomena in Monojet plus Missing Transverse Momentum Final States using 10fb-1 of pp Collisions at $\sqrt{s}=8$ TeV with the ATLAS detector at the LHC.
- [70] Search for new physics in monojet events in pp collisions at $\sqrt{s}=8$ TeV.
- [71] G. Aad, et al., Search for charginos nearly mass degenerate with the lightest neutralino based on a disappearing-track signature in pp collisions at $\sqrt{s}=8$ TeV with the ATLAS detector, Phys.Rev. D88 (11) (2013) 112006. [arXiv:1310.3675](#), [doi:10.1103/PhysRevD.88.112006](#).
- [72] Search for disappearing tracks in proton-proton collisions at $\sqrt{s} = 8$ TeV [arXiv:1411.6006](#).
- [73] S. Gori, S. Jung, L.-T. Wang, J. D. Wells, Prospects for Electroweakino Discovery at a 100 TeV Hadron Collider, JHEP 1412 (2014) 108. [arXiv:1410.6287](#), [doi:10.1007/JHEP12\(2014\)108](#).
- [74] K. Harigaya, K. Kaneta, S. Matsumoto, Gaugino coannihilations, Phys.Rev. D89 (2014) 115021. [arXiv:1403.0715](#), [doi:10.1103/PhysRevD.89.115021](#).

- [75] A. De Simone, G. F. Giudice, A. Strumia, Benchmarks for Dark Matter Searches at the LHC, JHEP 1406 (2014) 081. [arXiv:1402.6287](#), [doi:10.1007/JHEP06\(2014\)081](#).
- [76] T. Han, I. Lewis, Z. Liu, Colored Resonant Signals at the LHC: Largest Rate and Simplest Topology, JHEP 1012 (2010) 085. [arXiv:1010.4309](#), [doi:10.1007/JHEP12\(2010\)085](#).
- [77] G. Aad, et al., Search for new phenomena in the dijet mass distribution using $p - p$ collision data at $\sqrt{s} = 8$ TeV with the ATLAS detector, Phys.Rev. D91 (5) (2015) 052007. [arXiv:1407.1376](#), [doi:10.1103/PhysRevD.91.052007](#).
- [78] S. Chatrchyan, et al., Search for narrow resonances using the dijet mass spectrum in pp collisions at $\sqrt{s}=8$ TeV, Phys.Rev. D87 (11) (2013) 114015. [arXiv:1302.4794](#), [doi:10.1103/PhysRevD.87.114015](#).
- [79] P. Langacker, The Physics of Heavy Z' Gauge Bosons, Rev. Mod. Phys. 81 (2009) 1199–1228. [arXiv:0801.1345](#), [doi:10.1103/RevModPhys.81.1199](#).
- [80] K. A. Olive, et al., Review of Particle Physics, Chin. Phys. C38 (2014) 090001. [doi:10.1088/1674-1137/38/9/090001](#).
- [81] N. Craig, F. D’Eramo, P. Draper, S. Thomas, H. Zhang, The Hunt for the Rest of the Higgs Bosons, JHEP 06 (2015) 137. [arXiv:1504.04630](#), [doi:10.1007/JHEP06\(2015\)137](#).
- [82] J. Hajer, Y.-Y. Li, T. Liu, J. F. H. Shiu, Heavy Higgs Bosons at 14 TeV and 100 TeV [arXiv:1504.07617](#).
- [83] T. Han, J. Sayre, S. Westhoff, Top-Quark Initiated Processes at High-Energy Hadron Colliders, JHEP 04 (2015) 145. [arXiv:1411.2588](#), [doi:10.1007/JHEP04\(2015\)145](#).
- [84] M. A. G. Aivazis, J. C. Collins, F. I. Olness, W.-K. Tung, Leptoproduction of heavy quarks. 2. A Unified QCD formulation of charged and neutral current processes from fixed target to collider energies, Phys. Rev. D50 (1994) 3102–3118. [arXiv:hep-ph/9312319](#), [doi:10.1103/PhysRevD.50.3102](#).

- [85] T. P. Cheng, L.-F. Li, Neutrino Masses, Mixings and Oscillations in $SU(2) \times U(1)$ Models of Electroweak Interactions, Phys. Rev. D22 (1980) 2860. doi:10.1103/PhysRevD.22.2860.
- [86] R. N. Mohapatra, G. Senjanovic, Neutrino Masses and Mixings in Gauge Models with Spontaneous Parity Violation, Phys. Rev. D23 (1981) 165. doi:10.1103/PhysRevD.23.165.
- [87] P. Fileviez Perez, T. Han, G.-y. Huang, T. Li, K. Wang, Neutrino Masses and the CERN LHC: Testing Type II Seesaw, Phys. Rev. D78 (2008) 015018. arXiv:0805.3536, doi:10.1103/PhysRevD.78.015018.
- [88] H. Cai, H.-C. Cheng, J. Terning, A Spin-1 Top Quark Superpartner, Phys. Rev. Lett. 101 (2008) 171805. arXiv:0806.0386, doi:10.1103/PhysRevLett.101.171805.
- [89] C.-Y. Chen, A. Freitas, T. Han, K. S. M. Lee, New Physics from the Top at the LHC, JHEP 11 (2012) 124. arXiv:1207.4794, doi:10.1007/JHEP11(2012)124.
- [90] C.-Y. Chen, A. Freitas, T. Han, K. S. M. Lee, Heavy Color-Octet Particles at the LHC, JHEP 05 (2015) 135. arXiv:1410.8113, doi:10.1007/JHEP05(2015)135.
- [91] R. Foot, H. Lew, X. G. He, G. C. Joshi, Seesaw Neutrino Masses Induced by a Triplet of Leptons, Z. Phys. C44 (1989) 441. doi:10.1007/BF01415558.
- [92] A. Arhrib, B. Bajc, D. K. Ghosh, T. Han, G.-Y. Huang, I. Puljak, G. Senjanovic, Collider Signatures for Heavy Lepton Triplet in Type I+III Seesaw, Phys. Rev. D82 (2010) 053004. arXiv:0904.2390, doi:10.1103/PhysRevD.82.053004.
- [93] T. Li, X.-G. He, Neutrino Masses and Heavy Triplet Leptons at the LHC: Testability of Type III Seesaw, Phys. Rev. D80 (2009) 093003. arXiv:0907.4193, doi:10.1103/PhysRevD.80.093003.
- [94] M. Cacciari, G. P. Salam, G. Soyez, The Anti-k(t) jet clustering algorithm, JHEP 04 (2008) 063. arXiv:0802.1189, doi:10.1088/1126-6708/2008/04/063.

- [95] A. J. Larkoski, F. Maltoni, M. Selvaggi, Tracking down hyper-boosted top quarks, JHEP 06 (2015) 032. [arXiv:1503.03347](#), [doi:10.1007/JHEP06\(2015\)032](#).
- [96] P. Torrielli, Rare Standard Model processes for present and future hadronic colliders [arXiv:1407.1623](#).
- [97] J. Alwall, R. Frederix, S. Frixione, V. Hirschi, F. Maltoni, et al., The automated computation of tree-level and next-to-leading order differential cross sections, and their matching to parton shower simulations, JHEP 1407 (2014) 079. [arXiv:1405.0301](#), [doi:10.1007/JHEP07\(2014\)079](#).
- [98] A. Denner, S. Dittmaier, T. Kasprzik, A. Muck, Electroweak corrections to dilepton + jet production at hadron colliders, JHEP 06 (2011) 069. [arXiv:1103.0914](#), [doi:10.1007/JHEP06\(2011\)069](#).
- [99] M. Rubin, G. P. Salam, S. Sapeta, Giant QCD K-factors beyond NLO, JHEP 09 (2010) 084. [arXiv:1006.2144](#), [doi:10.1007/JHEP09\(2010\)084](#).
- [100] S. Moretti, M. R. Nolten, D. A. Ross, Weak corrections to four-parton processes, Nucl. Phys. B759 (2006) 50–82. [arXiv:hep-ph/0606201](#), [doi:10.1016/j.nuclphysb.2006.09.028](#).
- [101] G. Bell, J. H. Kuhn, J. Rittinger, Electroweak Sudakov Logarithms and Real Gauge-Boson Radiation in the TeV Region, Eur. Phys. J. C70 (2010) 659–671. [arXiv:1004.4117](#), [doi:10.1140/epjc/s10052-010-1489-x](#).
- [102] S. Dittmaier, A. Huss, C. Speckner, Weak radiative corrections to dijet production at hadron colliders, JHEP 11 (2012) 095. [arXiv:1210.0438](#), [doi:10.1007/JHEP11\(2012\)095](#).
- [103] J. R. Christiansen, T. Sjostrand, Weak Gauge Boson Radiation in Parton Showers, JHEP 04 (2014) 115. [arXiv:1401.5238](#), [doi:10.1007/JHEP04\(2014\)115](#).
- [104] B. W. Lee, C. Quigg, H. B. Thacker, Weak Interactions at Very High-Energies: The Role of the Higgs Boson Mass, Phys. Rev. D16 (1977) 1519. [doi:10.1103/PhysRevD.16.1519](#).

- [105] M. S. Chanowitz, M. K. Gaillard, The TeV Physics of Strongly Interacting W's and Z's, Nucl. Phys. B261 (1985) 379. doi:10.1016/0550-3213(85)90580-2.
- [106] G. L. Kane, W. W. Repko, W. B. Rolnick, The Effective W⁺⁻, Z⁰ Approximation for High-Energy Collisions, Phys. Lett. B148 (1984) 367–372. doi:10.1016/0370-2693(84)90105-9.
- [107] S. Dawson, The Effective W Approximation, Nucl. Phys. B249 (1985) 42–60. doi:10.1016/0550-3213(85)90038-0.
- [108] J. Chen, T. Han, R. Ruiz, B. Tweedie, In preparation.
- [109] M. Cvetič, P. Langacker, Rare decays as diagnostics for Z-prime gauge couplings at hadron colliders, Phys. Rev. D46 (1992) R14–R18. doi:10.1103/PhysRevD.46.R14.
- [110] T. G. Rizzo, Exploring new gauge bosons at a 100 TeV collider, Phys. Rev. D89 (9) (2014) 095022. arXiv:1403.5465, doi:10.1103/PhysRevD.89.095022.
- [111] J. Alwall, M. Herquet, F. Maltoni, O. Mattelaer, T. Stelzer, MadGraph 5 : Going Beyond, JHEP 06 (2011) 128. arXiv:1106.0522, doi:10.1007/JHEP06(2011)128.
- [112] T. Stelzer, W. F. Long, Automatic generation of tree level helicity amplitudes, Comput. Phys. Commun. 81 (1994) 357–371. arXiv:hep-ph/9401258, doi:10.1016/0010-4655(94)90084-1.
- [113] F. Maltoni, T. Stelzer, MadEvent: Automatic event generation with MadGraph, JHEP 02 (2003) 027. arXiv:hep-ph/0208156, doi:10.1088/1126-6708/2003/02/027.
- [114] A. G. Cohen, D. B. Kaplan, A. E. Nelson, The More minimal supersymmetric standard model, Phys. Lett. B388 (1996) 588–598. arXiv:hep-ph/9607394, doi:10.1016/S0370-2693(96)01183-5.
- [115] C. Brust, A. Katz, S. Lawrence, R. Sundrum, SUSY, the Third Generation and the LHC, JHEP 03 (2012) 103. arXiv:1110.6670, doi:10.1007/JHEP03(2012)103.

- [116] R. Essig, E. Izaguirre, J. Kaplan, J. G. Wacker, Heavy Flavor Simplified Models at the LHC, JHEP 01 (2012) 074. [arXiv:1110.6443](#), [doi:10.1007/JHEP01\(2012\)074](#).
- [117] M. Papucci, J. T. Ruderman, A. Weiler, Natural SUSY Endures, JHEP 09 (2012) 035. [arXiv:1110.6926](#), [doi:10.1007/JHEP09\(2012\)035](#).
- [118] M. Mangano, T. Melia, Rare exclusive hadronic W decays in a $t\bar{t}$ environment, Eur. Phys. J. C75 (6) (2015) 258. [arXiv:1410.7475](#), [doi:10.1140/epjc/s10052-015-3482-x](#).
- [119] O. Gedalia, G. Isidori, F. Maltoni, G. Perez, M. Selvaggi, et al., Top B Physics at the LHC, Phys.Rev.Lett. 110 (23) (2013) 232002. [arXiv:1212.4611](#), [doi:10.1103/PhysRevLett.110.232002](#).
- [120] F. Maltoni, M. L. Mangano, I. Tsinikos, M. Zaro, Top-quark charge asymmetry and polarization in $t\bar{t}W^\pm$ production at the LHC, Phys. Lett. B736 (2014) 252–260. [arXiv:1406.3262](#), [doi:10.1016/j.physletb.2014.07.033](#).
- [121] F. Maltoni, D. Pagani, I. Tsinikos, Associated production of a top-quark pair with vector bosons at NLO in QCD: impact on $t\bar{t}H$ searches at the LHC [arXiv:1507.05640](#).
- [122] R. M. Barnett, H. E. Haber, D. E. Soper, Ultraheavy Particle Production from Heavy Partons at Hadron Colliders, Nucl. Phys. B306 (1988) 697. [doi:10.1016/0550-3213\(88\)90440-3](#).
- [123] F. I. Olness, W.-K. Tung, When Is a Heavy Quark Not a Parton? Charged Higgs Production and Heavy Quark Mass Effects in the QCD Based Parton Model, Nucl. Phys. B308 (1988) 813. [doi:10.1016/0550-3213\(88\)90129-0](#).
- [124] R. D. Ball, et al., Parton distributions with LHC data, Nucl. Phys. B867 (2013) 244–289. [arXiv:1207.1303](#), [doi:10.1016/j.nuclphysb.2012.10.003](#).
- [125] J. C. Collins, Hard scattering factorization with heavy quarks: A General treatment, Phys. Rev. D58 (1998) 094002. [arXiv:hep-ph/9806259](#), [doi:10.1103/PhysRevD.58.094002](#).

- [126] Higgs Cross Section Working Group, <https://cern.ch/twiki/bin/view/LHCPhysics/LHCHXSWG>.
- [127] A. Papaefstathiou, Discovering Higgs boson pair production through rare final states at a 100 TeV collider, Phys. Rev. D91 (11) (2015) 113016. [arXiv:1504.04621](https://arxiv.org/abs/1504.04621), doi:10.1103/PhysRevD.91.113016.